JAERI-M
91-093

EFFECTS OF RADIAL CORE POWER PROFILE ON CORE THERMO-HYDRAULIC BEHAVIOR DURING REFLOOD PHASE IN SCTF CORE-I FORCED FEED TESTS

(Work done under Contract with the Government)

June 1991

Takamichi IWAMURA, Masahiro OSAKABE*, Yukio SUDO
Makoto SOBAJIMA, Akira OHNUKI, Yutaka ABE
Hiromichi ADACHI** and Yoshio MURAO

日本原子力研究所
Japan Atomic Energy Research Institute

JAERI-Mレポートは，日本原子力研究所が不定期に公刊している研究報告書です。
入手の問合わせは，日本原子力研究所技術情報部情報資料課（〒319-11茨城県那珂郡東海村）あて，お申しこしください。なお，このほかに財団法人原子力弘済会資料センター（〒319-11 茨城県那珂郡東海村日本原子力研究所内）で複写による実費領布をおこなっております。

JAERI-M reports are issued irregularly.
Inquiries about availability of the reports should be addressed to Information Division, Department of Technical Information, Japan Atomic Energy Research Institute, Tokai-mura, Naka-gun, Ibaraki-ken 319-11, Japan.

編集兼発行　日本原子力研究所
印　　刷　㈱原子力資料サービス

JAERI-M 91-093

Effects of Radial Core Power Profile on Core Thermo-Hydraulic Behavior during Reflood Phase in SCTF Core-I Forced Feed Tests

Takamichi IWAMURA, Masahiro OSAKABE*, Yukio SUDO+
Makoto SOBAJIMA++, Akira OHNUKI, Yutaka ABE
Hiromichi ADACHI** and Yoshio MURAO

Department of Reactor Engineering
Tokai Research Establishment
Japan Atomic Energy Research Institute
Tokai-mura, Naka-gun, Ibaraki-ken

(Received May 9, 1991)

An investigation of the effects of the radial core power profile on the thermo-hydraulic behavior during the reflood phase of the large break LOCA of a PWR has been conducted with the Slab Core Test Facility (SCTF). Since the power in an actual PWR is lower in the peripheral bundles than in the central bundles, the so called chimney effect due to radial core power profile is expected to improve the cooling of the higher power bundles. The SCTF simulates a full radius slab section of a PWR and therefore the effects of radial core power profile can be investigated.

The revealed results obtained from four forced-feed reflood tests (S1-01, S1-06, S1-08 and S1-11) in the SCTF Core-I are; (1) Two-dimensional flow in the core was induced by the radial power distribution. The direction of cross flow was from the central high power region to the peripheral low power region above the quench front and

---

The work was performed under contract with the Atomic Energy Bureau of Science and Technology Agency of Japan.
+ Department of HTTR Project
++ Department of Fuel Safety Research
* Tokyo Marine University
** Yamagata University

the direction was reversed below the quench front. (2) The heat transfer coefficient at the highest power bundle of the steep power profile test was higher than that of the flat power profile test under the same total core power condition.

Keywords: PWR Type Reactors, Reflood, Chimney Effects, Slab Core Test, Radial Core Power Profile, Collapsed Water Level, Heat Transfer, Loss of Coolant Accident, Cross Flow

JAERI－M　91－093

SCTF 第1次炉心強制注入試験における半径方向出力分布が再冠水時炉心内熱水力挙動に及ぼす影響

日本原子力研究所東海研究所原子炉工学部
岩村　公道・刑部　真弘*・数土　幸夫+・傍島　真++
大貫　晃・阿部　豊・安達　公道**・村尾　良夫

（1991年5月9日受理）

PWR 大破断 LOCA 時再冠水過程の熱水力学的挙動に及ぼす，半径方向出力分布の効果を，平板炉心試験装置（SCTF）を用いて調べた。実際の PWR では周辺バンドルでは中心バンドルよりも出力が低くなっているので，半径方向出力分布に起因するいわゆるチムニー効果のため，高出力バンドルでの冷却を促進することが期待される。SCTF は PWR の半径方向長さを模擬しているので，半径方向出力分布効果が調べられる。

SCTF 第1次炉心における4種類の強制注入試験（S1－01，S1－06，S1－08 及び S1－11）の試験結果より，以下の点が明らかになった。

(1) 半径方向出力分布により炉心内に二次元的な流れが引き起こされた。横流れの方向はクェンチフロント上方では中心の高出力部より周辺の低出力部に向かい，クェンチフロントの下方では横流れ方向が逆転した。

(2) 総出力が同一の場合の最高出力バンドルにおいては，急峻な出力分布の方が平坦出力分布の場合より熱伝達率が大きくなった。

本報告書は，電源開発促進対策特別会計法に基づき，科学技術庁からの受託により行った研究の成果である。

東海研究所：〒319－11　茨城県那珂郡東海村白方字白根2－4
＋　高温工学試験研究炉開発部
＋＋　燃料安全工学部
＊　東京商船大学
＊＊　山形大学

Contents

1. Introduction 1
2. Test Conditions and Procedure 2
3. Test Results and Discussions 3
3.1 Initial Cladding Temperature 3
3.2 Mass Flow Rate at Inlet and Outlet of Core 3
3.3 Cladding Temperature and Quench Behavior 3
3.4 Horizontal Differential Pressure and Cross Flow Behavior in Core 4
3.5 Characteristics of Heat Transfer Coefficient in High Power Bundles 5
4. Conclusions 6
Acknowledgments 6
References 7
Appendix A Slab Core Test Facility (SCTF) Core-I 23
Appendix B Selected Data for Test S1-06 (Run 512) 67
Appendix C Selected Data for Test S1-08 (Run 514) 79

目　　次

1. 緒　　言 …… 1
2. 試験条件及び手順 …… 2
3. 試験結果及び検討 …… 3
3.1 被覆管初期温度 …… 3
3.2 炉心入口及び出口の質量流量 …… 3
3.3 被覆管温度及びクェンチ挙動 …… 3
3.4 炉心内水平方向差圧及び横流れ挙動 …… 4
3.5 高出力バンドル内熱伝達率特性 …… 5
4. 結　　論 …… 6
謝　　辞 …… 6
文　　献 …… 7
付　　録 A　平板炉心試験装置（SCTF）第1次模擬炉心 …… 23
付　　録 B　試験S1－06（Run 512）のデータ …… 67
付　　録 C　試験S1－08（Run 514）のデータ …… 79

1. Introduction

A typical pressurized water reactor (PWR) with 1,100 MWe has 193 bundles with a non-uniform power distribution. Especially, the power is much lower in peripheral bundles than in central ones. As there is no partition plate between bundles, the cooling water can flow from one bundle to another and the accumulated water level tends to be equalized across the core. At the same time, the vapor generation rate in the higher power bundles is considered to increase and to induce a kind of chimney effect, *i.e.* more water is collected at the highest power bundle than the lower power bundle. The chimney effect is expected to improve the cooling of higher power bundles and results in lower peak cladding temperature and earlier quench[1]. However, most of the simulated core in the previous reflooding experiments have been too small to investigate adequately the effects of radial power profile in an actual reactor.

Slab Core Test Facility (SCTF)[2] is a part of the Large Scale Reflood Test Program along with the Cylindrical Core Test Facility (CCTF) at the Japan Atomic Energy Research Institute (JAERI). The major purpose of the SCTF, which has full-size radial width of the core, is to investigate the two-dimensional thermo-hydrodynamic behavior in the core during the reflood phase of a PWR-LOCA.

Four SCTF tests were analyzed to investigate the effect of radial core power profile on the core thermal-hydraulic behavior during the reflood phase. These tests consist of the base case test in which the bundle power profile simulates the initial core power profile of a Westinghouse type PWR, the 1.2 times higher power test than the base case test, the steep bundle power profile test and the flat bundle power profile test. To clarify the pre-cooling above the quench front at the highest power bundle, the transient heat transfer coefficient were calculated. The heat transfer coefficients at the highest power bundle were compared and discussed among the different bundle power profile tests. The effect on heat transfer at the highest power bundle due to the chimney effect was investigated.

The objective of the present report is to clarify the effects of radial power profile on the core thermo-hydrodynamic behavior during the reflood phase.

A brief description on the design of the SCTF is given in Appendix A. Selected test data from Tests S1-06 and S1-08 are given in Appendices B and C, respectively.

2. Test Conditions and Procedure

The tests investigated in this report are the base case test (Test S1-01), the flat radial power profile test (Test S1-11), the steep radial power profile test (Test S1-08) and the higher core heating power test (Test S1-06). Major test conditions for these tests are listed in Table 2.1

These tests were performed under the forced-feed flooding condition. That is, the downcomer was isolated from the lower plenum by inserting a blocking plate and ECC water was directly injected into the lower plenum. In this way, the core inlet water flow rate can be specified during the tests.

The test conditions in the base case test have been selected to reasonably represent the situation of the reflood phase of a PWR-LOCA. The intended values for the system pressure and the maximum cladding temperature at the start of reflood were 0.2MPa and 973 K, respectively. Nominal flooding velocities during the Acc injection and the LPCI periods are about 5 and 2.5 cm/s, respectively, which are corresponding to about 22.4 and 11.2 kg/s of injection rate. The core inlet water subcooling was set as low as possible, however the maximum subcooling varied within 15 to 18 K in accordance with the overshoot of system pressure.

Normalized radial power profiles for these tests are shown in Fig. 2.1. The radial power profile in the base case test was based on the startup profile of a 1,100 MWe Westinghouse type PWR. The radial power profile was changed to steep one (Test S1-08) or flat one (Test S1-11) but the total heating power was unchanged from the base case test. It should be noted here that the initial stored energy at the peak power bundles was set to be the same for each test while the total initial stored energy for whole bundle was different with each other. Power decay curves for these tests except Test S1-06 were the same and the sum of the ANS standard and the additional power generated by actinides and delayed neutron. On the other hand, in Test S1-06, the ANS standard was increased 1.2 times as much as the other tests. The normalized decay curve used in these tests is shown in Fig. 2.2.

The general test procedure for these tests is as follows. After setting the initial conditions, core heating is initiated. When four cladding temperature signals exceed 926 K, the Acc injection is initiated into the lower plenum and the core heating power remains constant. When the water level in the lower plenum reaches the bottom of the heated part of the

core, the core heating power begins to decrease following the specified decay power curve from 30 s after shutdown. After 20 s from the initiation of the Acc injection, the ECC injection is switched from the Acc injection to the LPCI. The tests are terminated at about 900 s after the initiation of the LPCI.

3. Test Results and Discussions

3.1 Initial Cladding Temperature

The initial cladding temperature at the start of reflood affects the core thermal-hydraulics during the reflood process[3]. The effect of power should be discussed under the same initial cladding temperature. Therefore, the initial cladding temperatures at the highest power bundle 4 were set to be the same in the four tests as shown in Fig. 3.1. The distribution of the initial cladding temperature is approximately proportional to the power profile shown in Fig. 2.1. For an example, the distribution of the initial cladding temperature at elevation 1.735 m is shown in Fig. 3.2.

3.2 Mass Flow Rate at Inlet and Outlet of Core

Shown in Fig. 3.3 are injected water flow rate, effluent total (water and steam) and steam flow rates. The effluent steam flow rate was measured with a venturi flow meter after the steam/water separator. The effluent total flow rate was obtained by subtracting the water accumulation rate in the core from the injected water flow rate. The effluent total and steam flow rates are the same in Tests S1-01 (base case), S1-08 (steep power profile) and S1-11 (flat power profile). The effluent total and steam flow rates in Test S1-06 (high power) are little higher than those in the other tests.

3.3 Cladding Temperature and Quench Behavior

Shown in Fig. 3.4 is the typical transient of cladding temperature. The time before the start of reflood is the heating-up period. After the start of reflood, rods are cooled and quenched to the saturation temperature. The temperature rise to the turnaround temperature ΔT_{rise}, and the quench time are defined in Fig. 3.4. Comparisons of the temperature rise ΔT_{rise}, at the highest power bundle 4 are shown in Fig. 3.5. Circles show the comparison between Test S1-06 (high power) and Test S1-01 (base case). Triangles show the comparison between Test S1-08 (steep power) and Test S1-11 (flat power). The ΔT_{rise} in Test S1-06 (ordinate in Fig. 3.5)

core, the core heating power begins to decrease following the specified decay power curve from 30 s after shutdown. After 20 s from the initiation of the Acc injection, the ECC injection is switched from the Acc injection to the LPCI. The tests are terminated at about 900 s after the initiation of the LPCI.

3. Test Results and Discussions

3.1 Initial Cladding Temperature

The initial cladding temperature at the start of reflood affects the core thermal-hydraulics during the reflood process[3]. The effect of power should be discussed under the same initial cladding temperature. Therefore, the initial cladding temperatures at the highest power bundle 4 were set to be the same in the four tests as shown in Fig. 3.1. The distribution of the initial cladding temperature is approximately proportional to the power profile shown in Fig. 2.1. For an example, the distribution of the initial cladding temperature at elevation 1.735 m is shown in Fig. 3.2.

3.2 Mass Flow Rate at Inlet and Outlet of Core

Shown in Fig. 3.3 are injected water flow rate, effluent total (water and steam) and steam flow rates. The effluent steam flow rate was measured with a venturi flow meter after the steam/water separator. The effluent total flow rate was obtained by subtracting the water accumulation rate in the core from the injected water flow rate. The effluent total and steam flow rates are the same in Tests S1-01 (base case), S1-08 (steep power profile) and S1-11 (flat power profile). The effluent total and steam flow rates in Test S1-06 (high power) are little higher than those in the other tests.

3.3 Cladding Temperature and Quench Behavior

Shown in Fig. 3.4 is the typical transient of cladding temperature. The time before the start of reflood is the heating-up period. After the start of reflood, rods are cooled and quenched to the saturation temperature. The temperature rise to the turnaround temperature ΔT_{rise}, and the quench time are defined in Fig. 3.4. Comparisons of the temperature rise ΔT_{rise}, at the highest power bundle 4 are shown in Fig. 3.5. Circles show the comparison between Test S1-06 (high power) and Test S1-01 (base case). Triangles show the comparison between Test S1-08 (steep power) and Test S1-11 (flat power). The ΔT_{rise} in Test S1-06 (ordinate in Fig. 3.5)

is about 50% higher than that in Test S1-01 (abscissa in Fig. 3.5) under the bundle power ratio of 1.2. The ΔT_{rise} in Test S1-08 (ordinate in Fig. 3.5) is only about 20% higher than that in Test S1-11 (abscissa in Fig. 3.5) in spite of the same bundle power ratio (1.2) as that of Test S1-06 to Test S1-01. Quench time distributions for eight bundles at elevations 2.33, 1.735 and 0.95 m are shown in Fig. 3.6. The quench time of Test S1-06 is delayed from the other tests, suggesting the effect of the higher total bundle power. It is noticed that nearly the same quench time at bundle 4 is obtained in Tests S1-01, S1-08 and S1-11 in spite of the different bundle power. The later quench time is obtained in Test S1-06 than that of Test S1-01 under the condition of 1.2 times the bundle power. The quench time in Test S1-08 is approximately the same as that in Test S1-11 in spite of almost the same bundle power ratio of 1.2. Shown in Fig. 3.7 are the quench temperatures at bundle 4. The quench temperature depends on the elevation, but the difference is very small among four tests.

3.4 Horizontal Differential Pressure and Cross Flow Behavior in Core

Figures 3.8 and 3.9 show the horizontal differential pressures in the core for Tests S1-08 (steep power) and S1-11(flat power), respectively. The measurement locations and the quench front propagation profiles are also shown in these figures.

It is clearly observed in Fig.3.8 (steep power test) that the pressure in Bundle 5 is higher than the pressure in Bundle 8 until 200 s at elevation 1.905 m and also until 120 s at elevation 1.365 m. As shown in Fig.3.8, the times of 120 s and 200s are corresponding to the times when the quench front in Bundle 5 reaches the elevations 1.365 and 1.905 m, respectively. After those times, the pressure at the Bundle 8 side becomes larger than the pressure at the Bundle 5 side. The positive horizontal differential pressure between Bundles 5 and 8 indicates the occurrence of cross flow from the Bundle 5 side to the Bundle 8 side. Therefore, it is concluded that the direction of cross flow is from the center bundle to the peripheral bundle above the quench front and the direction is reversed below the quench front. Between Bundles 1 and 5 at elevation 1.905 m, no net cross flow is observed. At the upper part of the core (elevation 3.235 m), horizontal differential pressure is approximately zero during the initial 240 s and then becomes negative. This is explained by the development of non-uniform water accumulation in the upper plenum as indicated in Fig.3.10. That is, the collapsed water level in the upper plenum is higher in the Bundle 8 side than in the other side and the difference increases

with time. The higher pressure in the core in Bundle 8 is induced by the higher water head above Bundle 8.

On the other hand, as shown in Fig.3.9 (flat power test), the horizontal differential pressures between Bundles 5 and 8 are almost zero during the initial 140 s and then become negative. The negative horizontal differential pressures at the later period are also due to the non-uniform water accumulation behavior shown in Fig.3.11. It should be noted that the variation of radial power profile has little effect on the non-uniform water accumulation behavior in the upper plenum.

3.5 Characteristics of Heat Transfer Coefficient in High Power Bundles

Figures 3.12 and 3.13 show the heat transfer coefficients with respect to the time after reflood and to the distance from the quench front for the steep power profile test (Test S1-08) and flat power profile test (Test S1-11) at the elevations of 2.33 and 1.735 m of Bundle 4, respectively. Heat transfer coefficients are calculated with "HEATT" code[4] developed for the SCTF tests. Figures 3.14 and 3.15 are for the high power test (Test S1-06) and the base case test (Test S1-01). The power rate of rods in Bundle 4 of the steep power test is 1.2 times that of the flat power test. The power rate of rods in Bundle 4 of the high power test is also 1.2 times that of the base case test.

From Fig. 3.12 and 3.13 it is easily understood that the heat transfer coefficient during the major period of the reflood for the steep power profile test is slightly higher than that for the flat power test at both elevations of 2.33 m and 1.735 m. The sharp rise of heat transfer coefficient corresponds the quench. The quench occurred at almost the same time at the same elevations in the two tests though the power rate is higher in the steep power test as mentioned before. This result shows the enhancement of cooling of rods in the higher power bundles in the steep power profile test.

On the other hand, as shown in Fig. 3.14 and 3.15, the heat transfer coefficient for the high power test is almost the same as that for the base case test at the elevations 2.33 and 1.735 m with respect to the distance from the quench front. As already mentioned, the power rate in the high power test is 1.2 times that of the base case test. Therefore, the quench of the rods for the high power test is delayed much in comparison to the base case test because of the same characteristic in heat transfer. This result implies that the similar bundle power profile does not give the enhancement of cooling of higher power rods but the steeper bundle power

profile does.

4. Conclusions

The effects of radial core power profile and total core power on the cooling characteristics of heater rods in the higher power bundles have been investigated with the Slab Core Test Facility (SCTF) Core-I. The initial stored energy at the peak power bundle was set to be the same for each test while the total initial stored energy of the core was different with each other.

Major conclusions are as follows:

(1) Even with different radial core power profile, almost the same transients were obtained for the core exit steam flow rate and total effluent rate under the same total core power.

(2) Under the same total core power, almost the same quench times of heater rods in the higher power bundles were obtained in spite of different power level in the higher power bundles in the radial power profile tests.

(3) Two-dimensional flow in the core was induced by the radial power distribution. The direction of cross flow was from the central high power region to the peripheral low power region above the quench front and the direction was reversed below the quench front.

(4) The heat transfer coefficient at the highest power bundle of the steep power profile test was higher than that of the flat power profile test under the same total core power condition.

Acknowledgments

The authors would like to express their gratitude to Mr. T. Iguchi, Dr. J. Sugimoto, Dr. H. Akimoto and Mr. T. Okubo of JAERI for discussions and suggestions. They are indebted deeply to Dr. K. Hirano for encouragements during this study.

profile does.

4. Conclusions

The effects of radial core power profile and total core power on the cooling characteristics of heater rods in the higher power bundles have been investigated with the Slab Core Test Facility (SCTF) Core-I. The initial stored energy at the peak power bundle was set to be the same for each test while the total initial stored energy of the core was different with each other.

Major conclusions are as follows:

(1) Even with different radial core power profile, almost the same transients were obtained for the core exit steam flow rate and total effluent rate under the same total core power.

(2) Under the same total core power, almost the same quench times of heater rods in the higher power bundles were obtained in spite of different power level in the higher power bundles in the radial power profile tests.

(3) Two-dimensional flow in the core was induced by the radial power distribution. The direction of cross flow was from the central high power region to the peripheral low power region above the quench front and the direction was reversed below the quench front.

(4) The heat transfer coefficient at the highest power bundle of the steep power profile test was higher than that of the flat power profile test under the same total core power condition.

Acknowledgments

The authors would like to express their gratitude to Mr. T. Iguchi, Dr. J. Sugimoto, Dr. H. Akimoto and Mr. T. Okubo of JAERI for discussions and suggestions. They are indebted deeply to Dr. K. Hirano for encouragements during this study.

profile does.

4. Conclusions

The effects of radial core power profile and total core power on the cooling characteristics of heater rods in the higher power bundles have been investigated with the Slab Core Test Facility (SCTF) Core-I. The initial stored energy at the peak power bundle was set to be the same for each test while the total initial stored energy of the core was different with each other.

Major conclusions are as follows:

(1) Even with different radial core power profile, almost the same transients were obtained for the core exit steam flow rate and total effluent rate under the same total core power.

(2) Under the same total core power, almost the same quench times of heater rods in the higher power bundles were obtained in spite of different power level in the higher power bundles in the radial power profile tests.

(3) Two-dimensional flow in the core was induced by the radial power distribution. The direction of cross flow was from the central high power region to the peripheral low power region above the quench front and the direction was reversed below the quench front.

(4) The heat transfer coefficient at the highest power bundle of the steep power profile test was higher than that of the flat power profile test under the same total core power condition.

Acknowledgments

The authors would like to express their gratitude to Mr. T. Iguchi, Dr. J. Sugimoto, Dr. H. Akimoto and Mr. T. Okubo of JAERI for discussions and suggestions. They are indebted deeply to Dr. K. Hirano for encouragements during this study.

References

(1) Hirano, K., Murao, Y.: J. At. Energy Soc. Japan, (in Japanese), 22[10], 681 (1980).

(2) Adachi, H., et al.: JAERI-M 82-075, (1982).

(3) Yadigaroglu, G.: Nucl. Safety, 19[1], 20 (1978).

(4) Osakabe, M., Sudo, Y.: J. Nucl. Sci. Technol., 20[7], 559 (1983).

Table 2.1 Test conditions

TEST NO.	S1-01	S1-06	S1-08	S1-11
Test type	Forced flooding	Forced flooding	Forced flooding	Forced flooding
System pressure	0.2 MPa	0.2 MPa	0.2 MPa	0.2 MPa
Core inlet velocity Acc for 10 sec LPCI after Acc	 5 cm/s 2.5 cm/s	 5 cm/s 2.5 cm/s	 5 cm/s 2.5 cm/s	 5 cm/s 2.5 cm/s
Max. core inlet subcooling	15.5 K	17.8 K	17.5 K	16.5 K
Max. cladding temp. at start of reflood	970 K	970 K	970 K	960 K
Power type	Base case	High power	Steep power	Flat power

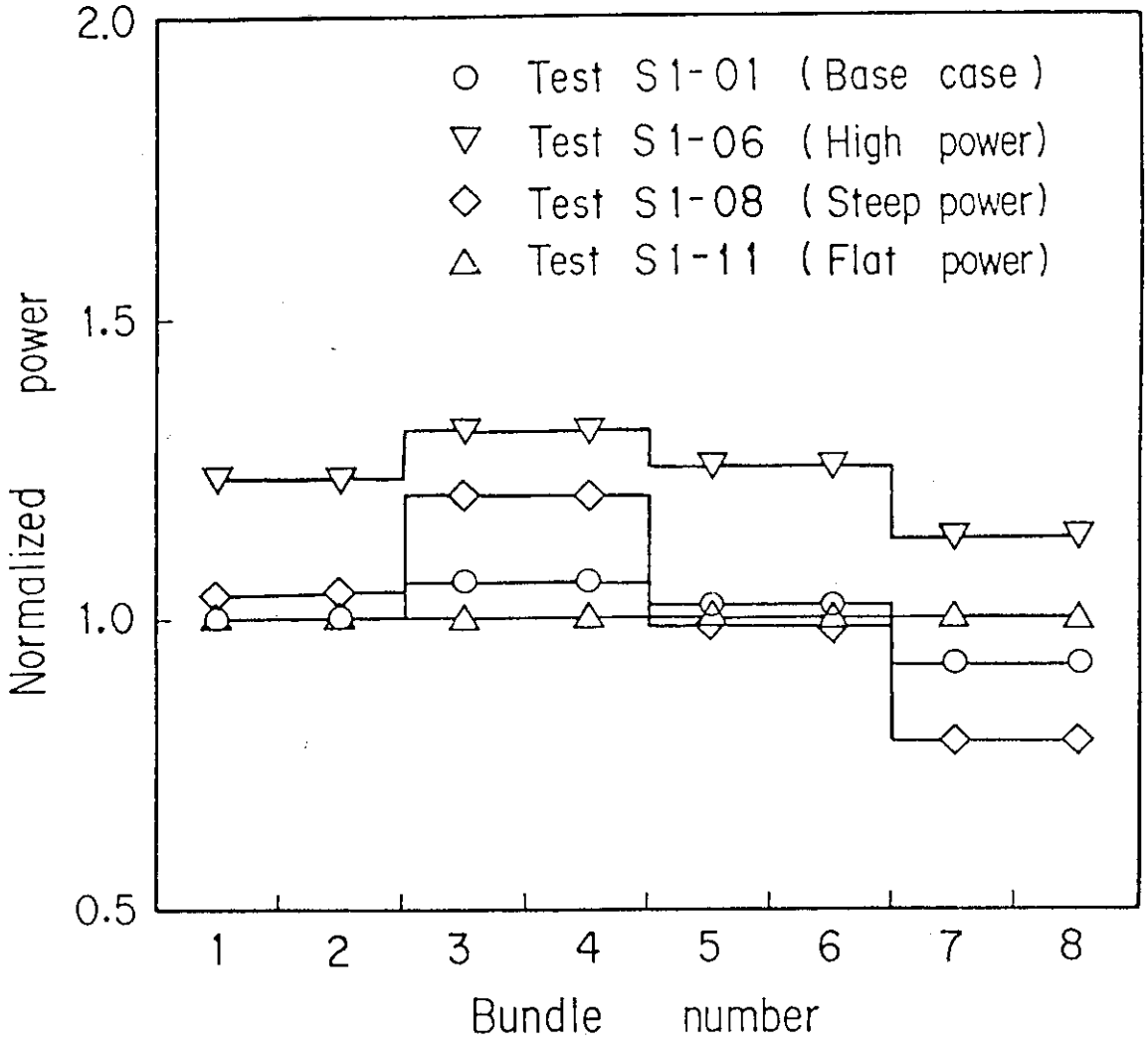

Fig. 2.1 Power profiles in core

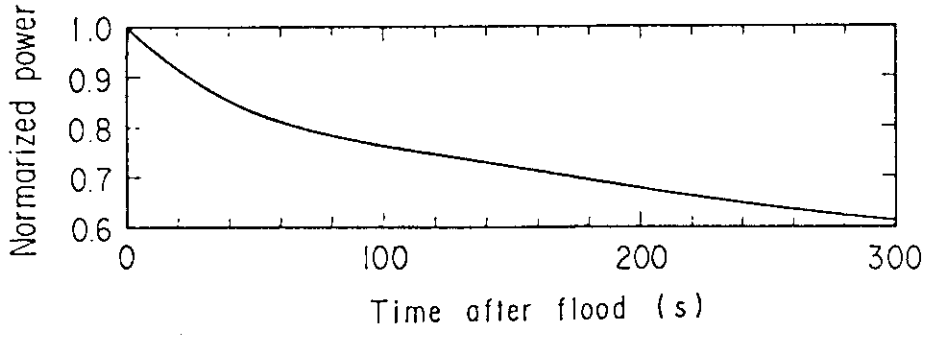

Fig. 2.2 Normarized decay curve

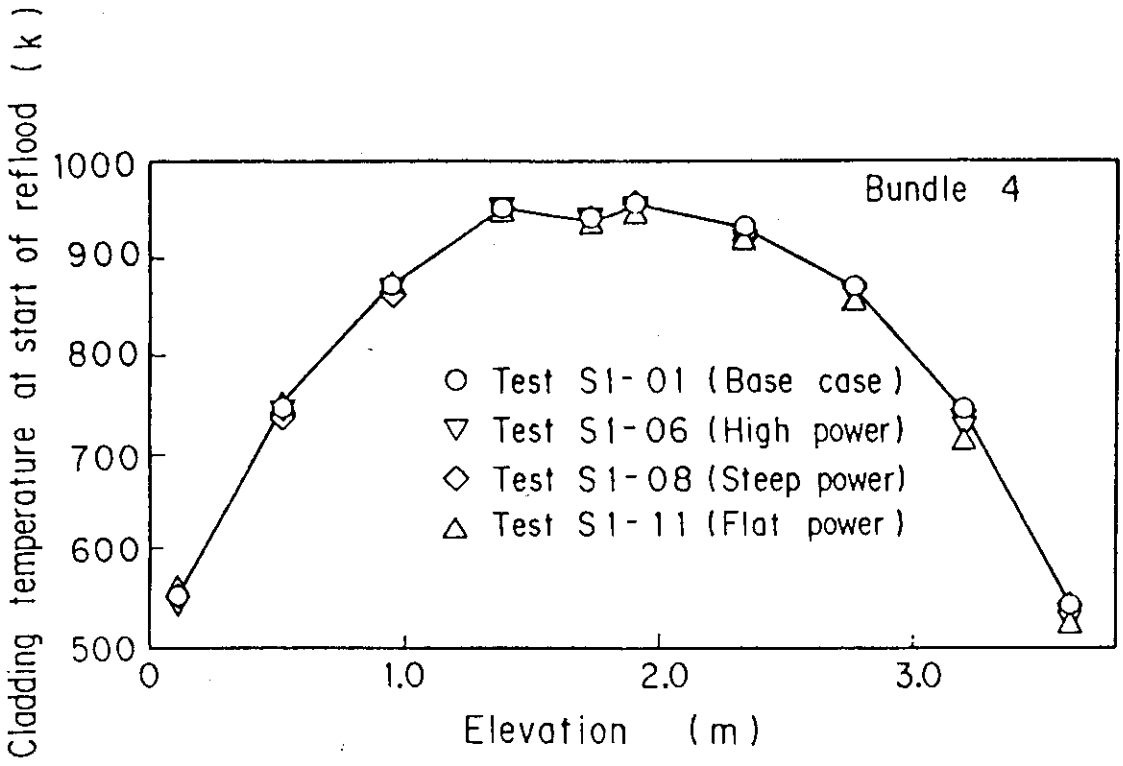

Fig. 3.1 Initial cladding temperature at start of reflood

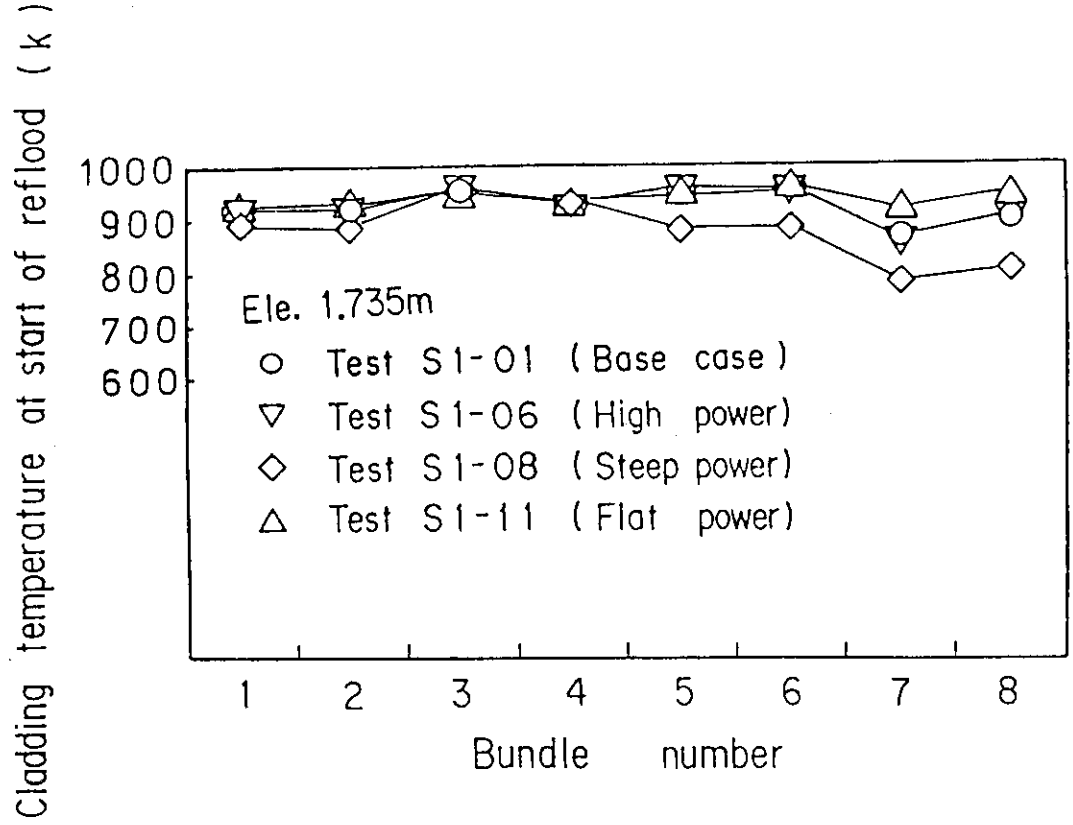

Fig. 3.2 Initial cladding temperature profile in core

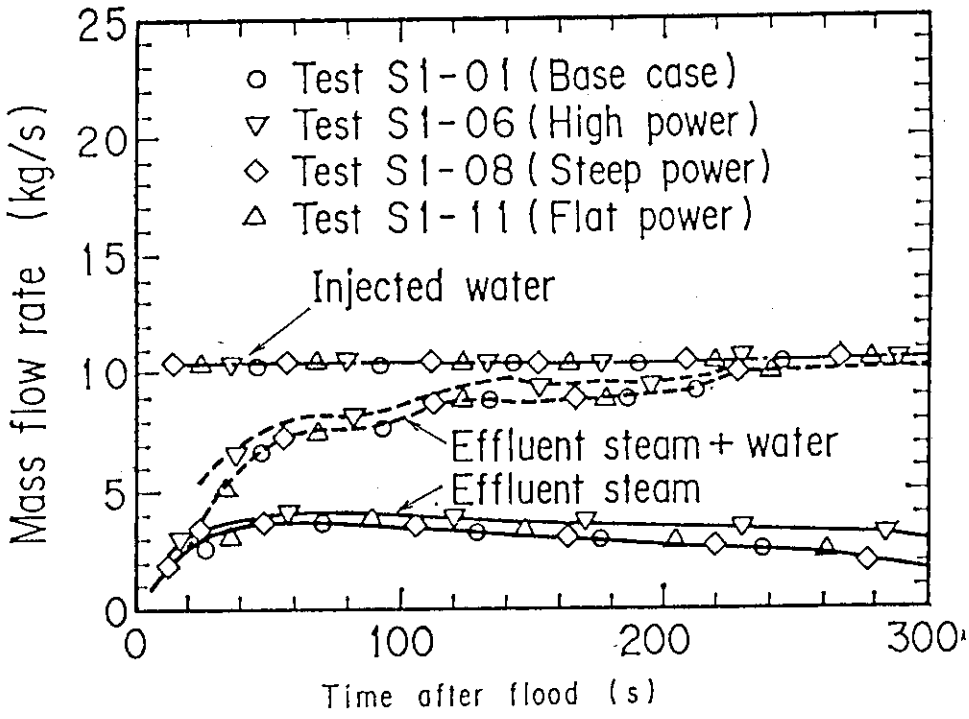

Fig.3.3 Mass flow rate at inlet and outlet of core

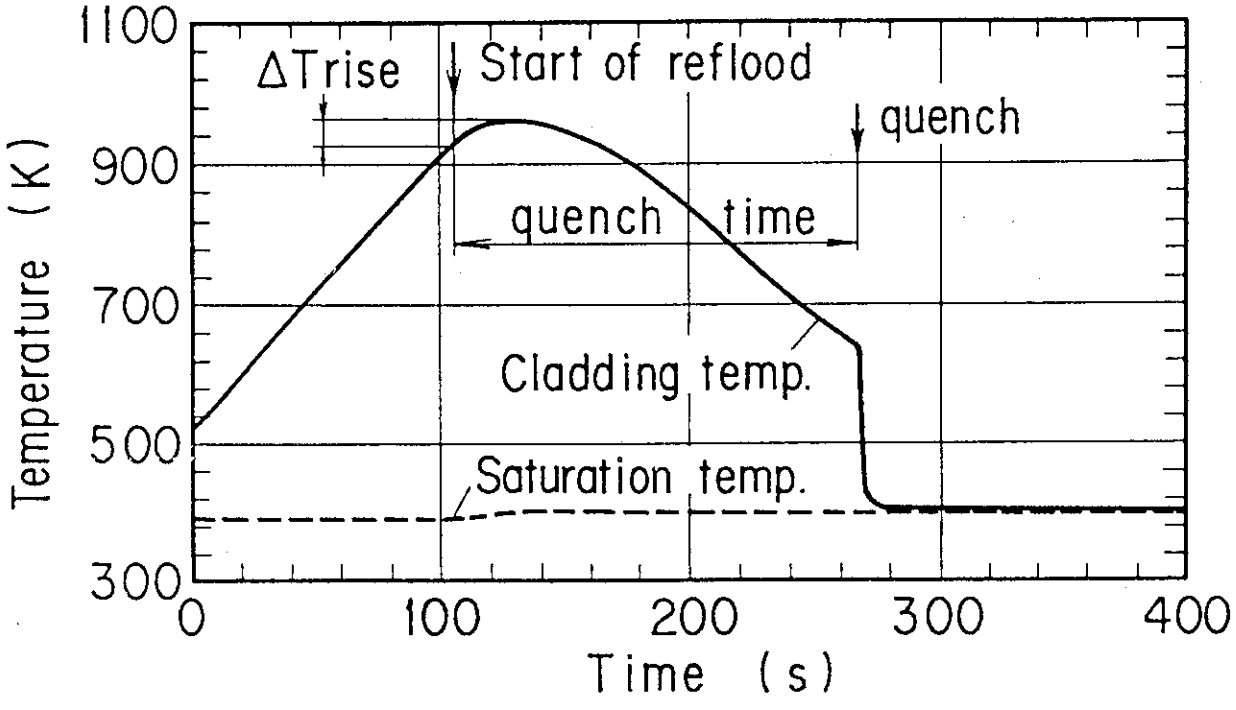

Fig. 3.4 Transient of cladding temperature

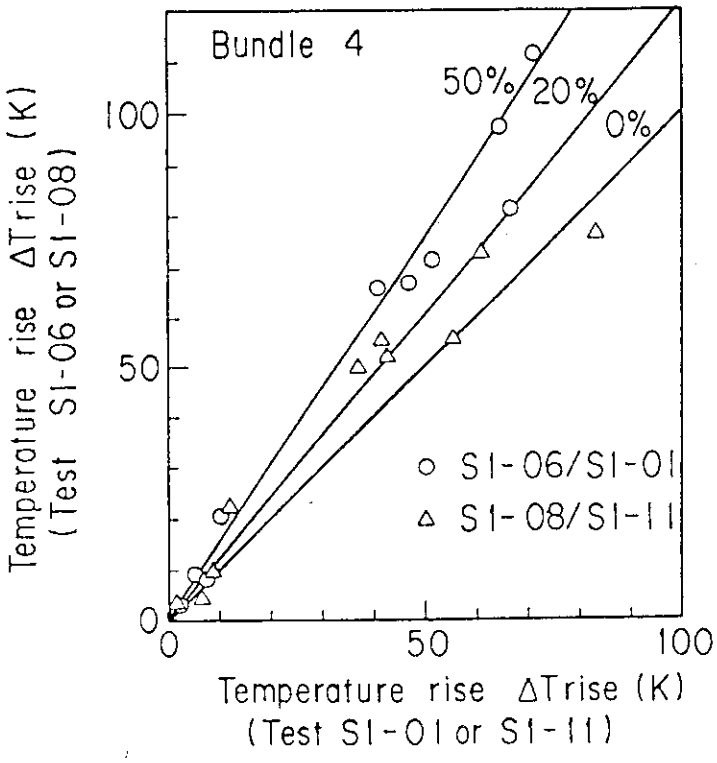

Fig. 3.5 Temperature rise to peak cladding temperature

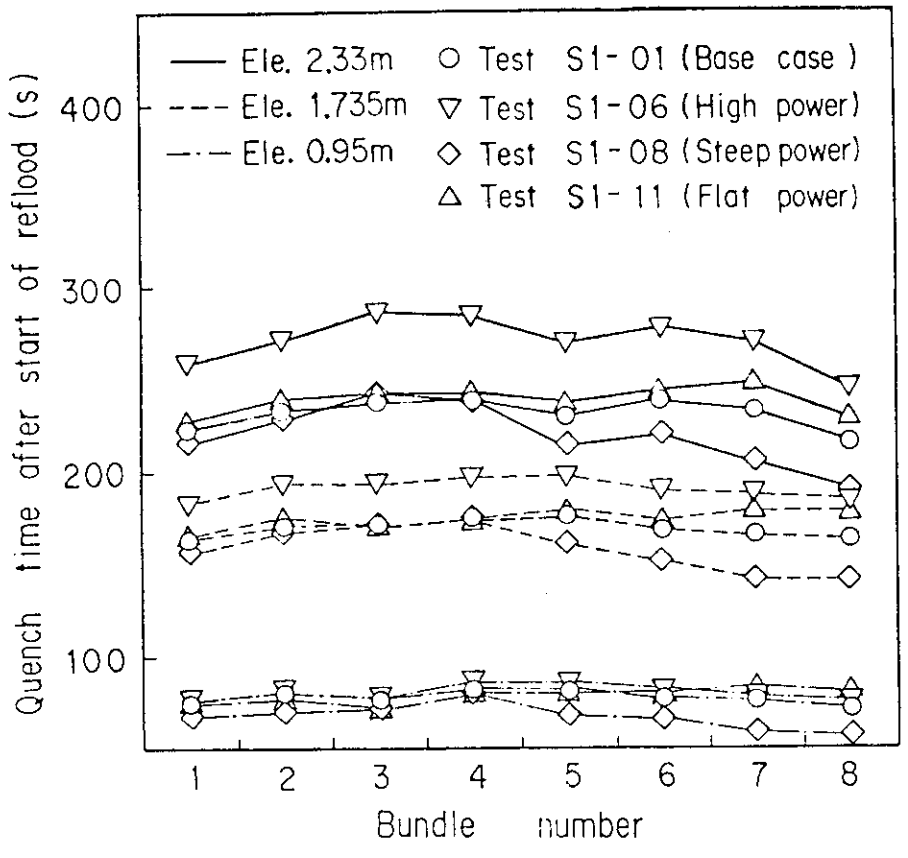

Fig. 3.6 Quench time distribution in core

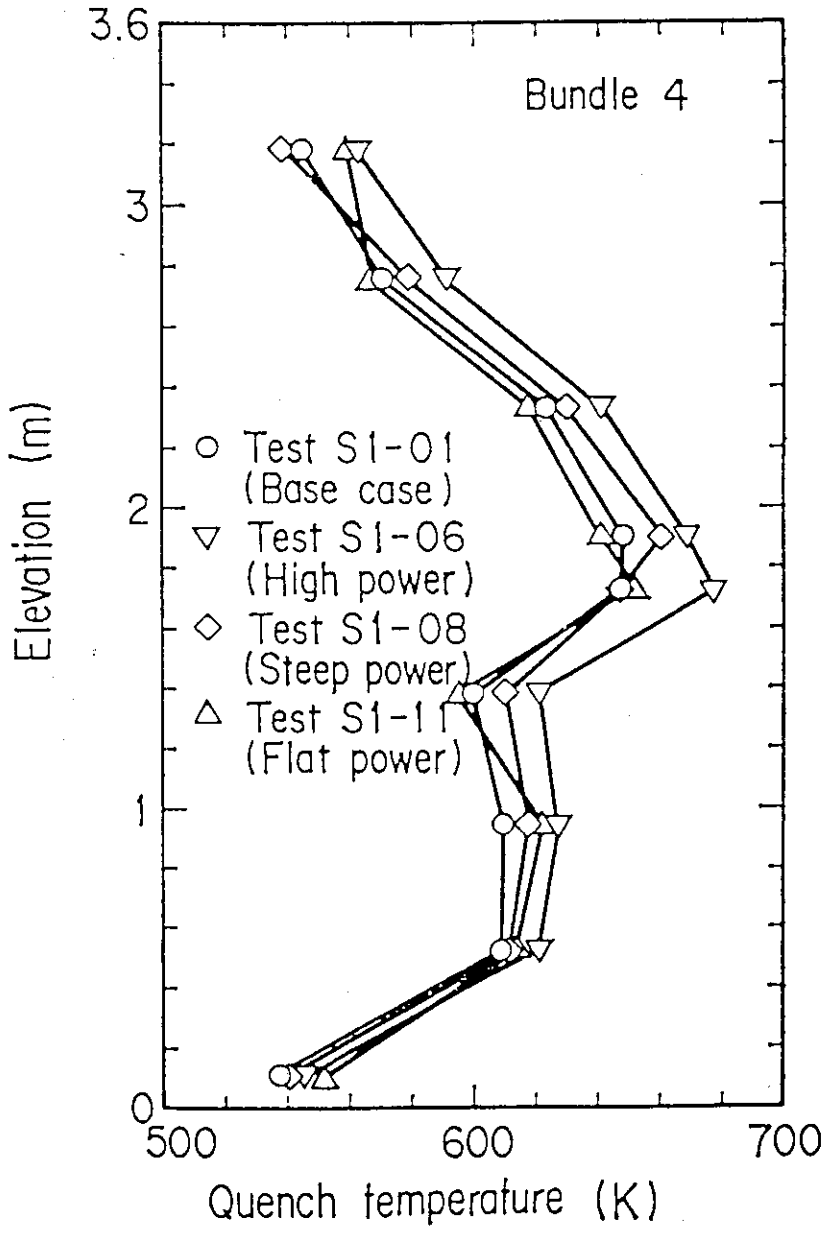

Fig. 3.7 Axial distribution of quench temperature

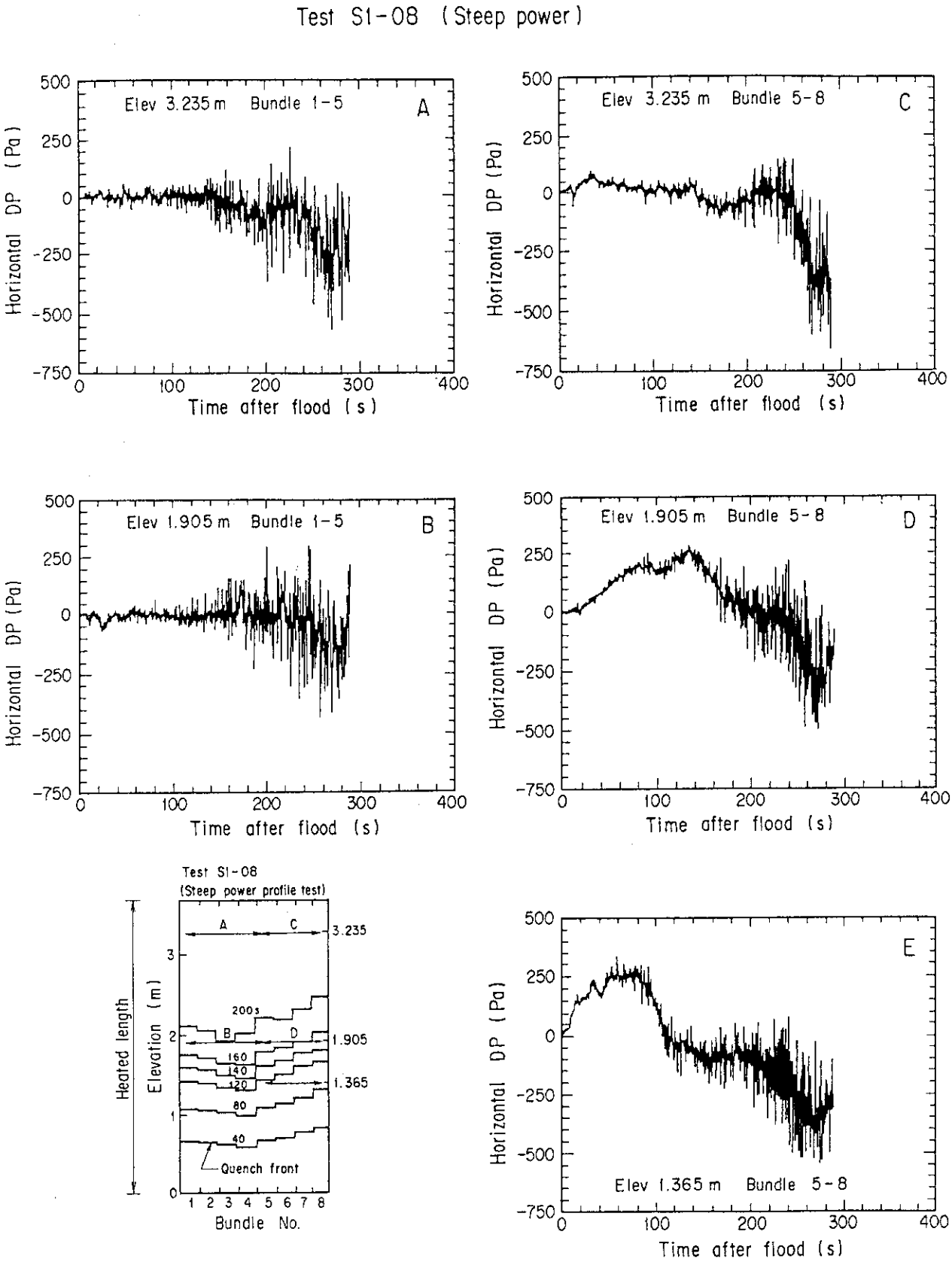

Fig. 3.8 Horizontal differential pressures in Test S1-08

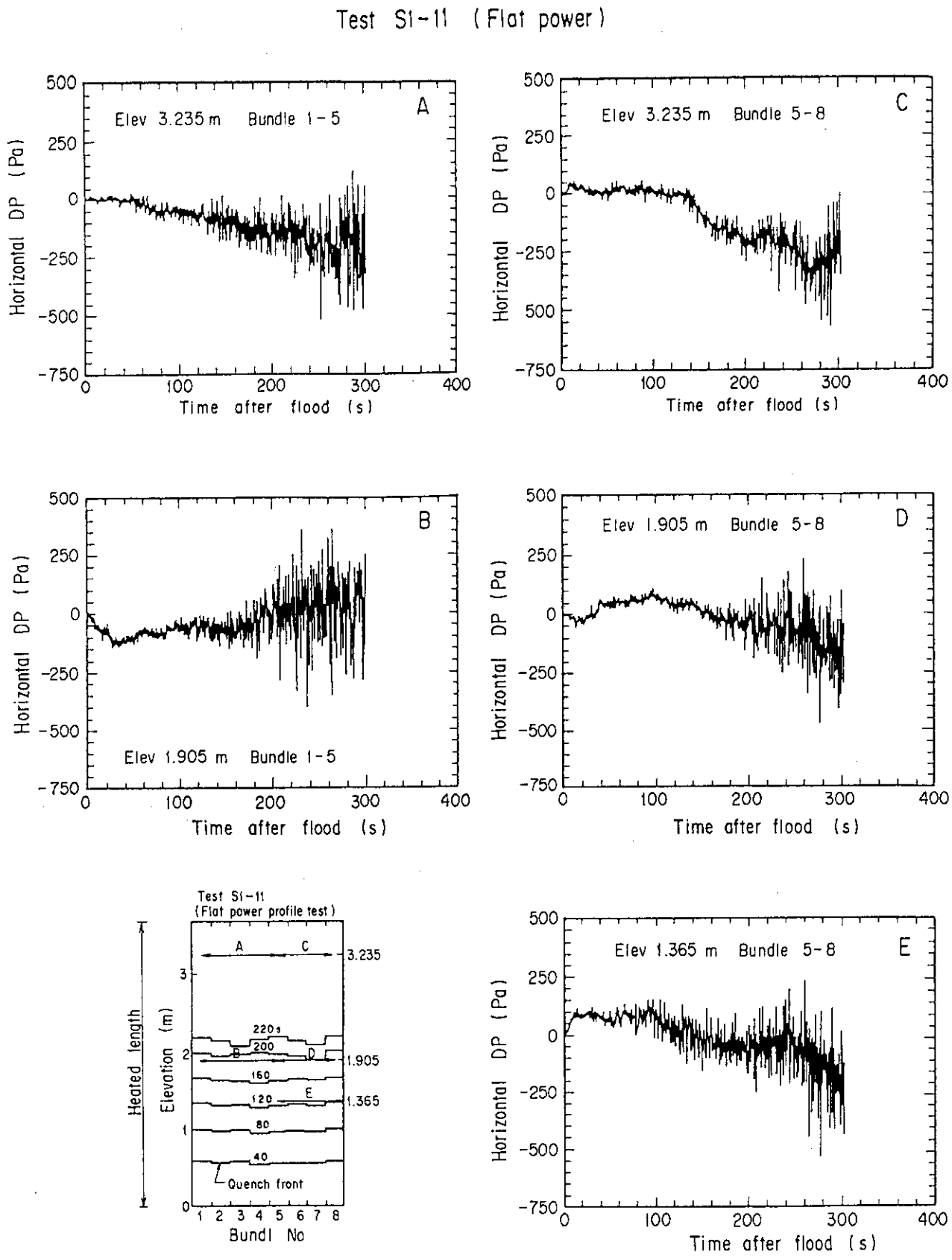

Fig. 3.9 Horizontal differential pressures in Test S1-11

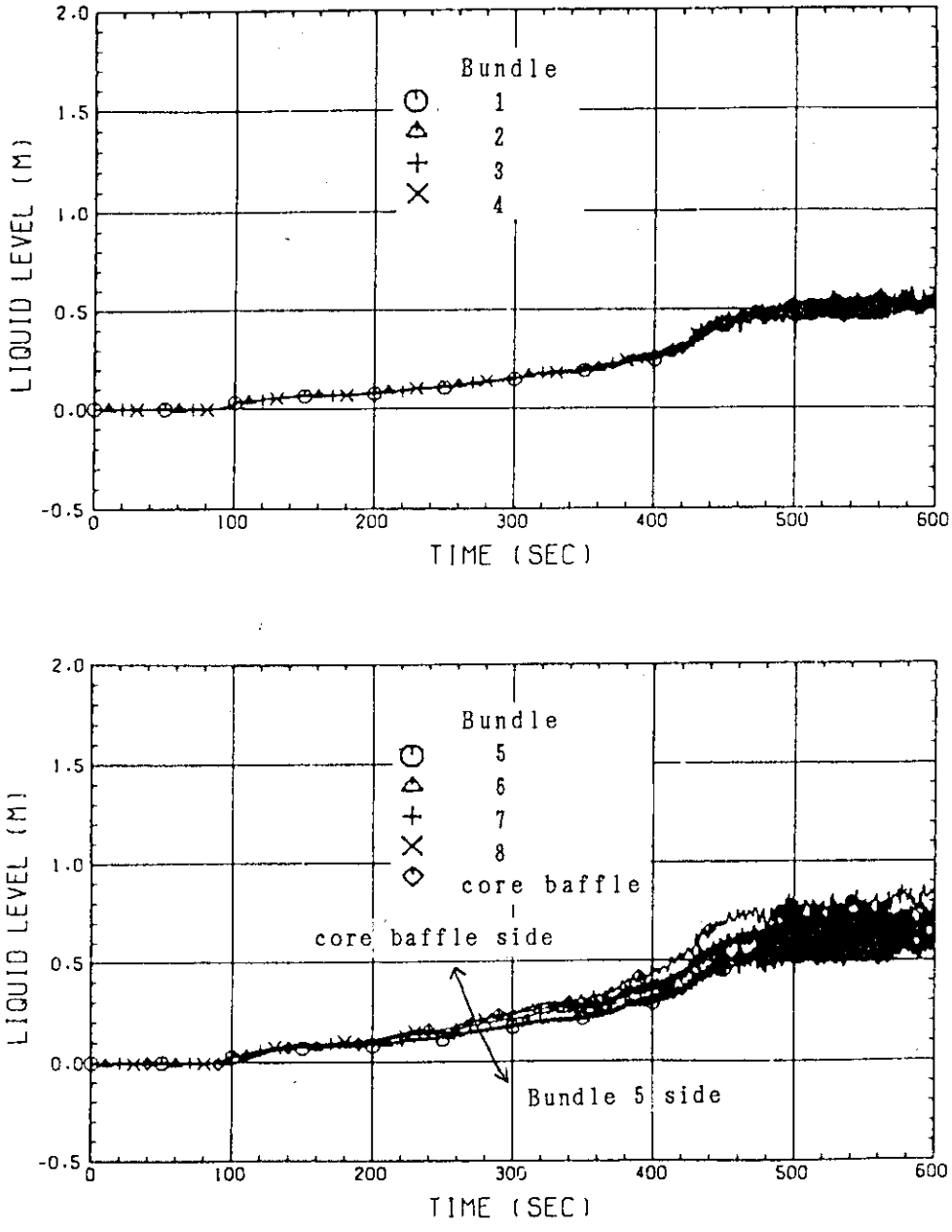

Fig. 3.10 Collapsed water level in upper plenum (Test S1-08)

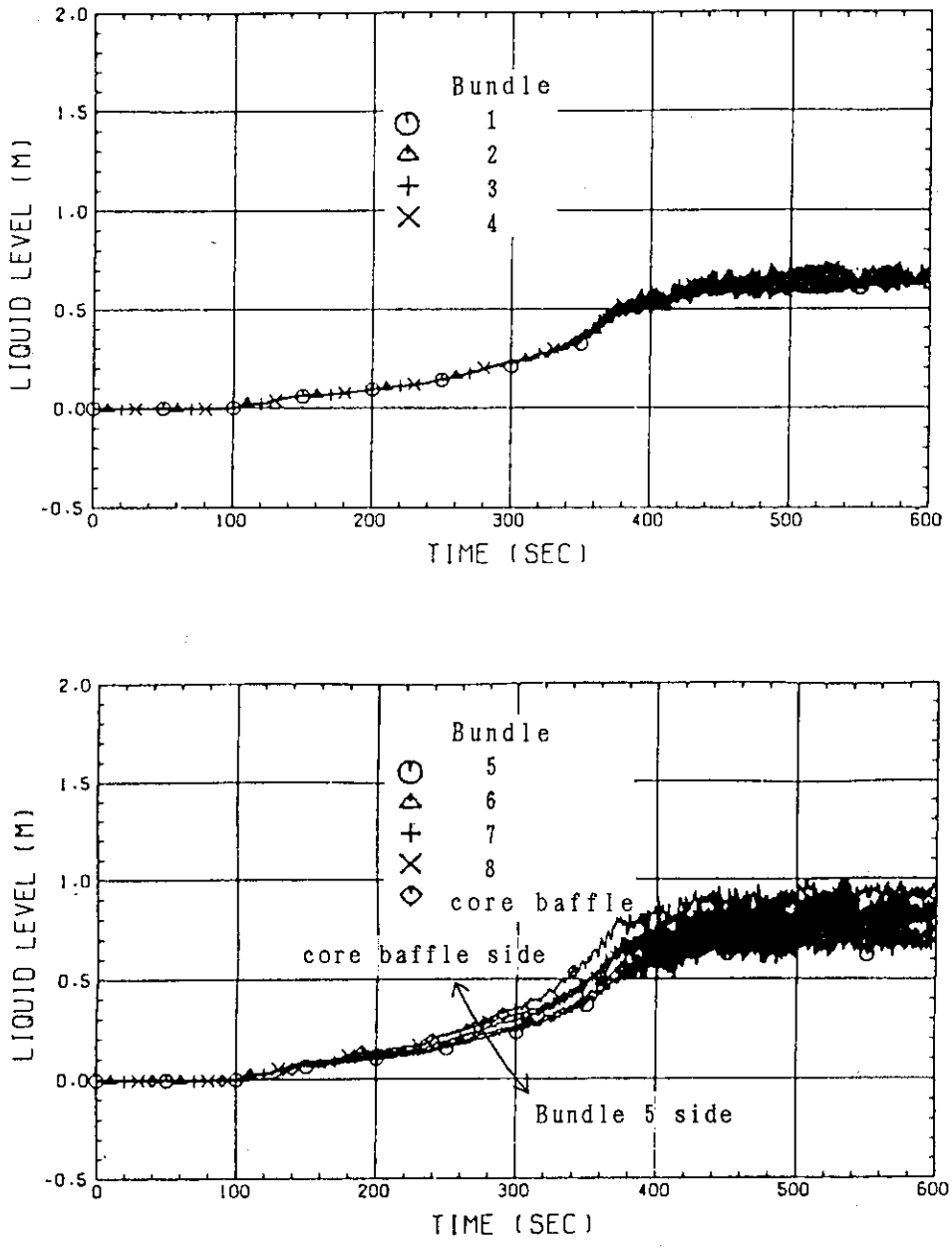

Fig. 3.11 Collapsed water level in upper plenum (Test S1-11)

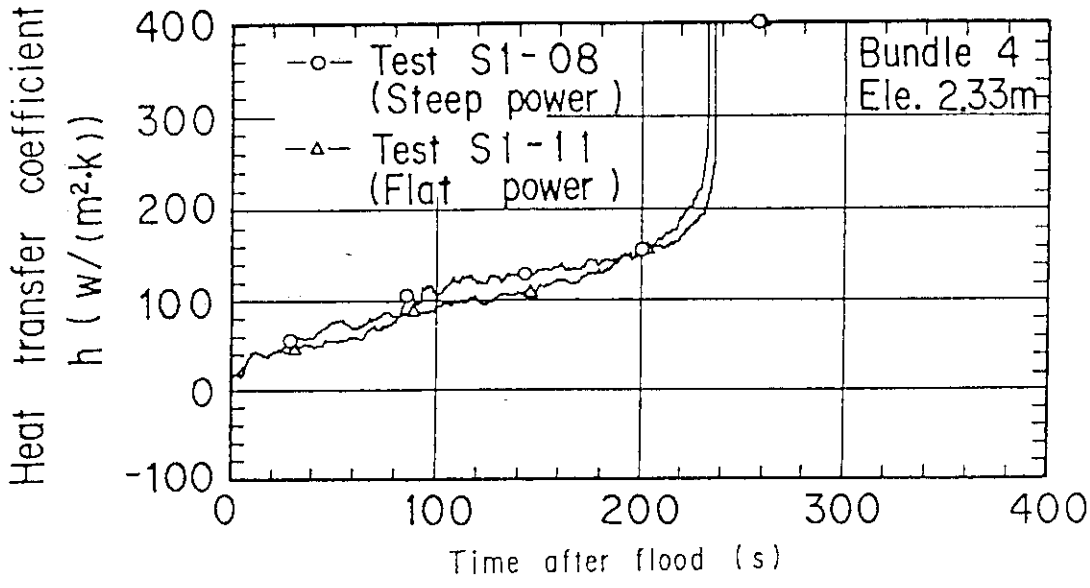

(a)

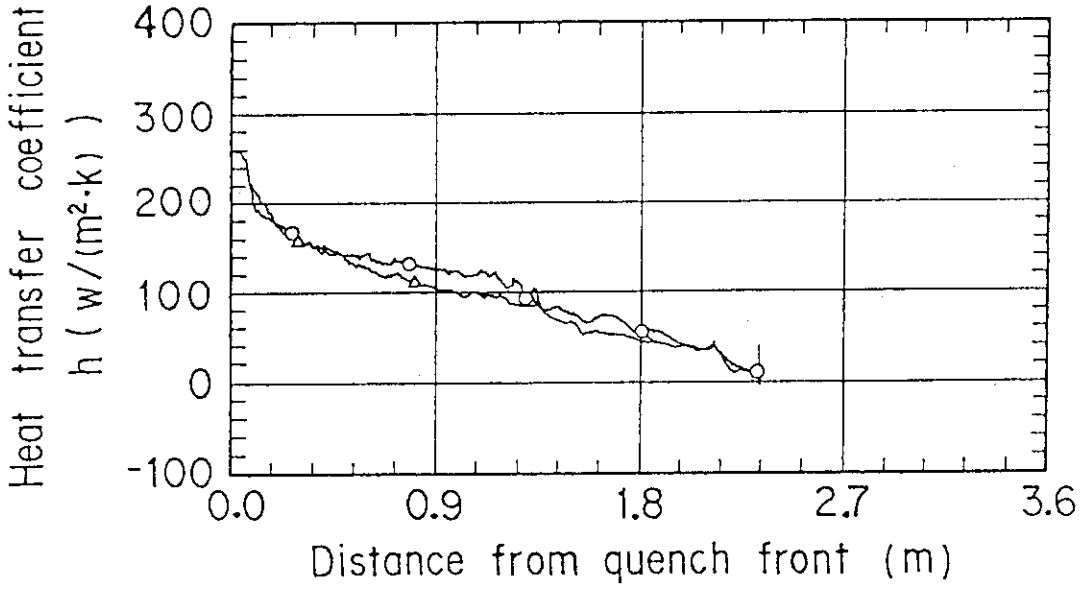

(b)

Fig. 3.12 Effects of bundle power profile at elevation 2.33 m
(a) Heat transfer coefficient vs. time
(b) Heat transfer coefficient vs. distance from quench front

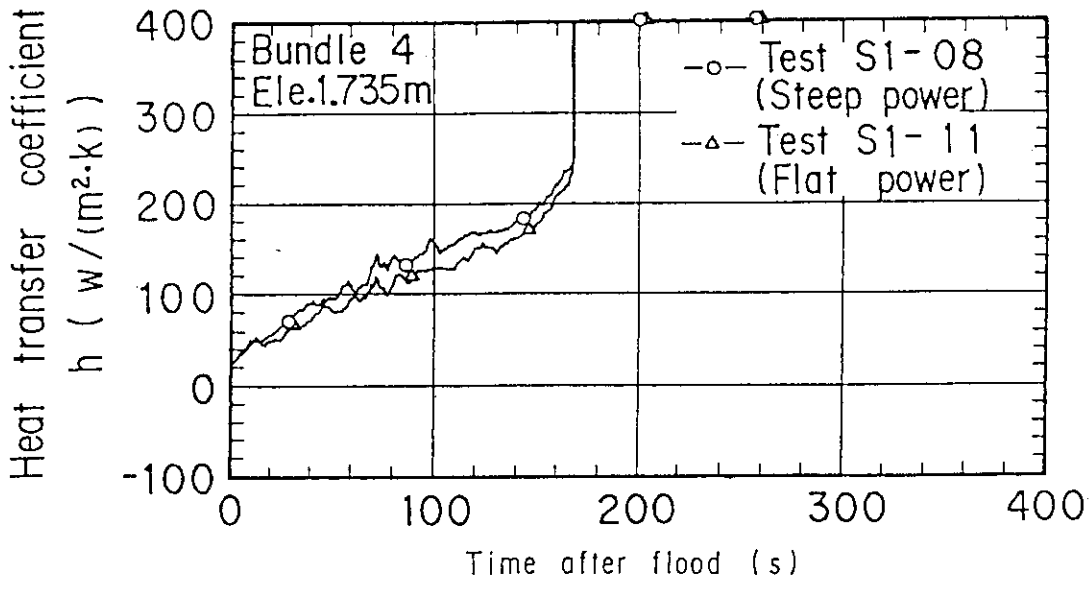

(a)

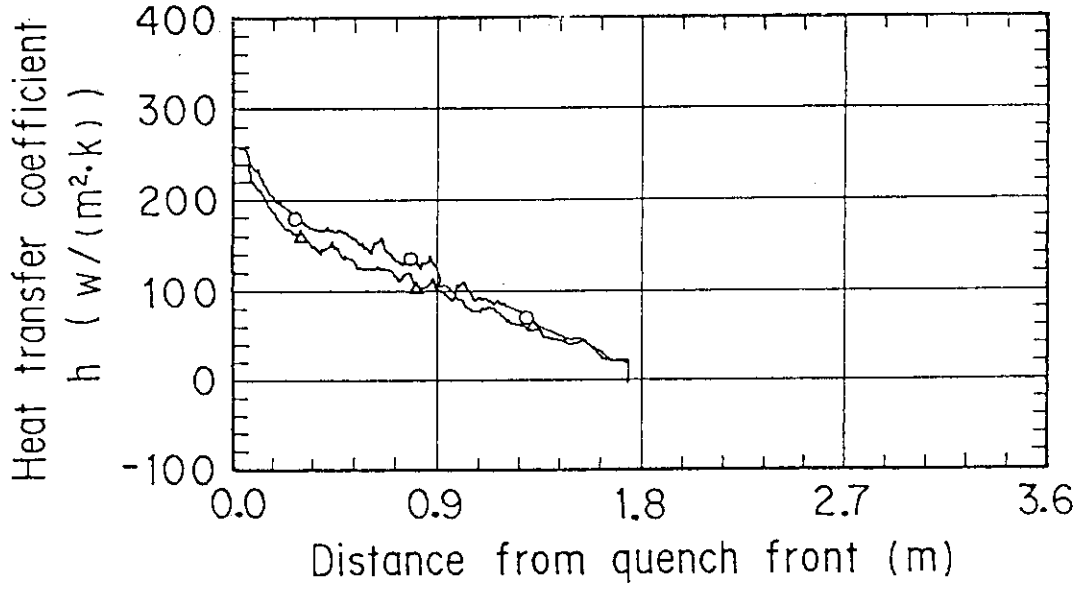

(b)

Fig. 3.13 Effects of bundle power profile at elevation 1.735 m
(a) Heat transfer coefficient vs. time
(b) Heat transfer coefficient vs. distance from quench front

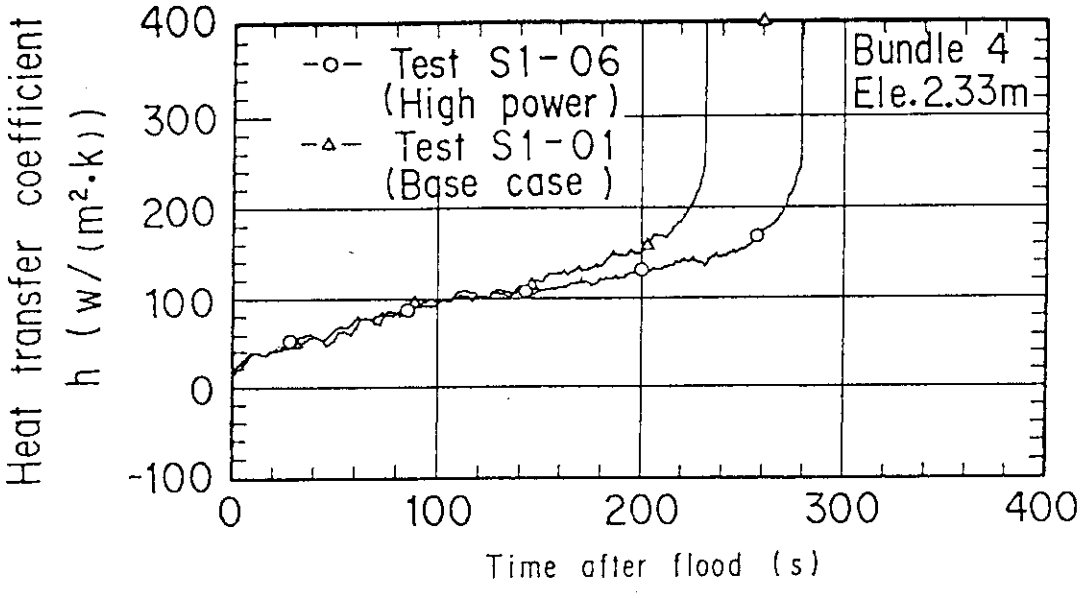

(a)

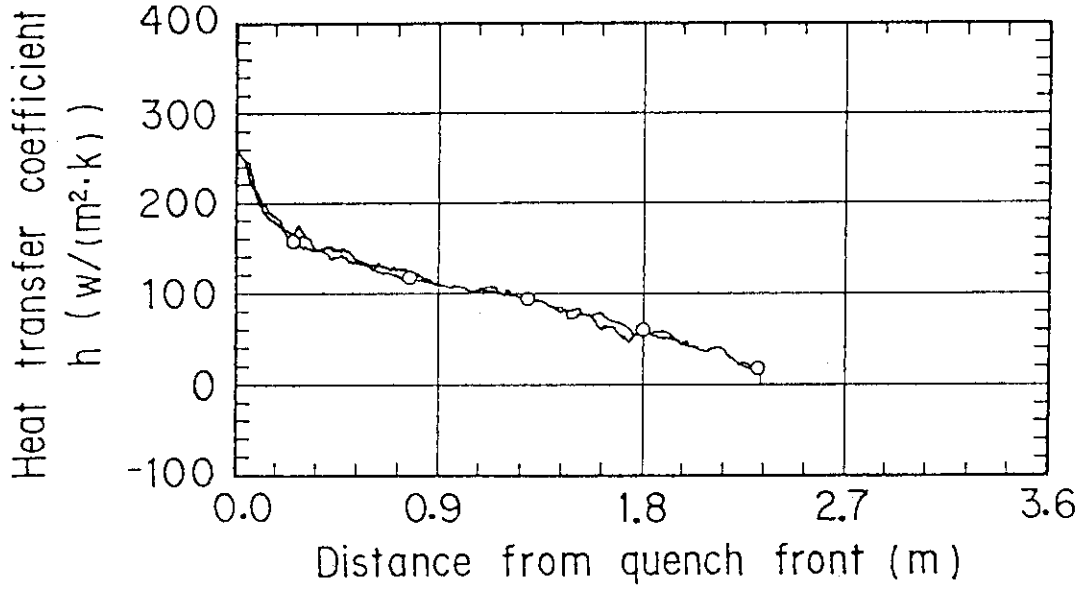

(b)

Fig. 3.14 Effects of bundle power at elevation 2.33 m
(a) Heat transfer coefficient vs. time
(b) Heat transfer coefficient vs. distance from quench front

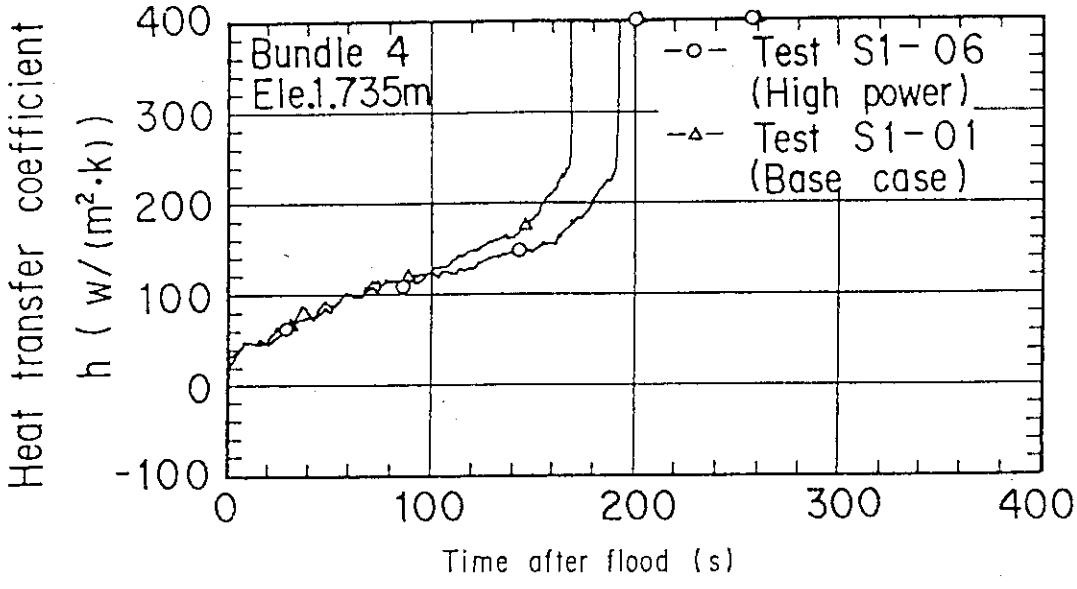

(a)

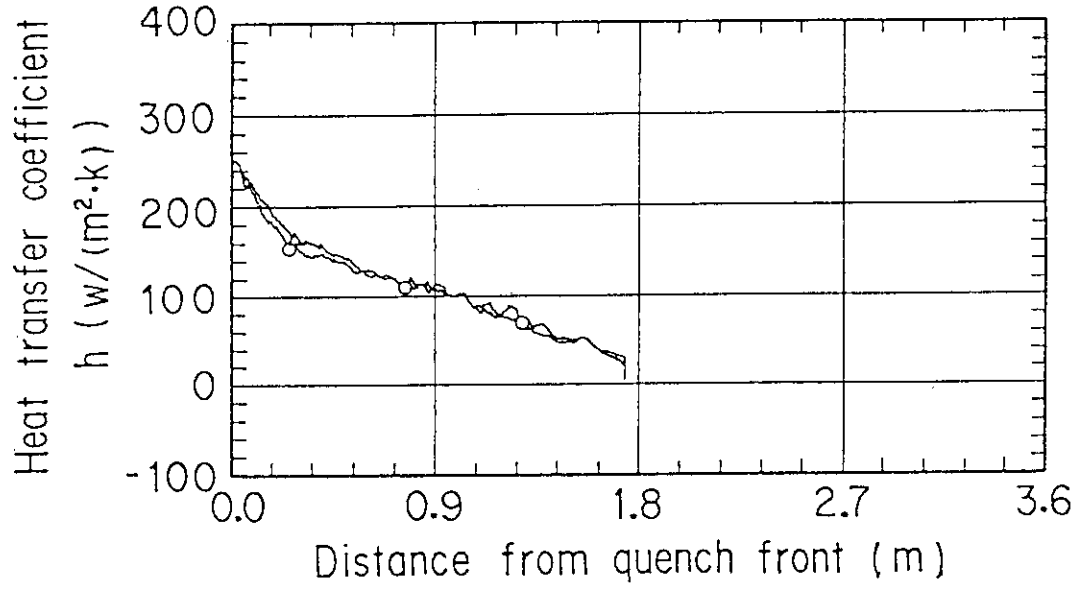

(b)

Fig. 3.15 Effects of bundle power at elevation 1.735 m
(a) Heat transfer coefficient vs. time
(b) Heat transfer coefficient vs. distance from quench front

Appendix A Slab Core Test Facility (SCTF) Core-I

A.1 Test Facility

The Slab Core Test Facility was designed under the following design phylosophy and design criteria:

a. Design Philosophy

(1) The facility should provide the capability to study the two-dimensional, thermohydraulic behavior and core flow within the reactor vessel especially due to the radial power distribution during the end of blowdown, refill and reflood phases of a simulated LOCA for a pressurized water reactor.

(2) To properly simulate the core heat transfer and hydrodynamics, a special emphasis is put on the proper simulation of the components in the pressure vessel. As the components in the pressure vessels are provided a simulated core, downcomer, core baffle region, lower plenum, upper plenum and upper head. On the other hand, simplified primary coolant loops are provided. As the primary coolant loops are provided a hot leg, an intact cold leg, broken cold legs and a steam water separator. The object of the steam/water separator is to measure the flow rate of carryover water coming out of the upper plenum.

b. Design Criteria

(1) The reference reactor for simulation to the SCTF is the Trojan reactor in the United States which is a four loop 3300 MWt PWR. The Ooi reactor in Japan is also referred which is of the similar type to the Trojan reactor.

(2) A full scale radial and axial section of a pressurized water reactor is provided as a simulated core of the SCTF with single bundle width.

(3) The simulated core consists of 8 bundles arranged in a row. Each bundle has electrically heated rods simulating fuel rods and non-heated rod with 16×16 array.

(4) The flow area and fluid volume of components are scaled down based on the core flow area scaling.

(5) To properly simulate the flow behavior of carryover water and entrainment, the elevations of hot leg and cold legs are designed to be the same as the PWRs as much as possible.

(6) The honeycomb structure is used as the side walls which accomodate the slab core, upper plenum and the upper part of lower plenum, so as to minimize the effect of walls on the disturbance of the core heat transfer and hydrodynamics.

(7) To investigate the effect of flow resistance in the primary loops are provided the orifices of which dimension is changeable.

(8) The maximum allowable temperature of the simulated fuel rods is 1900 ˚C and the maximum allowable pressure of the facility is 6 kg/cm^2 absolute.

(9) The facility is equipped with a hot leg equivalent to four actual hot legs connecting the upper plenum and the steam water separator, an intact cold leg equivalent to three actual intact cold legs connecting the steam water separator and the downcomer and two broken cold legs, one is for the steam water separator side and the other for the pressure vessel side.

(10) The ECCS consists of an Acc., a LPCI and a combined injection systems.

(11) ECC water injection ports are the cold leg, hot leg, upper plenum, downcomer, lower plenum and above the upper core support plate. These portions are to be chosen according to the object of the test.

(12) For better simulation of lower plenum flow resistance, simulated fuel rods do not penertrate through the bottom plate of the lower plenum but terminate below the bottom of the core.

(13) For measurements in the pressure vessel including core measurements, the feature of the slab geometry of the pressure vessel is utilized as much as possible. Design and arrangement of the instruments are done so as to be able to carry out installation, calibration and removal of the instruments.

(14) View windows are provided where flow pattern recognition is important. The locations are, the interface between the core and the upper plenum, the hot leg, the pressure vessel side broken cold leg and the downcomer.

(15) The blocked bundle test is carried out in Core-I in order to investigate the effect of the ballooned fuel rods and the unblocked normal bundle test for the Core-II and -III.

(16) Simulated types of break are cold leg break and hot leg break.

(17) The components and systems such as the containment tanks and ECC water supply system in the CCTF are shared with the SCTF to the maximum extent.

The overall schematic diagram of the SCTF is shown in Fig. A-1. The principal dimensions of the facility is shown in Table A-1, and the comparison of dimensions between the SCTF and the referred PWR is shown in Fig. A-2.

A.1.1 Pressure Vessel and Internals

The pressure vessel is of slab geometry as shown in Fig. A-3. The height of the components in the pressure vessel is almost the same as the reference reactor's, and the flow area and the fluid volume of each component are scaled down based on the nominal core flow area scaling.

The core consists of 8 bundles in a row and each bundle includes simulated fuel rods and non-heated rods with 16×16 array. The core arrangement for the SCTF Core-I is shown in Fig. A-4, which includes 6 normal bundles and 2 blocked bundles. The core is enveloped by the honeycomb thermal insulator which is attached on the barrel.

The downcomer is located at one end of the pressure vessel which corresponds to the periphery of the actual reactor. The core baffle region is, on the other hand, located between the core and the downcomer. For better understanding, the cross section of the pressure vessel at the elevation of midplane of the core is shown in Fig. A-5.

The design of upper plenum internals is based on that of the new Westinghouse 17×17 array fuel assemblies. The internals consist of control rod guide tubes, support columns, orifice plates and open holes and those arrangements is shown in Fig. A-6. The radius of each internal is scaled down by factor 8/15 from that of an actual reactor. Flow resistance baffles are inserted into the guide tubes. The elevation and the configuration of baffles plates are shown in Fig. A-7 and A-8.

The height of the hot leg and cold legs are designed as close to the actual PWR as possible. However, in order to avoid the interference of the nozzles in the downcomer, the height of nozzles for the broken cold leg and the intact cold leg are shifted down compared to that of the hot leg as shown in Fig. A-3.

A.1.2 Heater Rod Assembly

The heater rod assembly for the SCTF Core-I consists of 8 bundles arranged in a row. These bundles are composed of 6 normal unblocked bundles which are located at the 1st, 2nd and 5th to 8th bundles and 2 blocked bundles which are 3rd and 4th bundles as shown in Fig. A-4. Each bundle has 234 electrically heated rods and 22 non-heated rods. The dimensions of the heater rods are based on a 15×15 fuel rod bundle, and the heated length and the outer diameter of each heater rod are 3.66 m and 10.7 mm, respectively. A heater rod consists of a nichrome heater element, magnesium oxide (MgO) and Nichrofer-7216 sheath (equialent to Inconel 600). The sheath wall thickness is about 1.0 mm and is thicker than the actual fuel cladding because of the requirements for thermocouple installation. The heating element is a helical coil and has a 17 step chopped cosine axial power profile as shown in Fig. A-9. The peaking factor is 1.4.

Non-heated rods are either stainless steel pipes or solid rods of 13.8 mm O.D. The heater rods and non-heated rods are fixed at the top of the core allowing the rods to move downward when the thermal expansion occurs. In Fig. A-10 the axial position where blockage sleeves for simulating the balooned fuel rod are equipped is shown. The blockage sleeves consist of three types of sleeve, one is used for the rods at the corner adjacent to the next blocked bundle, another for the rods adjacent to the side walls and the third for the rods except for the periphery of the blocked bundle. These are named A, B and C respectively in the Fig. A-11 and these configurations for these are shown in Fig. A-12.

For better simulation for flow resistance in the lower plenum the simulated rods do not penetrate through the bottom plate of the lower plenum as shown in Fig. A-10.

A.1.3 Primary Loops and ECCS

Primary loops consist of a hot leg equivalent to the four actual hot legs, a steam/water separator for measuring the flow rate of carry over water, an intact cold leg equivalent to the three actual intact loops, a broken cold leg on the pressure vessel side and a broken cold leg on the steam water separator side. These two broken cold legs are connected to two containment tanks through break valves, respectively. The arrangement of the primary loops is shown in Fig. A-13. The flow area of each loop is scaled down based on the core flow area scaling. It should be

emphasized that the cross section of the hot leg is an elongated circle to realize the proper flow pattern in the hot leg. The steam/water separator has a steam generator inlet plenum simulator to realize the flow characteristics of carryover water. The cross section of the hot leg and the configuration of the steam generator inlet plenum simulator are shown in Fig. A-14.

A pump simulator and a loop seal part are provided for the intact cold leg. The arrangement of the intact cold leg is shown in Fig. A-15. The pump simulator consists of the casing and duct simulators and an orifice plate as shown in Fig. A-16. The loop resistance is adjusted with the orifice plate.

In principle, ECCS consists of an accumulator and a low pressure injection system. The injection port is located as already described in the design criteria. Besides, the UCSP extraction system is provided and the UCSP water injection and extraction systems will be used for combined injection tests.

A.1.4 Containment Tanks and Auxiliary System

Two containment tanks are provided to the SCTF. The containment tank-I is connected with the downcomer through the pressure vessel side broken cold leg and the containment tank-II is connected with the steam/water separator through the steam/water separator side broken cold leg. Especially in the containment tank-I, carryover water from the downcomer is measured by phase separation. These containment tanks and auxiliary system such as a pressurizer for injecting water from the Acc. tank, etc. are shared with the CCTF.

A.2 Instrumentation

The instrumentation in the SCTF has been provided both by JAERI and USNRC. The JAERI-provided instrumentation includes the measurement of temperatures, pressures, differential pressures, liquid levels, flow velocities, and heating powers. USNRC has provided film probes, impedance probes, string probes, liquid level detectors (LLDs), fluid distribution grids (FDGs), turbine meters, drag disks, γ-densitometers, spool pieces and video optical probes. The measurement items of the JAERI- and USNRC-provided instruments are listed in Table A-2 and A-3,

respectively. Location of each instrument is shown in Fig. A-17 through A-30.

Table A-1 Principal dimensions of test facility (1/2)

1. Core Dimension	
(1) Quantity of Bundle	8 Bundles
(2) Bundle Array	1 × 8
(3) Bundle Pitch	230 mm
(4) Rod Array in a Bundle	16 × 16
(5) Rod Pitch in a Bundle	14.3 mm
(6) Quantity of Heater Rod in a Bundle	234 rods
(7) Quantity of Non-Heated Rod in a Bundle	22 rods
(8) Total Quantity of Heater Rods	234 × 8 = 1872 rods
(9) Total Quantity of Non-Heated Rods	22 × 8 = 176 rods
(10) Effective Heated Length of Heater Rod	3660 mm
(11) Diameter of Heater Rod	10.7 mm
(12) Diameter of Non-Heateed Rod	13.8 mm
2. Flow Area & Fluid Volume	
(1) Core Flow Area* (nominal)	0.227 m^2
(2) Core Fluid Volume	0.92 m^3
(3) Baffle Region Flow Area	0.10 m^2
(4) Baffle Region Fluid Volume	0.36 m^3
(5) Downcomer Flow Area	0.121 m^2
(6) Upper Annulus Flow Area	0.158 m^2
(7) Upper Plenum Horizontal Flow Area	0.525 m^2
(8) Upper Plenum Fluid Volume	1.16 m^2
(9) Upper Head Fluid Volume	0.86 m^3
(10) Lower Plenum Fluid Volume	1.38 m^3
(11) Steam Generator Inlet Plenum Simulator Flow Area	0.626 m^2
(12) Steam Generator Inlet Plenum Simulator Fluid Volume	0.931 m^3
(13) Steam Water Separator Fluid Volume	5.3 m^3
(14) Flow Area at the Top Plate of Steam Generator Inlet Plenum Simulator	0.195 m^2
(15) Hot Leg Flow Area	0.0826 m^2
(16) Intact Cold Leg Flow Area (Diameter = 297.9 mm)	0.0697 m^2
(17) Broken Cold Leg Flow Area (Diameter = 151.0 mm)	0.0179 m^2

* Flow area in the core is 0.35 m^2, including the excess flow area of gaps between the bundle and the surface of thermal insulator and between the core barrel and the pressure vessel wall.

Table A-1 Principal dimensions of test facility (2/2)

(18) Containment Tank I Fluid Volume	30 m^3
(19) Containment Tank II Fluid Volume	50 m^3

3. Elevation & Height

(1) Top Surface of Upper Core Support Plate (UCSP)	0 mm
(2) Bottom Surface of UCSP	-76 mm
(3) Top of the Effective Heated Length of Heater Rod	-393 mm
(4) Bottom of the Skirt in the Lower Plenum	-5270 mm
(5) Bottom of Intact Cold Leg	+724 mm
(6) Bottom of Hot Leg	+1050 mm
(7) Top of Upper Plenum	+2200 mm
(8) Bottom of Steam Generator Inlet Plenum Simulator	+1933 mm
(9) Centerline of Loop Seal Bottom	-2281 mm
(10) Bottom Surface of End Box	- 185.1 mm
(11) Top of the Upper Annulus	+2234 mm
(12) Height of Steam Generator Inlet Plenum Simulator	1595 mm
(13) Height of Loop Seal	3140 mm
(14) Inner Height of Hot Leg Pipe	737 mm
(15) Bottom of Lower Plenum	-5770 mm
(16) Top of Upper Head	+2887 mm

Table A-2 Measurement items of SCTF (JAERI-provided instruments) (1/5)

LOCATION	ITEM	PROBE	QUANTITY
1. CORE			
center	pressure	DP cell	1
short range of core	diff. press.	DP cell	22
half length of core	diff. press.	DP cell	16
full length of core	diff. press.	DP cell	8
across spacers	diff. press.	DP cell	7
across end box	diff. press.	DP cell	8
across 4 assemblies	diff. press.	DP cell	3
across 8 assemblies	diff. press.	DP cell	3
below and above end box	steam velocity	Pitot-tube	3
sub channel	steam velocity	Pitot-tube	13
below end box hole	fluid temp.	T/C	16
above end box hole	fluid temp.	T/C	16
core baffle	fluid temp.	T/C	6
non-heating rods	fluid temp.	T/C	96
	steam temp.	SSP	16
	clad temp.	T/C	108
heater rods	clad temp.	T/C	640
side walls	wall temp.	T/C	36
core baffle	wall temp.	T/C	6
core baffle	liquid level	DP cell	1
short range of core baffle	liquid level	DP cell	6
heated rod	power		8
			sum(1039)
2. UPPER PLENUM			
centre	pressure	DP cell	1
across end box tie plate	diff. press.	DP cell	8
core outlet-hot leg inlet	diff. press.	DP cell	4
periphery of UCSP hole	fluid temp.	T/C	8
centre of UCSP hole	fluid temp.	T/C	8
250mm & 1000mm above UCSP	fluid temp.	T/C	8
surface of UCSP	fluid temp.	T/C	8
above UCSP hole	steam temp.	SSP	8

Table A-2 Measurement items of SCTF (JAERI-provided instruments) (2/5)

LOCATION	ITEM	PROBE	QUANTITY
surface of structure	wall temp.	T/C	15
side walls	wall temp.	T/C	8
above end box tie plate	liquid level	DP cell	8
above UCSP	liquid level	DP cell	9
above UCSP (v.)	steam velocity	Pitot-tube	2
inter-structures (h.)	steam velocity	Pitot-tube	2
			sum(97)
3. LOWER PLENUM			
below bottom spacer	pressure	DP cell	1
lower plenum - upper plenum	diff. press.	DP cell	1
core inlet	fluid temp.	T/C	8
inlet from downcomer	fluid temp.	T/C	2
side & bottom walls	wall temp.	T/C	4
below bottom spacer	liquid level	DP cell	1
			sum(17)
4. DOWNCOMER			
upper position	pressure	DP cell	1
horizontal direction	diff. press.	DP cell	1
four levels	fluid temp.	T/C	8
side wall	wall temp.	T/C	2
inner wall	wall temp.	T/C	2
below cold leg level	liquid level	DP cell	1
above cold leg level	liquid level	DP cell	1
below core inlet level	liquid level	DP cell	1
bottom	momentum flux	Drag disk	2
			sum(19)
5. HOT LEG			
full length	diff. press.	DP cell	1
multiple points	fluid temp.	T/C	3
	steam temp.	SSP	3
	wall temp.	T/C	1
	liquid level	DP cell	2
			sum(10)

Table A-2 Measurement items of SCTF (JAERI-provided instruments) (3/5)

LOCATION	ITEM	PROBE	QUANTITY
6. S/W SEPARATOR SIDE BROKEN COLD LEG			
across resistance simulator	diff. press.	DP cell	1
S/W separator to containment tank II	flow rate	venturi	1
multiple points	fluid temp.	T/C	1
	steam temp.	SSP	1
	wall temp.	T/C	1
			sum(5)
7. INTACT COLD LEG			
full length	diff. press.	DP cell	1
across resistance simulator	diff. press.	DP cell	1
across pump simulator	diff. press.	DP cell	1
	flow rate	venturi	1
near resistance simulator	fluid temp.	T/C	1
pump simulator	fluid temp.	T/C	3
	wall temp.	T/C	1
			sum(9)
8. PV SIDE BROKEN COLD-LEG			
	pressure	DP cell	1
full length	diff. press.	DP cell	1
across resistance simulator	diff. press.	DP cell	1
multiple points	fluid temp.	T/C	4
	wall temp.	T/C	2
	liquid level	DP cell	2
			sum(11)
9. VENT LINE			
across the length	diff. pres.	DP cell	1
			sum(1)

Table A-2 Measurement items of SCTF (JAERI-provided instruments) (4/5)

LOCATION	ITEM	PROBE	QUANTITY
10. S/W SEPARATOR			
	pressure	DP cell	1
between inlet and outlet	diff. press.	DP cell	1
SG plenum simulator	diff. press.	DP cell	1
SG plenum simulator	fluid temp.	T/C	2
top and bottom	fluid temp.	T/C	2
wall	wall temp.	T/C	2
full height	liquid level	DP cell	1
liquid extraction	flow rate	DP cell	1
			sum(11)
11. CONTAINMENT TANK-I			
	pressure	DP cell	1
downcomer-CT-I	diff. press.	DP cell	1
CT-I - CT-II	diff. press.	DP cell	1
	flow rate	DP cell	1
full height	liquid level	DP cell	1
		float	1
top, middle & bottom	fluid temp.	T/C	3
wall	wall temp.	T/C	1
			sum(10)
12. CONTAINMENT TANK-II			
	pressure	DP cell	1
upper plenum - CT-II	diff. press.	DP cell	1
separator - CT-II	diff. press.	DP cell	1
steam blow line	flow rate	DP cell	1
full height	liquid level	DP cell	1
top, middle & bottom	fluid temp.	T/C	3
			sum(8)
13. ECC INJECTION SYSTEM			
ACC tank	pressure	DP cell	1
total and LPCI	flow rate	E-M flow meter	2
			1
ACC tank	fluid temp.	T/C	1

Table A-2 Measurement items of SCTF (JAERI-provided instruments) (5/5)

LOCATION	ITEM	PROBE	QUANTITY
13. ECC INJECTION SYSTEM			
header	fluid temp.	T/C	2
ACC tank	liquid level	DP cell	1
			sum(8)
14. UCSP WATER EXTRACTION SYSTEM			
extraction line	flow rate	E-M flow meter	4
steam line	flow rate	DP cell	4
extraction line	fluid temp.	T/C	5
steam line	fluid temp.	T/C	1
extraction line	liquid level	DP cell	4
			sum(18)
15. SATURATED WATER TANK			
	fluid temp	T/C	1
	liquid level	DP cell	1
			sum(2)
16. NITROGEN GAS SYSTEM			
	flow rate	DP cell	1
injection port	fluid temp.	T/C	1
			sum(2)

Total 1267

Table A-3 Measurement items of SCTF (USNRC-provided instruments) (1/2)

LOCATION	ITEM	PROBE	QUANTITY
1. CORE			
non-heated rods	liquid level	LLD	20×4 = 80
non-heated rods	film thickness and velocity	film probe	6
non-heated rods	void fraction and droplet velocity	flag probe	8
side walls	film thickness and velocity	film probe	8
sub-channel	fluid density	γ-densitometer	10
end box	fluid density	γ-densitometer	5
end box	flow pattern	video optical probe	1
2. UPPER PLENUM			
full height	liquid level	FDG	8×8 = 64
structure surface	film thickness and velocity	film probe	6
side walls	film thickness and velocity	film probe	6
inter structure	void fraction	prong probe	8
above UCSP hole	velocity	turbine	8
inter structure	velocity	turbine	4
inter structure	fluid density	γ-densitometer	4
hot leg inlet	flow pattern	video optical probe	1
3. LOWER PLENUM			
core inlet	velocity	turbine	4
bottom	reference conductivity	reference probe	1
4. DOWNCOMER			
full height	liquid level	FDG	2×3×7 = 42
two levels	velocity	drag disk	3
two levels	void fraction	string probe	3

Table A-3 Measurement items of SCTF (USNRC-provided instruments) (2/2)

LOCATION	ITEM	PROBE	QUANTITY
5. HOT LEG	mass flow rate fluid density void fraction	spool piece	1
6. PV SIDE BROKEN COLD-LEG	mass flow rate fluid density void fraction	spool piece	1
7. VENT LINE	mass flow rate void fraction	spool piece	1

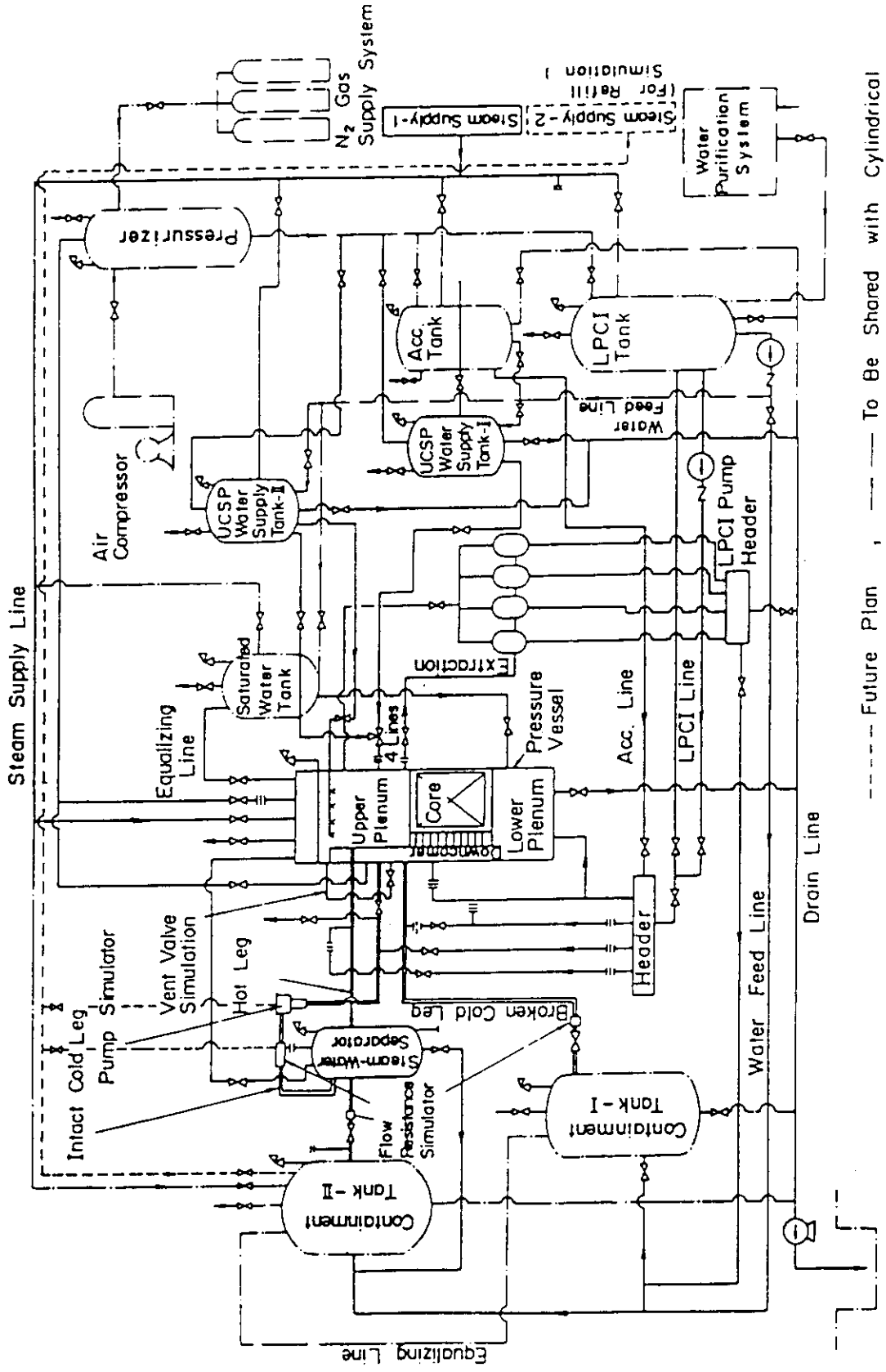

Fig. A-1 Schematic diagram of slab core test facility

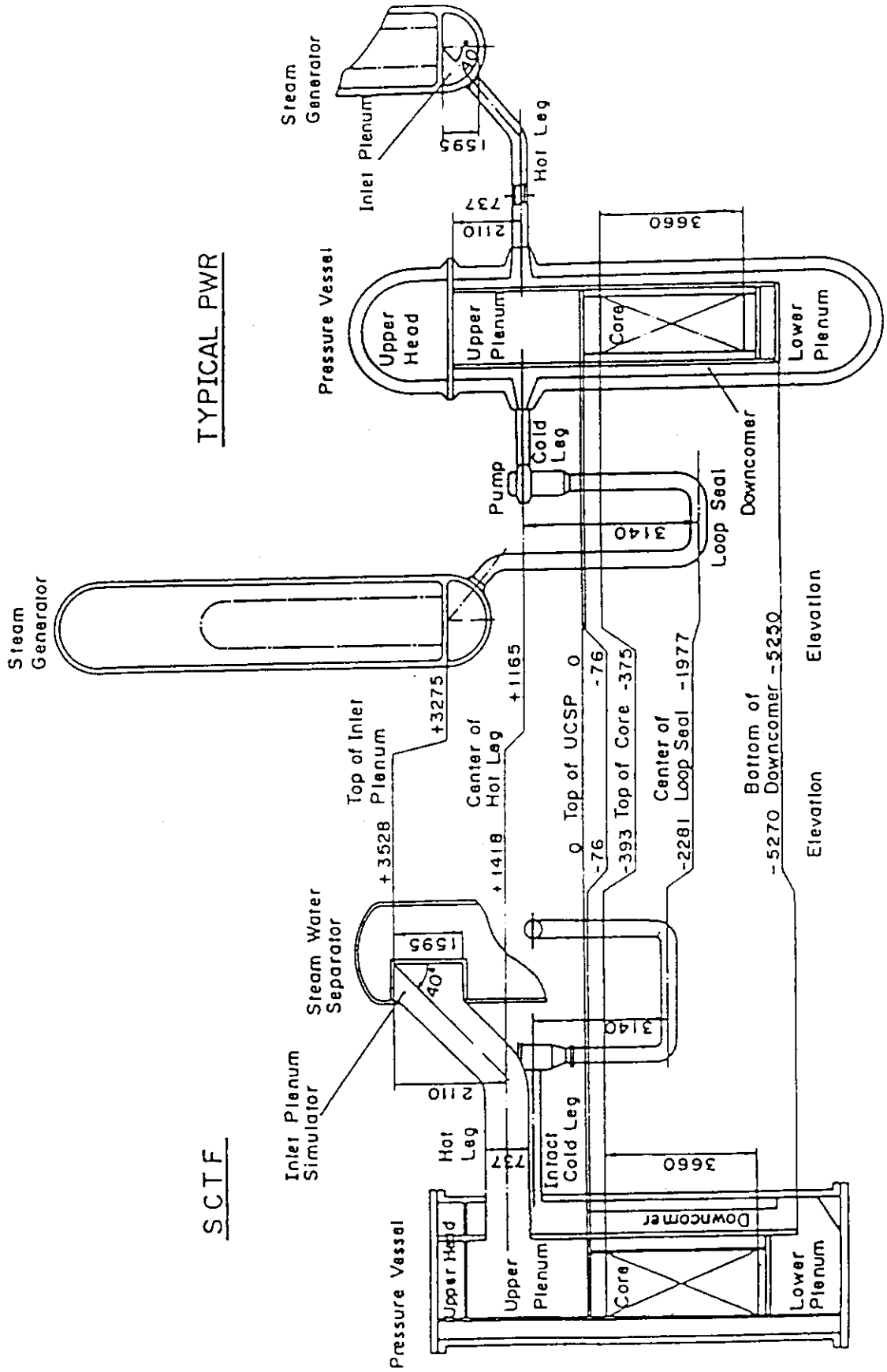

Fig. A-2 Comparison of dimensions between SCTF and a reference PWR

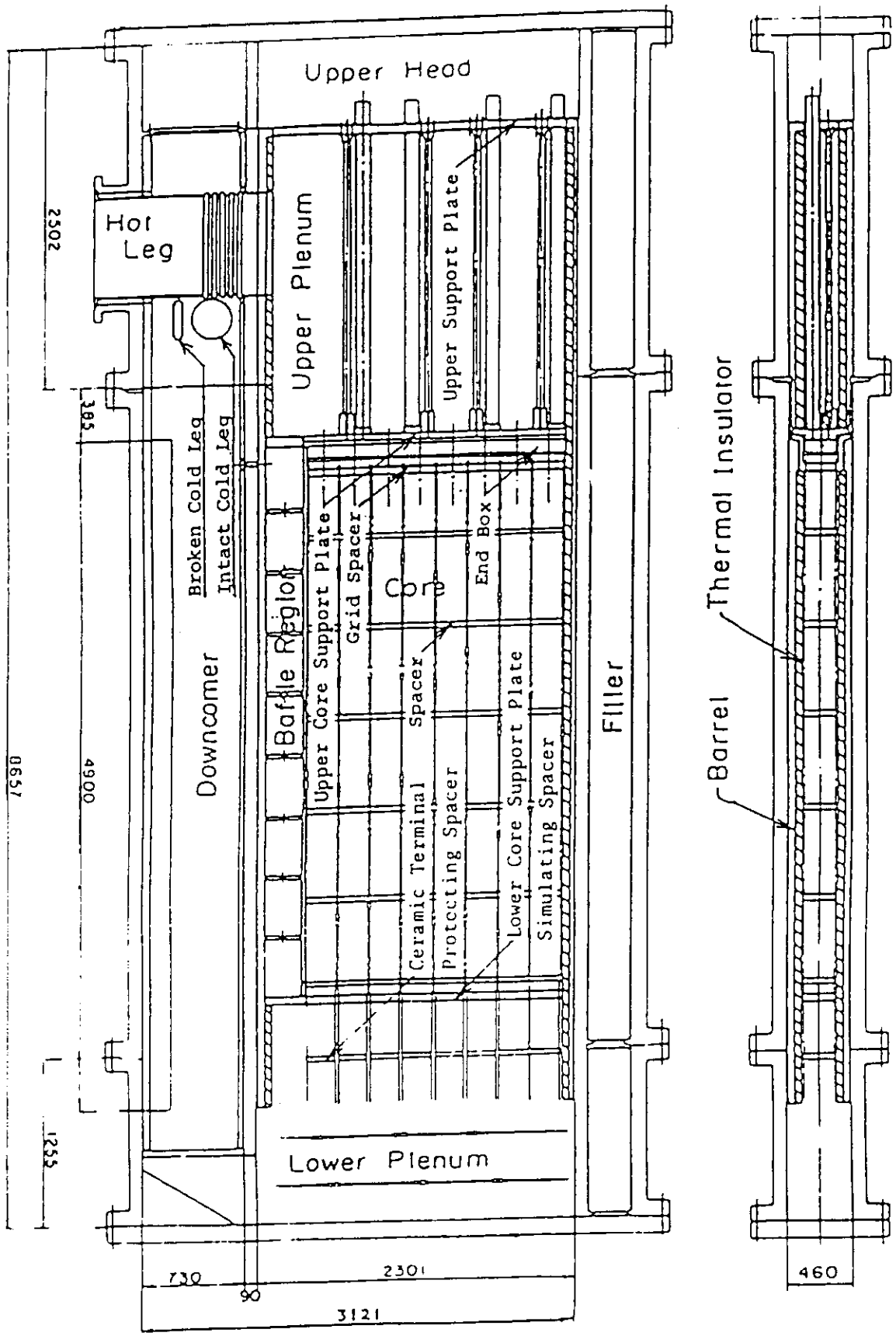

Fig. A-3 Verical cross section of the pressure vessel

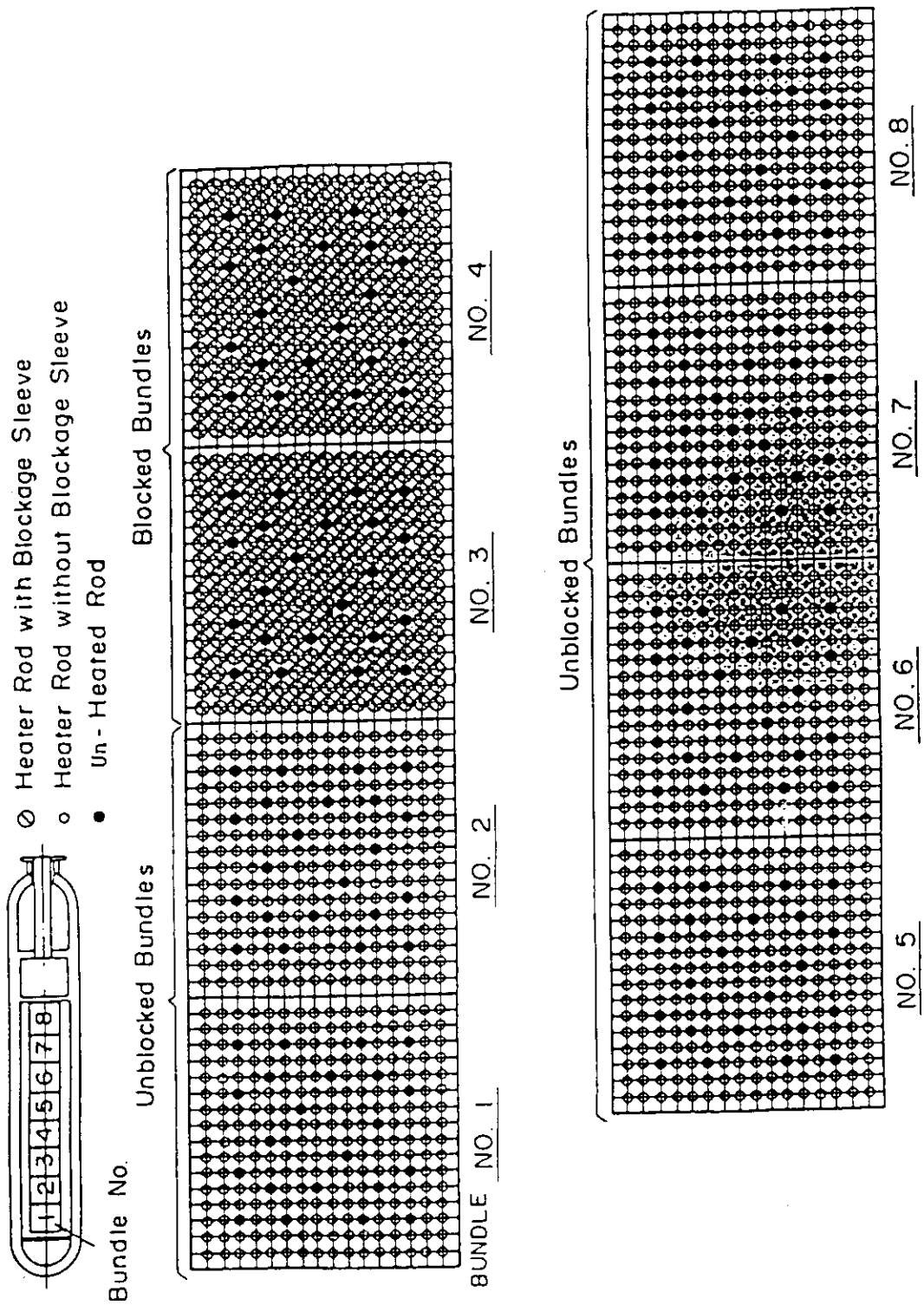

Fig. A-4 Arrangement of heater bundles

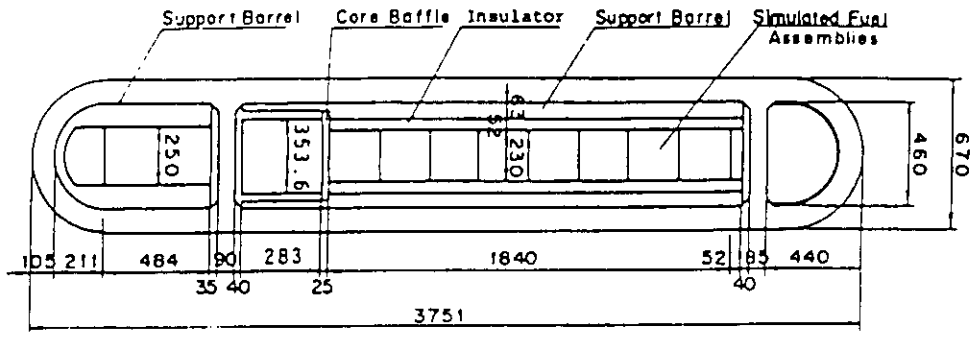

Fig. A-5 Horizontal cross section of the pressure vessel (1)

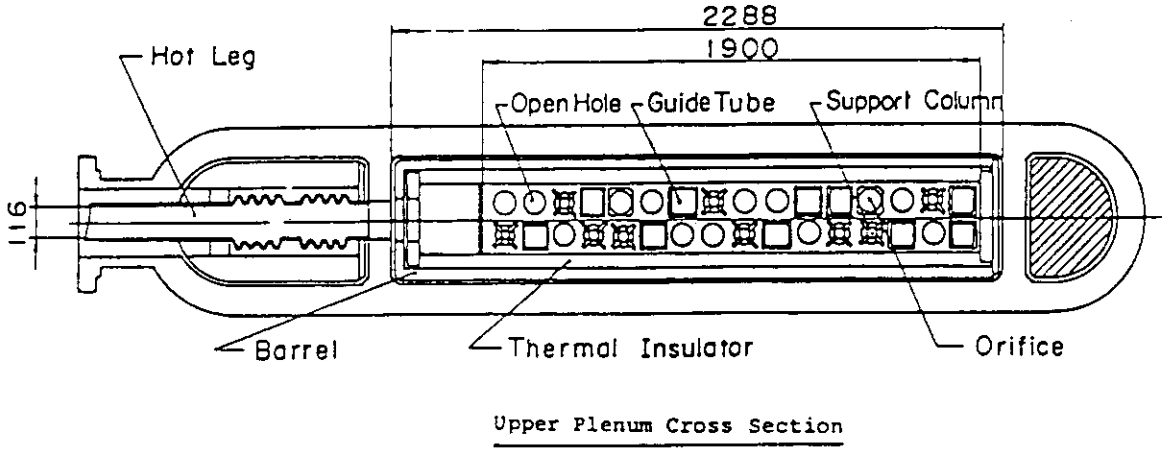

Fig. A-6 Horizontal cross section of the pressure vessel (2)

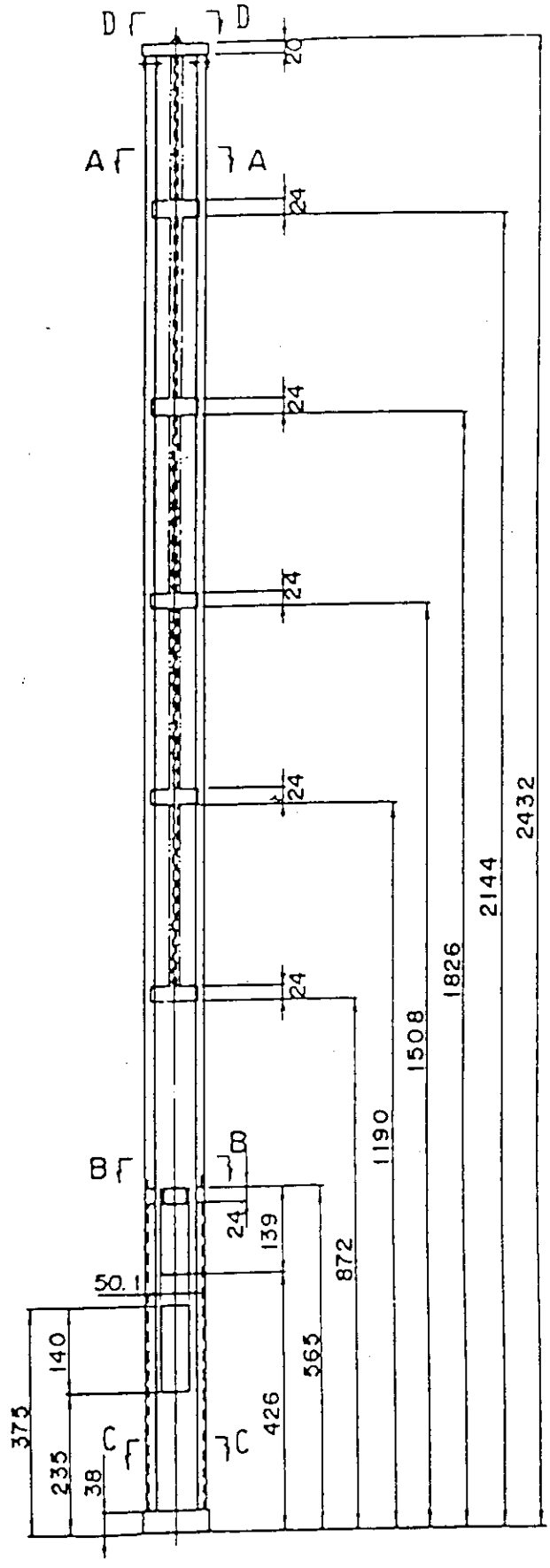

Fig. A-7 Dimension of guide tube (1)

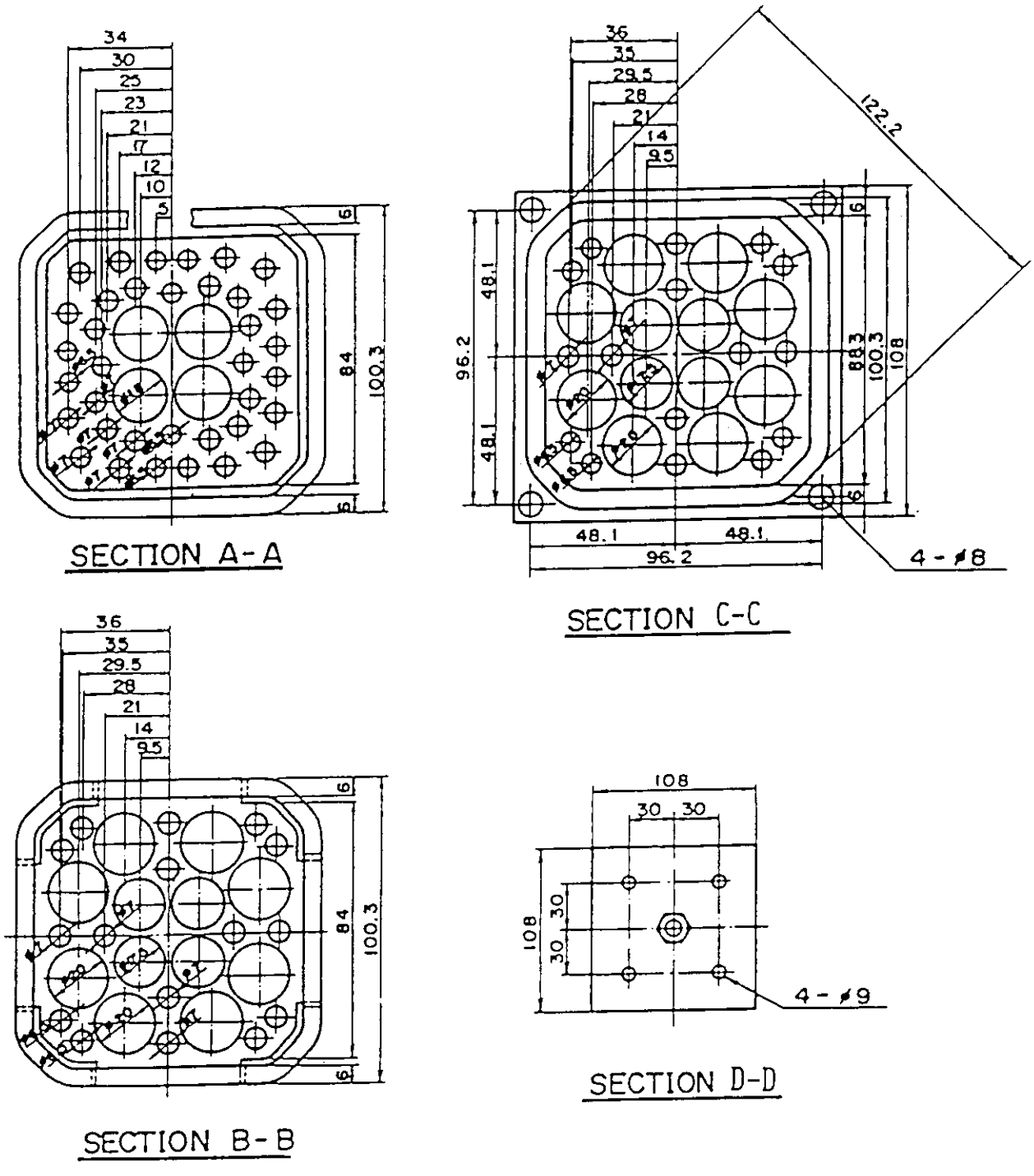

Fig. A-8 Dimension of guide tube (2)

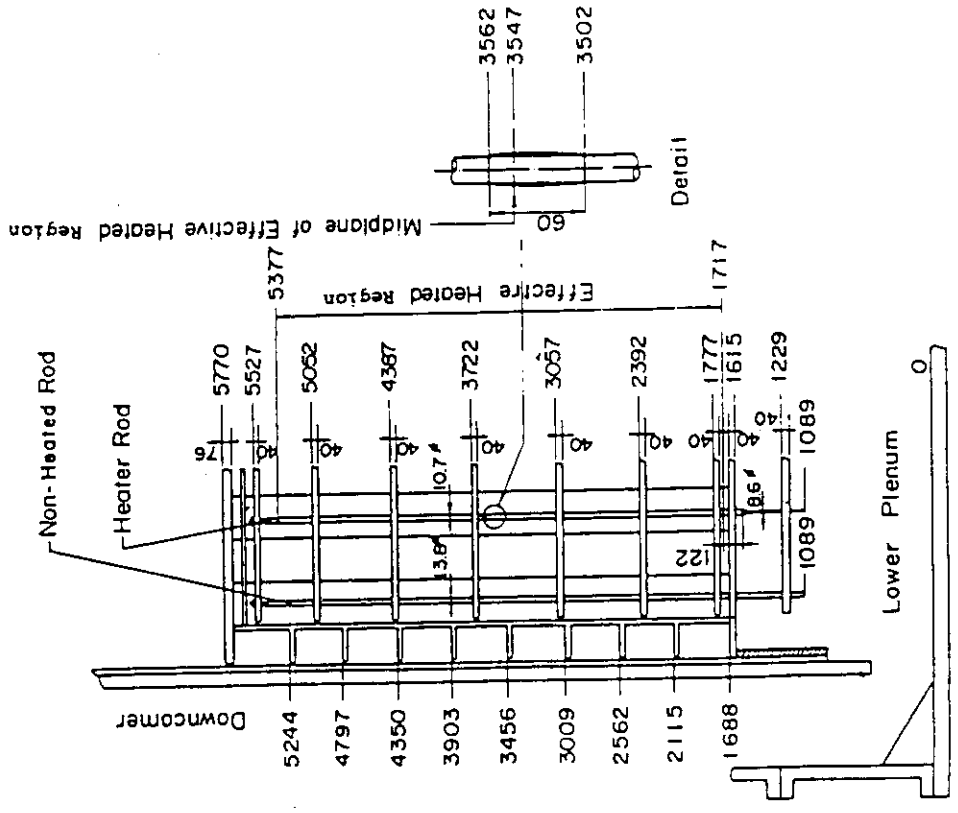

Fig. A-10 Relative elevation and dimension of the core in SCTF

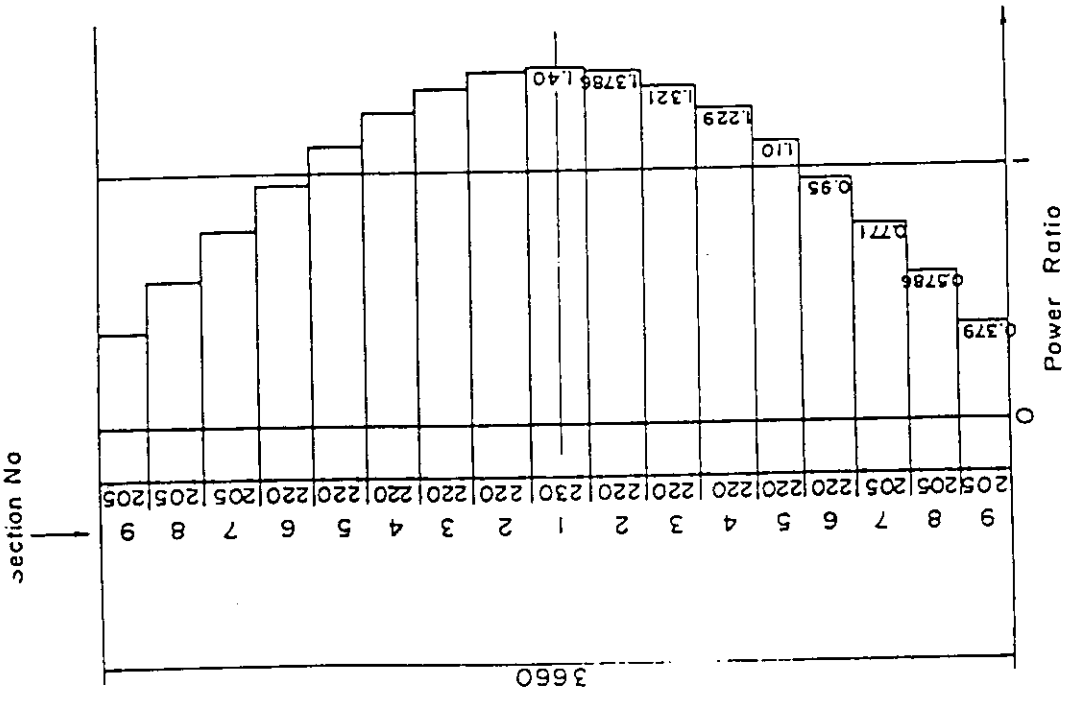

Fig. A-9 Axial power distribution of heater rod

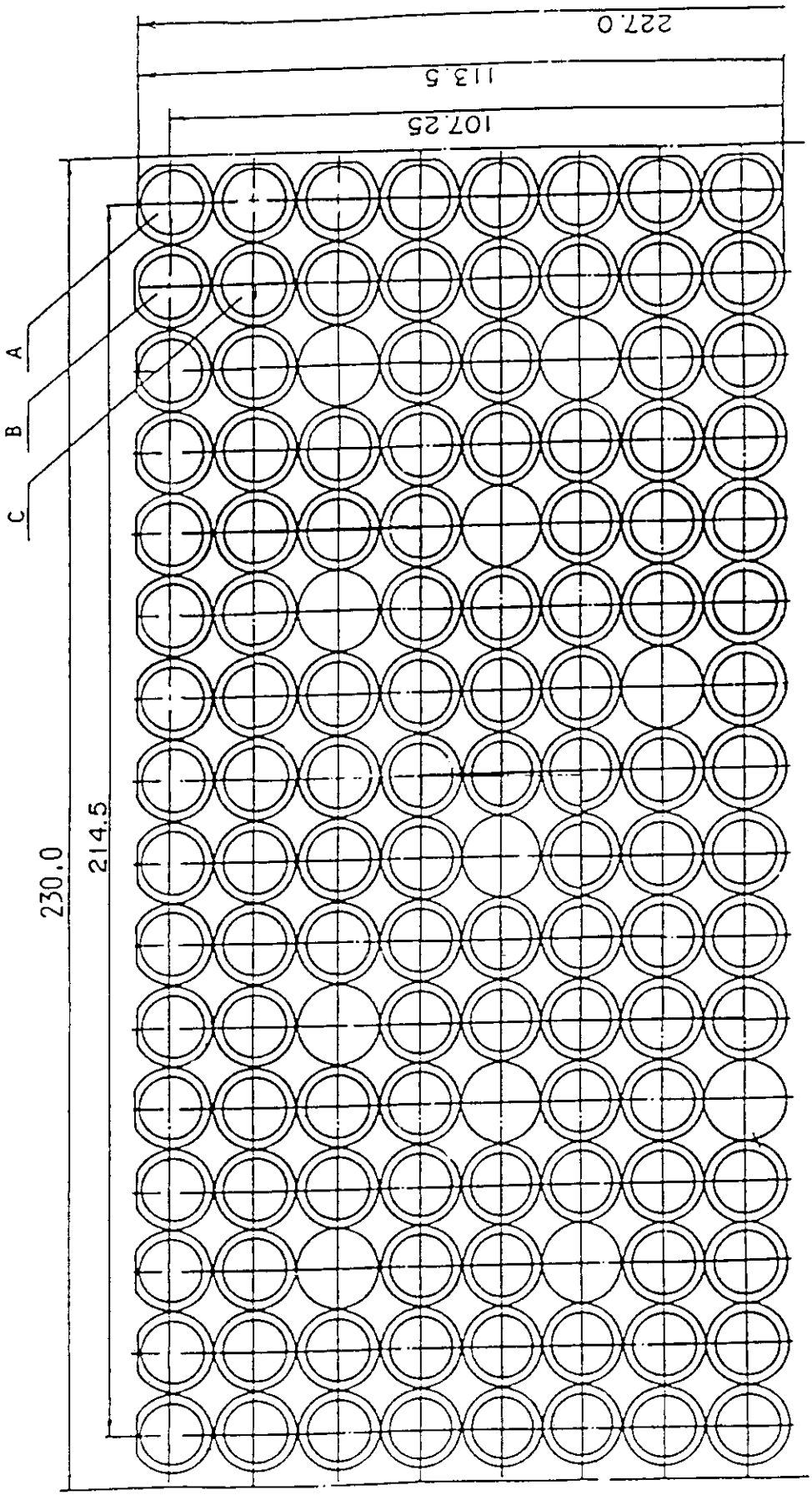

Fig. A-11 Arrangement of the heater rods with three kinds of blockage sleeve

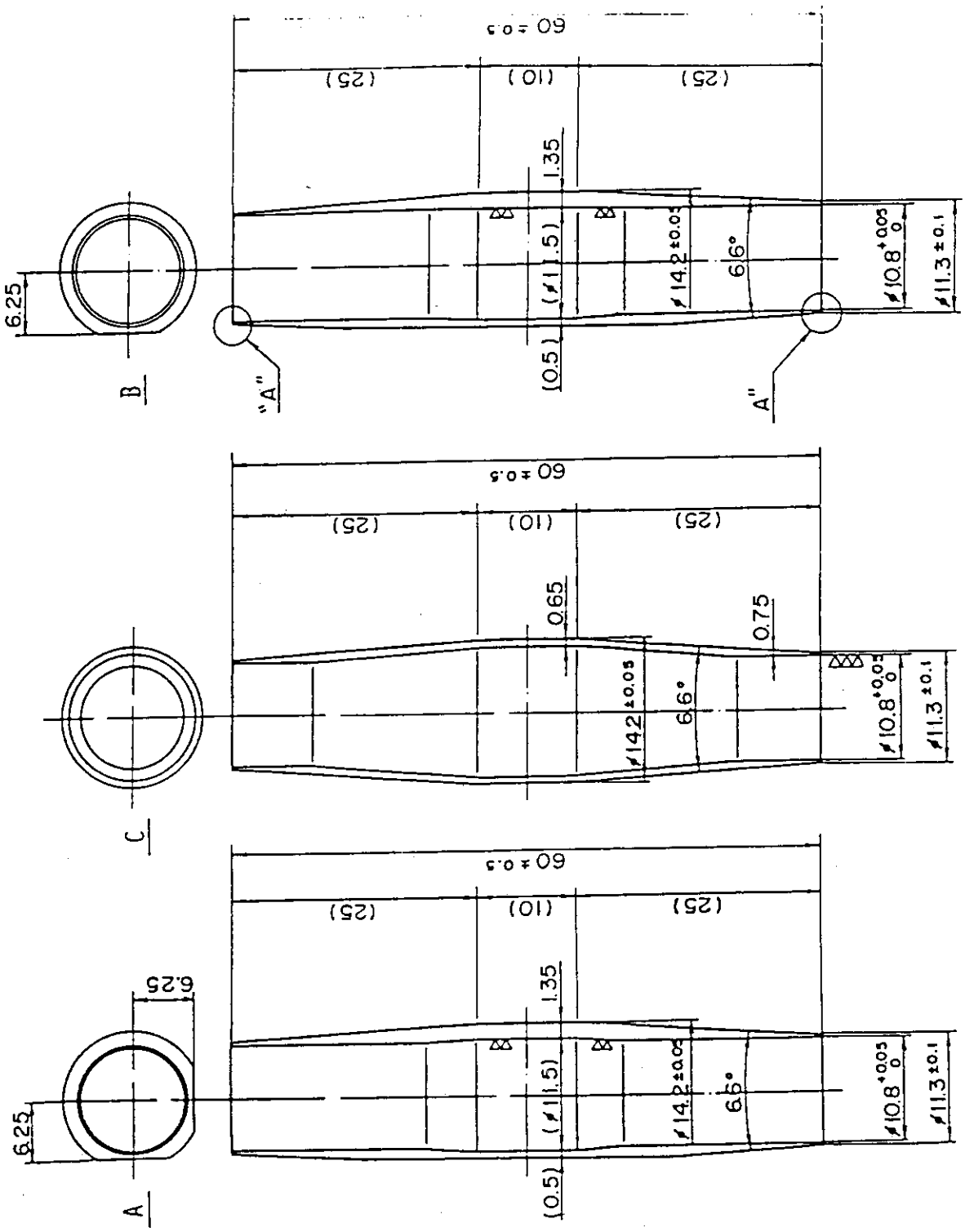

Fig. A-12 Configuration and dimension of the thre blockage sleeves

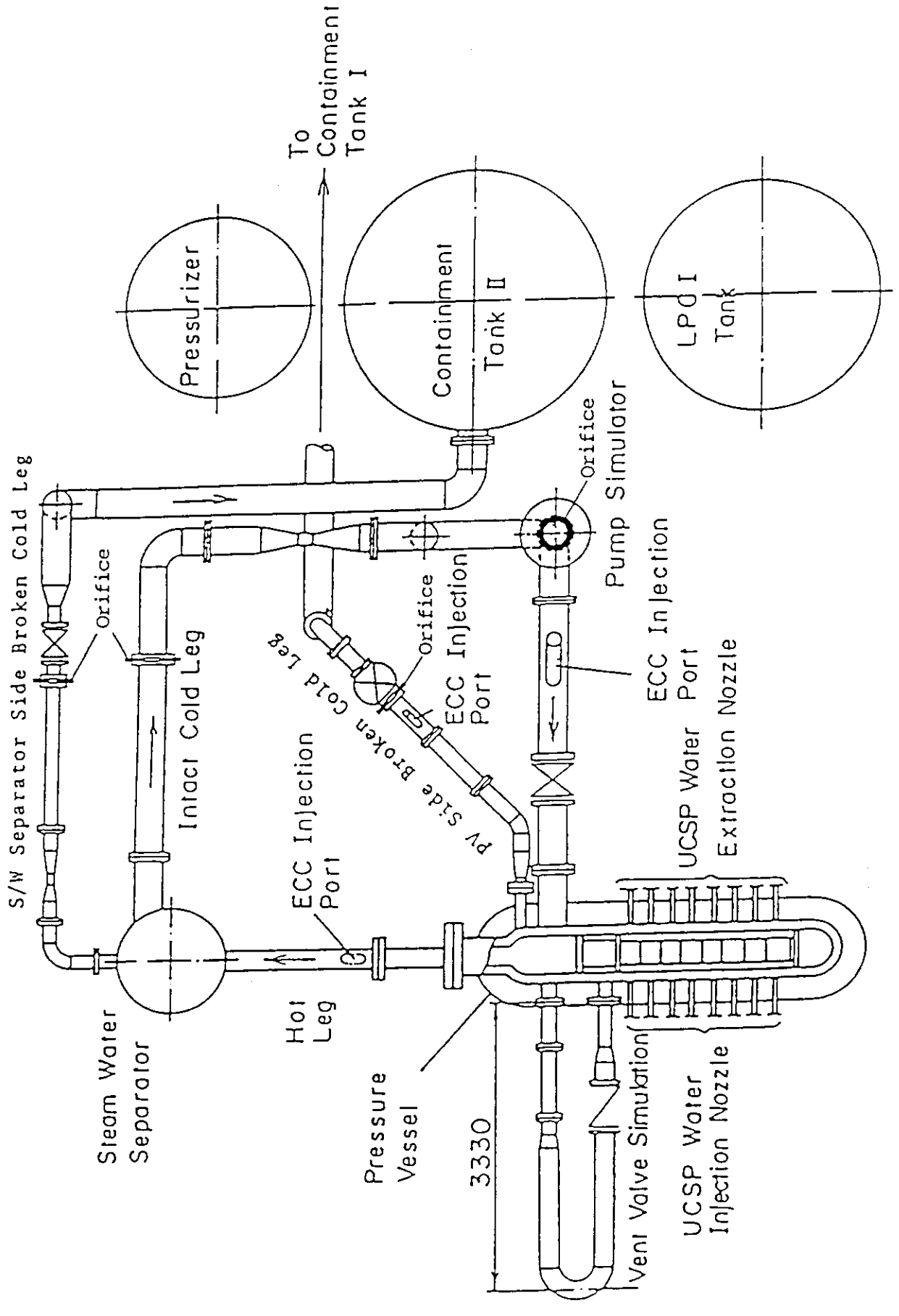

Fig. A-13 Overview of the arrangements of the SCTF

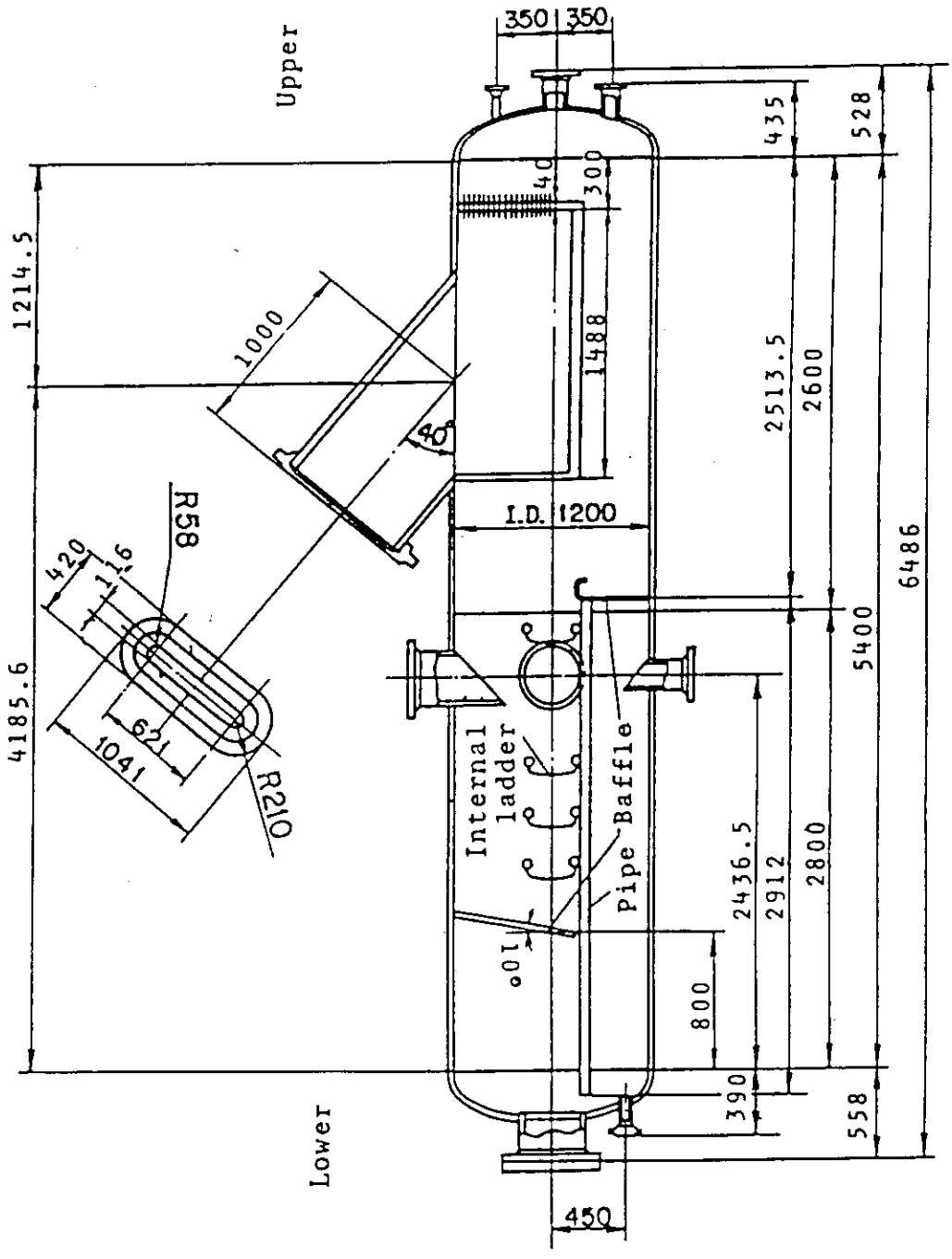

Fig. A-14 Steam-water separator

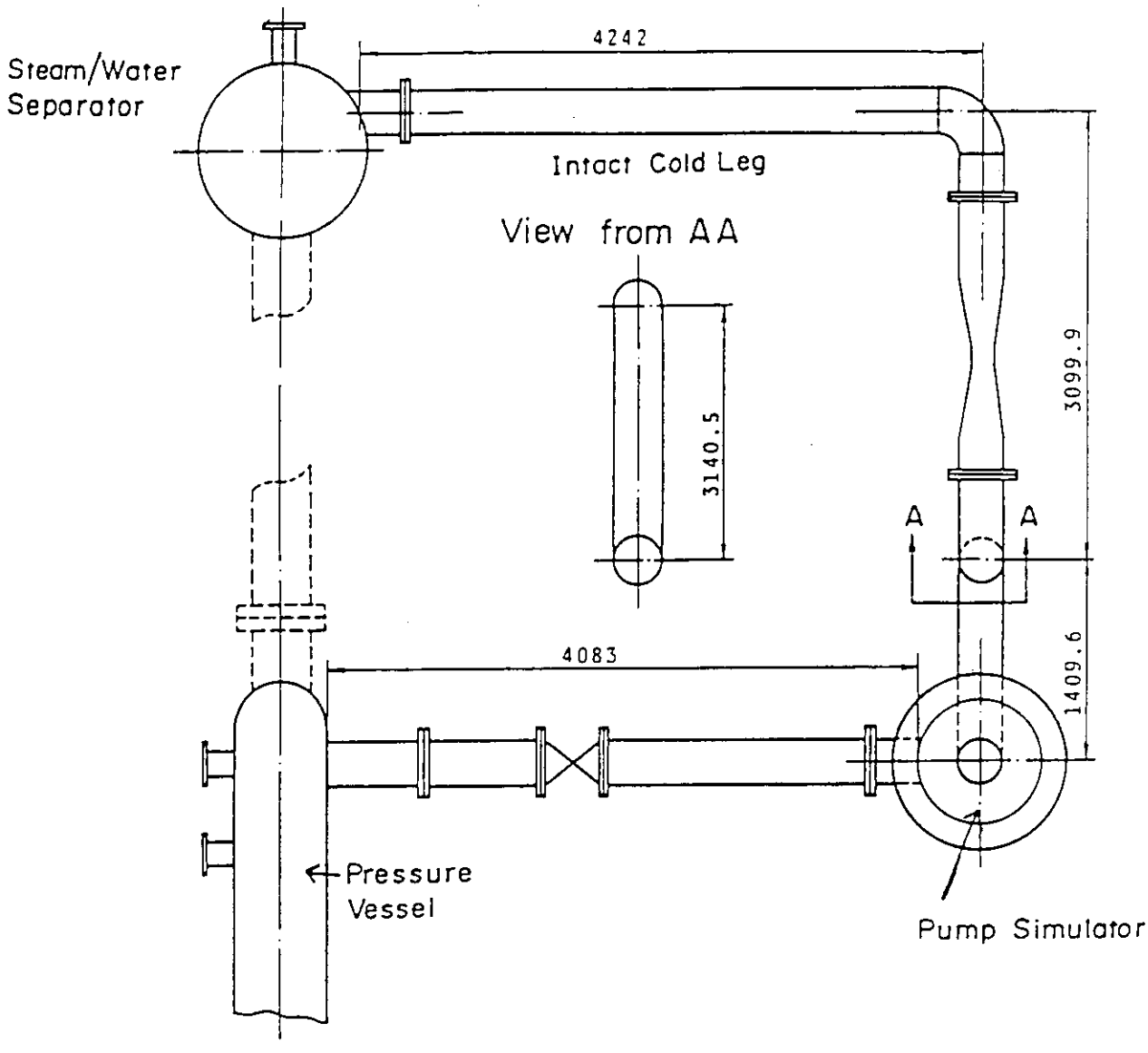

Fig. A-15 Arrangement of intact cold leg

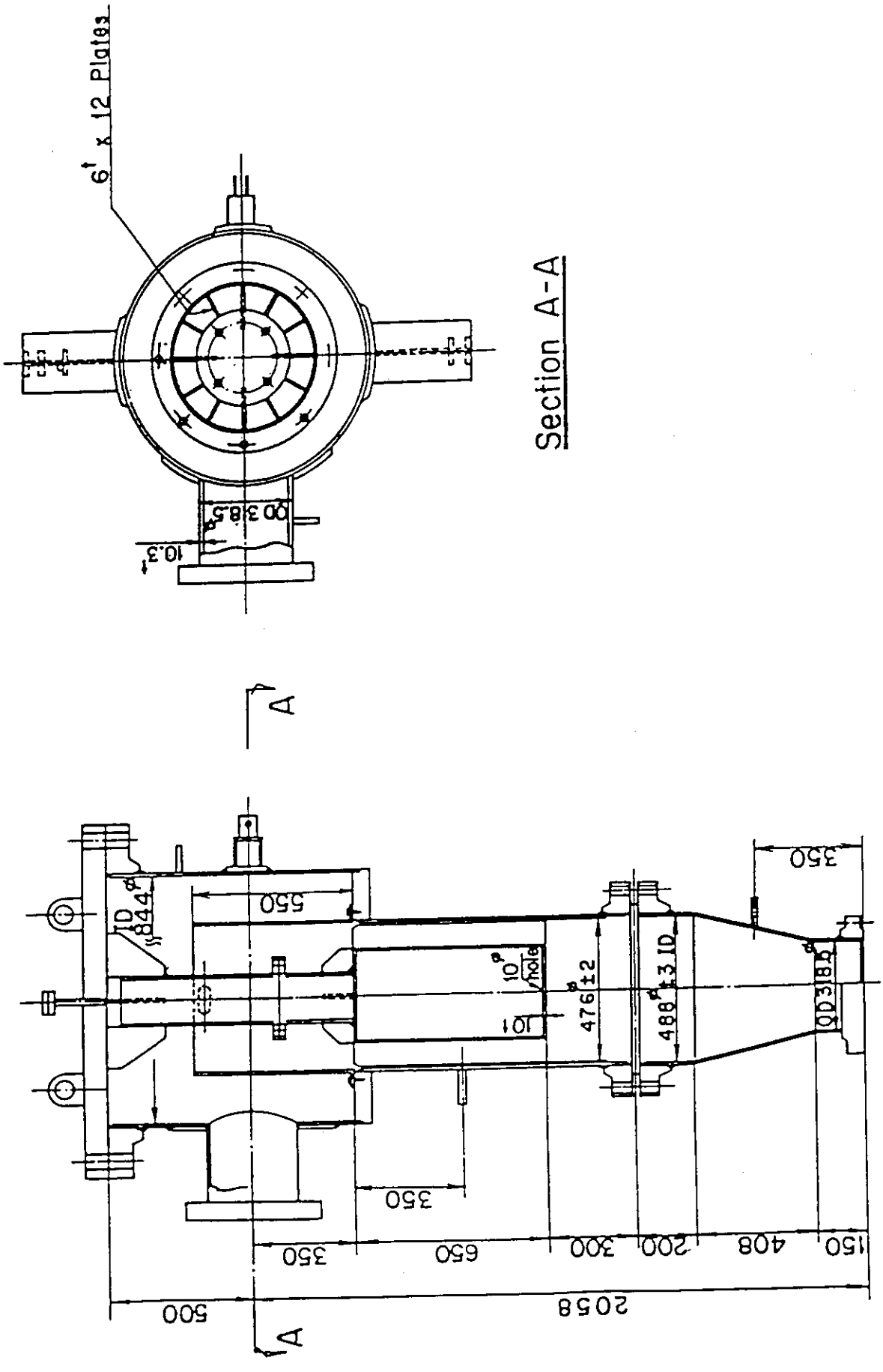

Fig. A-16 Configuration and dimension of pump simulator

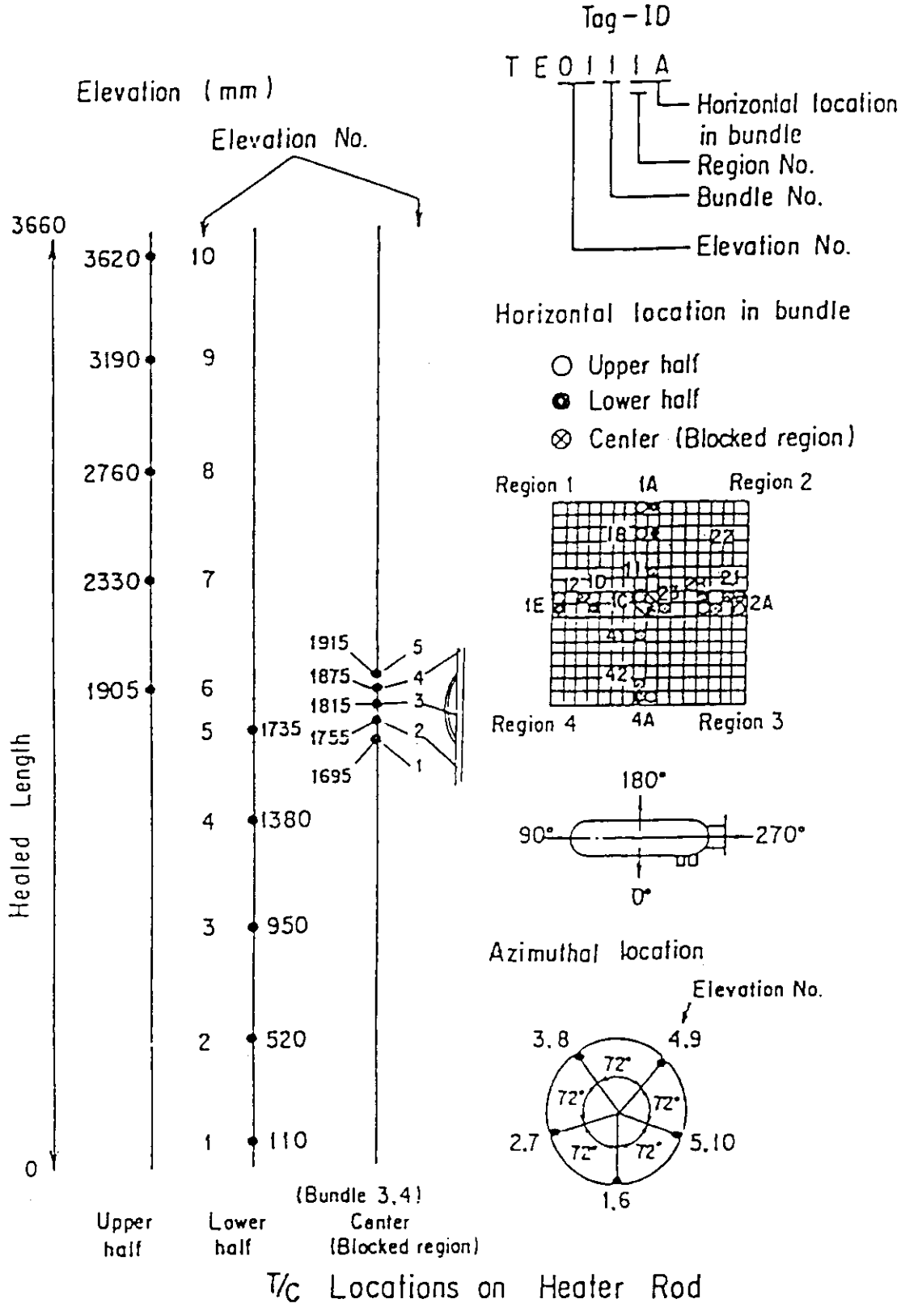

Fig. A-17 Thermocouple locations of heater rod surface temperature measurements

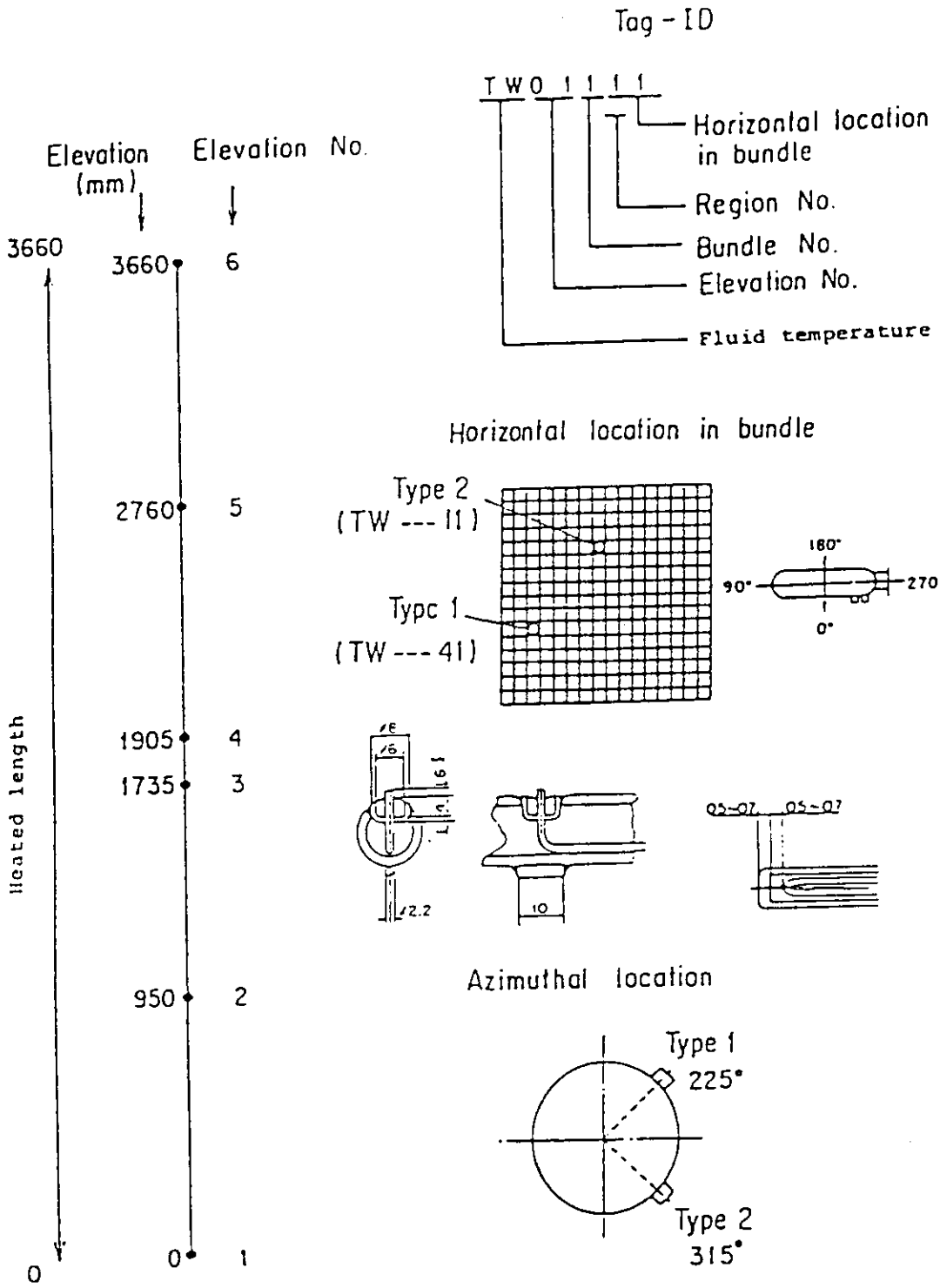

Fig. A-18 Thermocouple locations of fluid temperature measurements in core

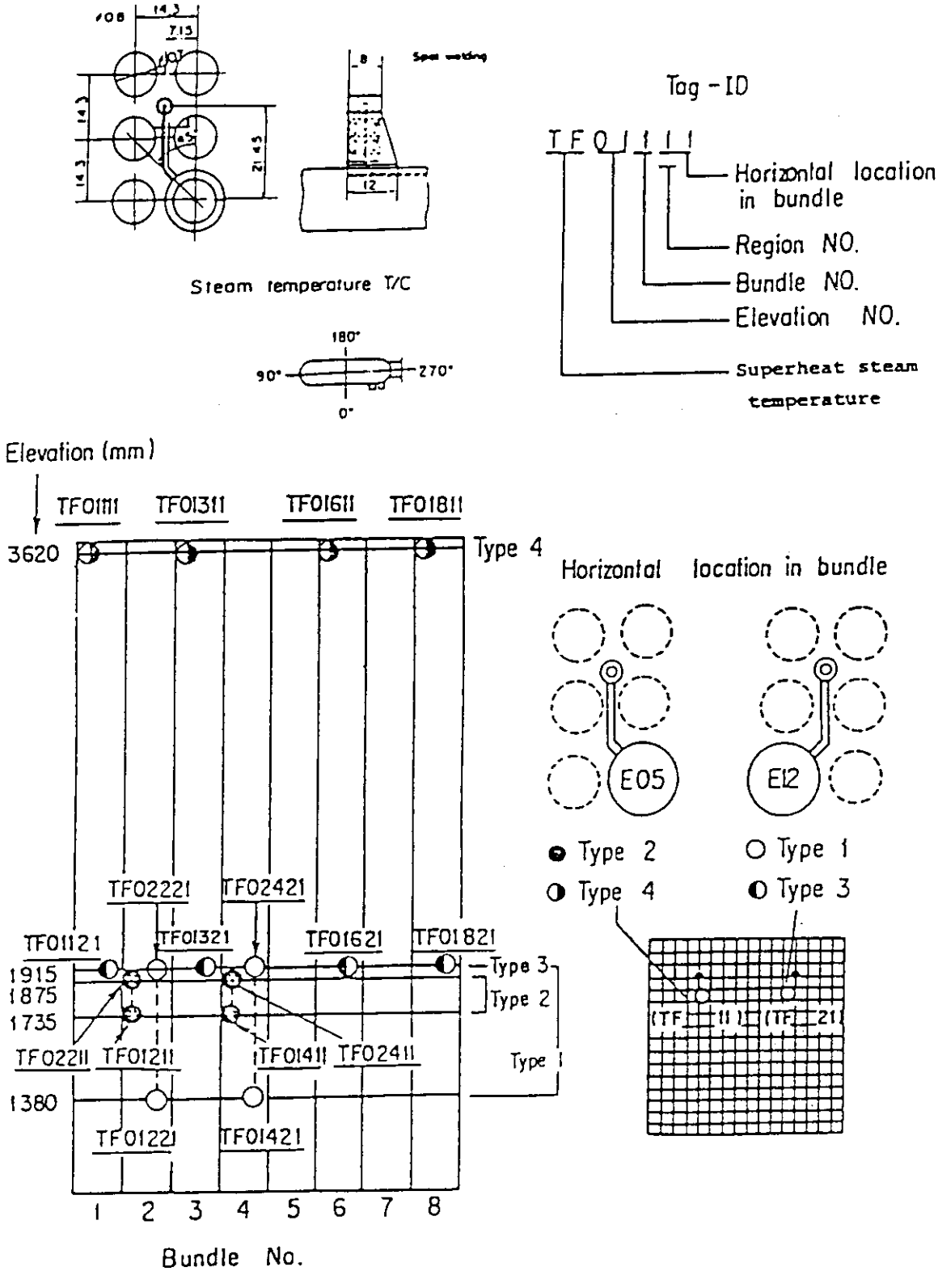

Fig. A-19 Thermocouple locations of steam temperature measurements in core

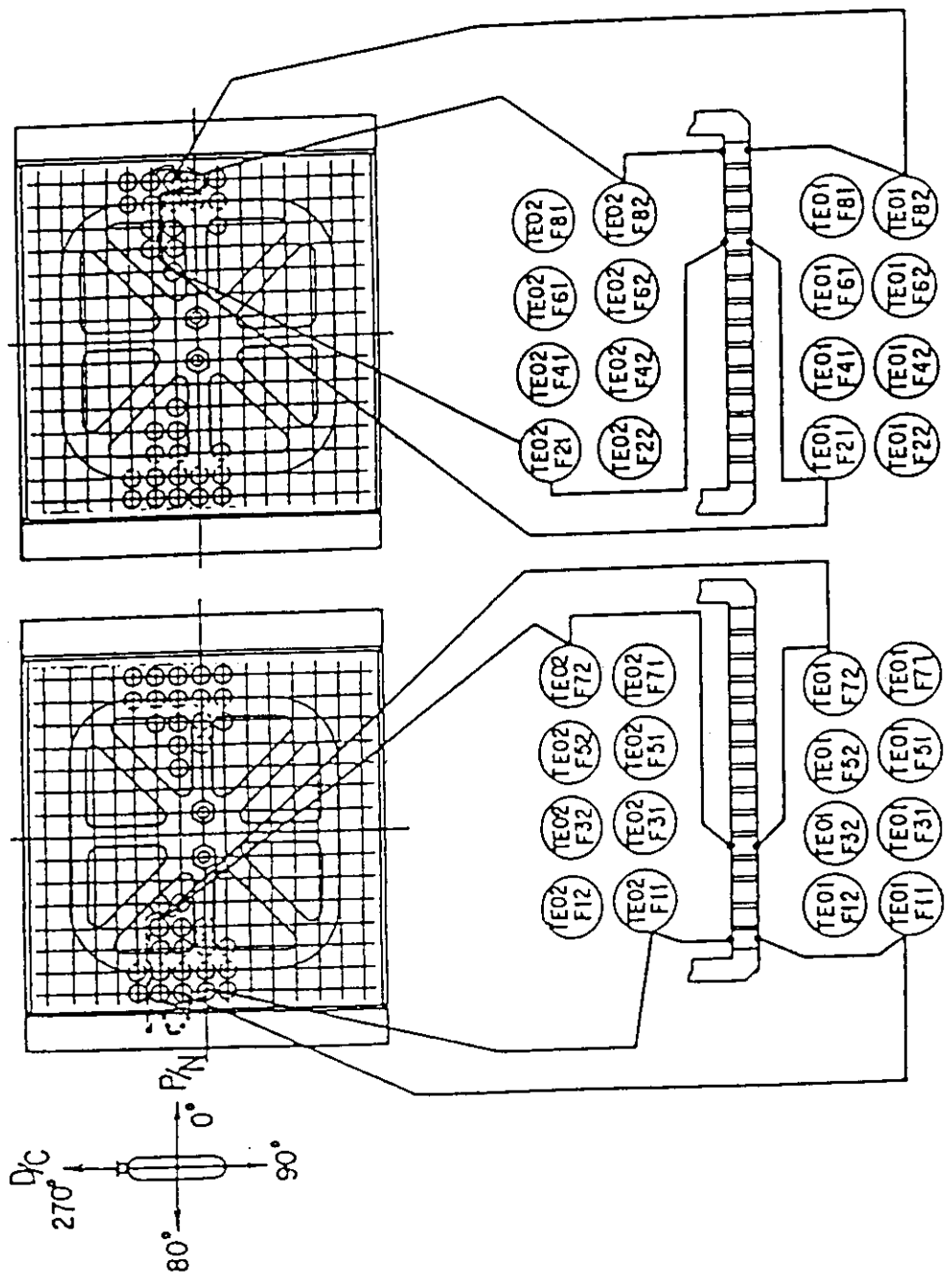

Fig. A-20 Thermocouple locations of fluid temperature measurements just above and below end box tie plate

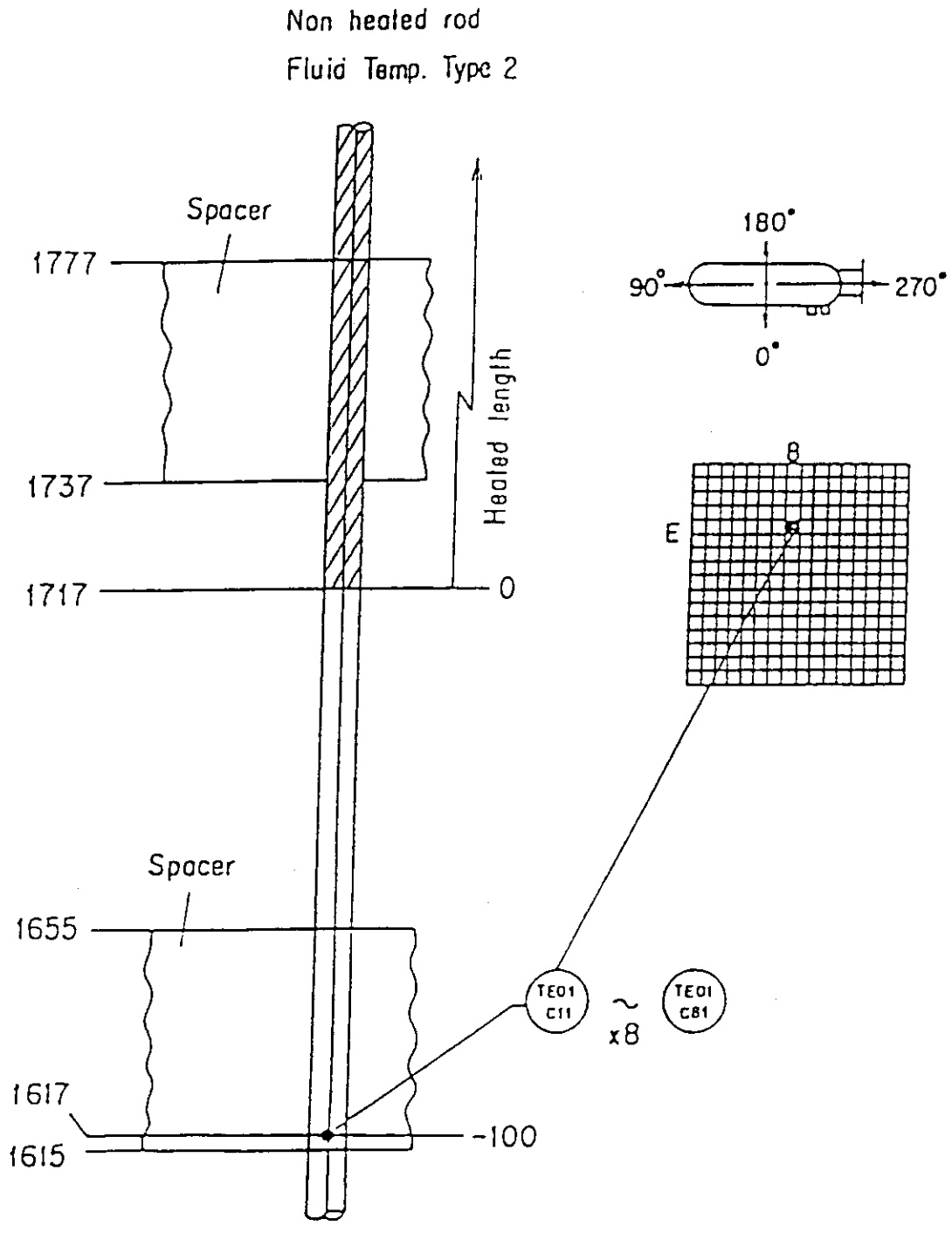

Fig. A-21 Thermocouple locations of fluid temperature measurements at core inlet

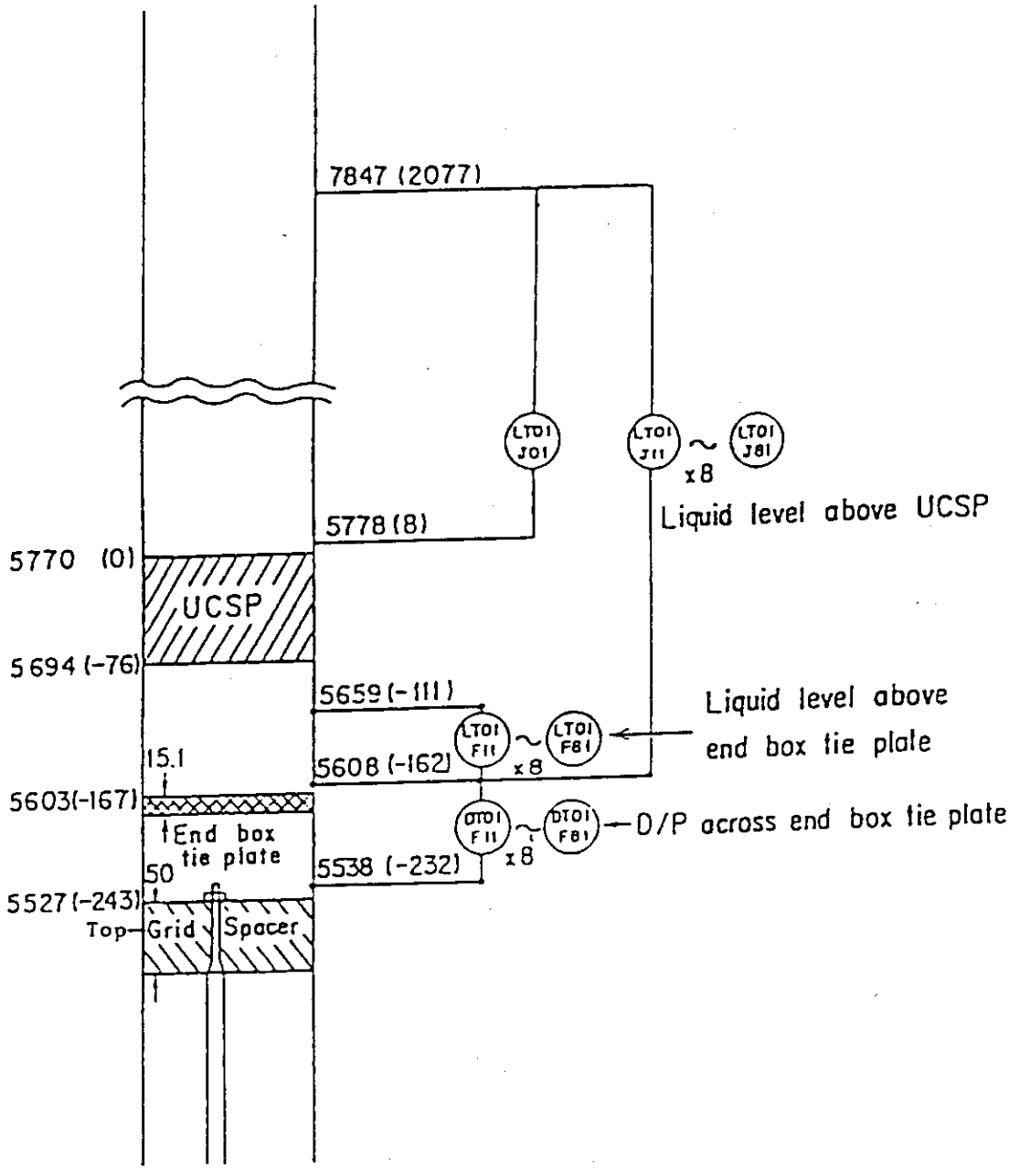

Fig. A-22 Locations of differential pressure measurements across end box tie plate and liquid level measurements above UCSP and end box tie plate

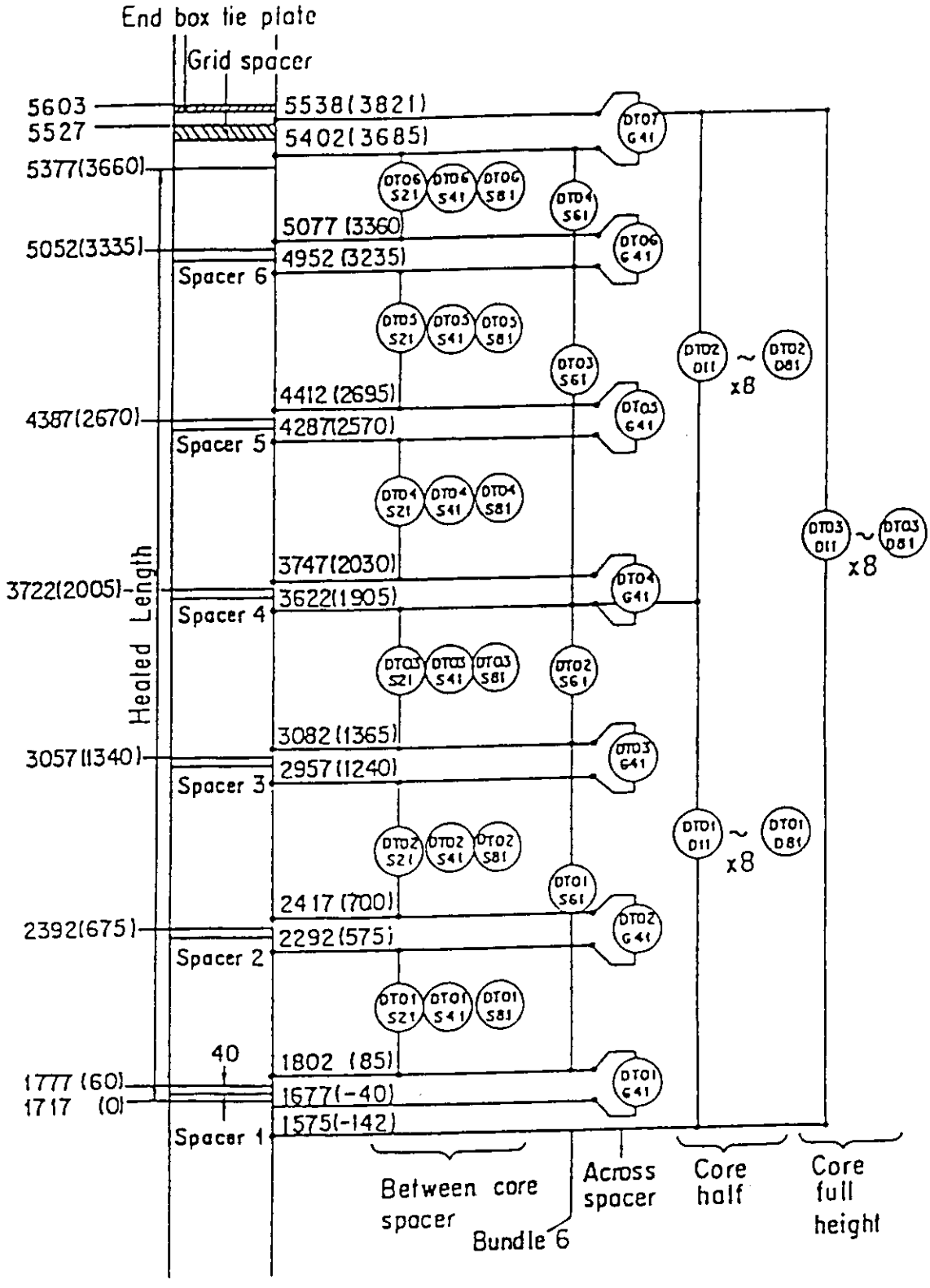

Fig. A-23 Locations of vertical differential pressure measurements in core

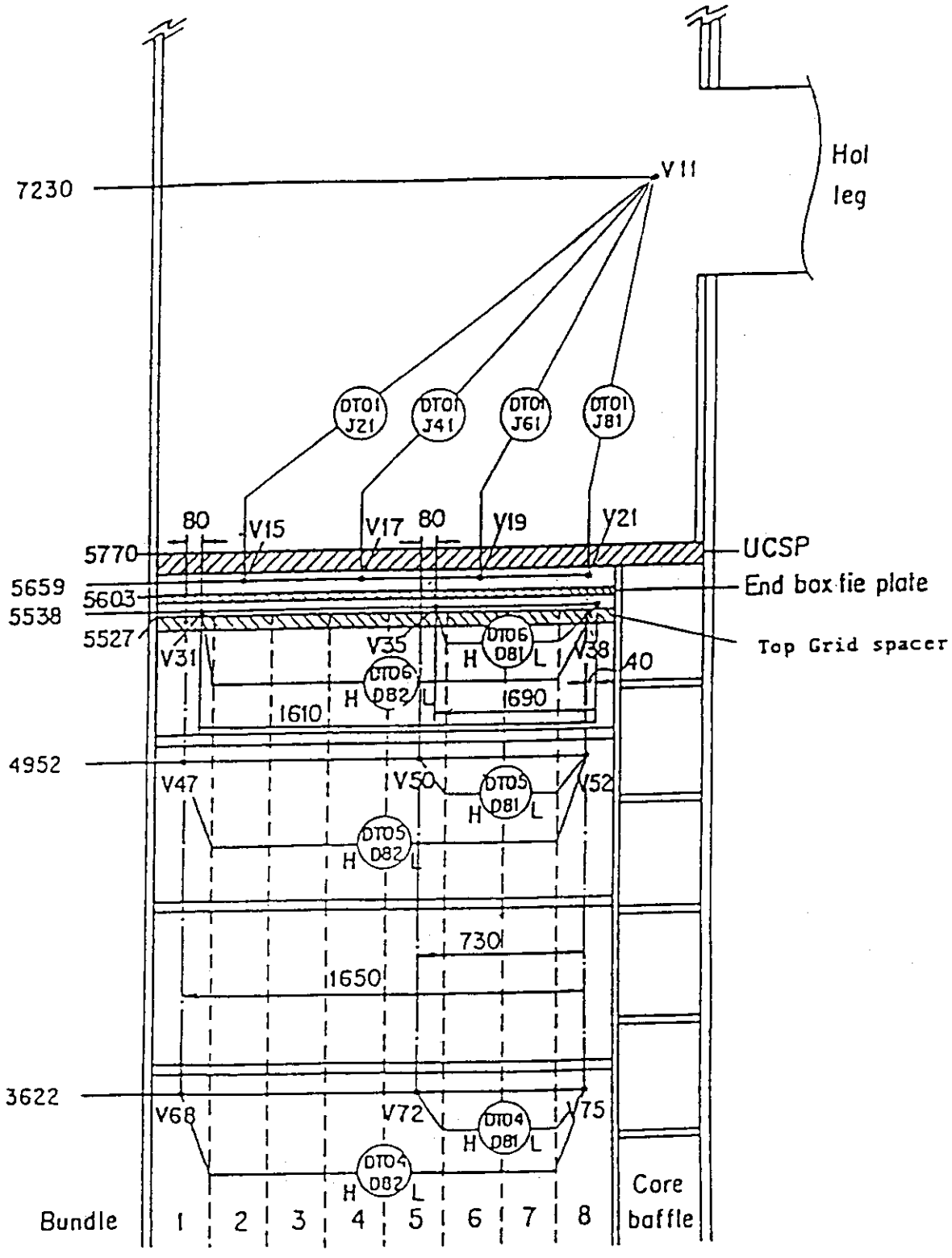

Fig. A-24 Locations of horizontal differential pressure measurements in core and differential pressure measurements between end box and inlet of hot leg

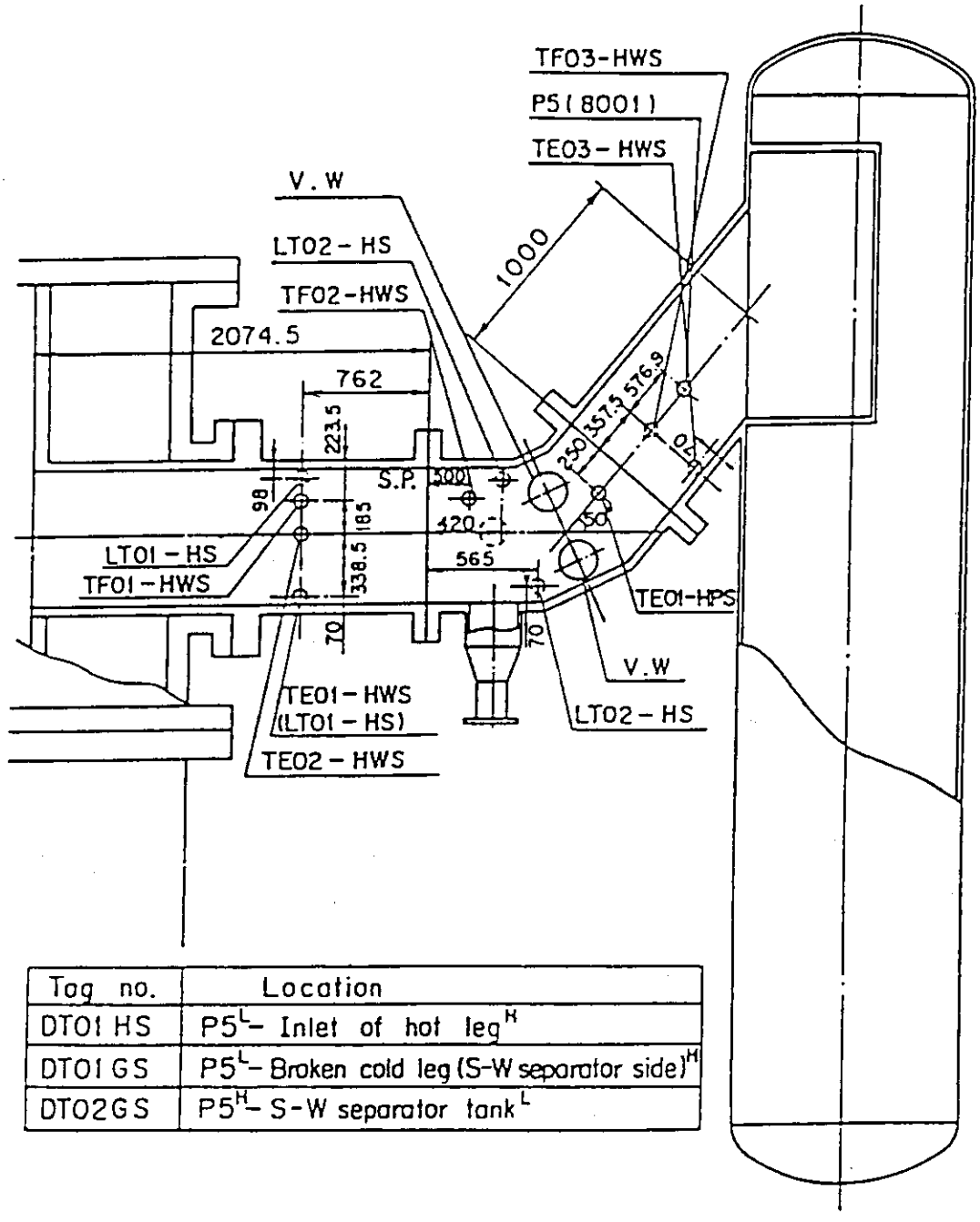

Tag no.	Location
DT01HS	$P5^{L}$ – Inlet of hot leg^{H}
DT01GS	$P5^{L}$ – Broken cold leg (S-W separator side)^{H}
DT02GS	$P5^{H}$ – S-W separator tank^{L}

Fig. A-25 Locations of hot leg instrumentation

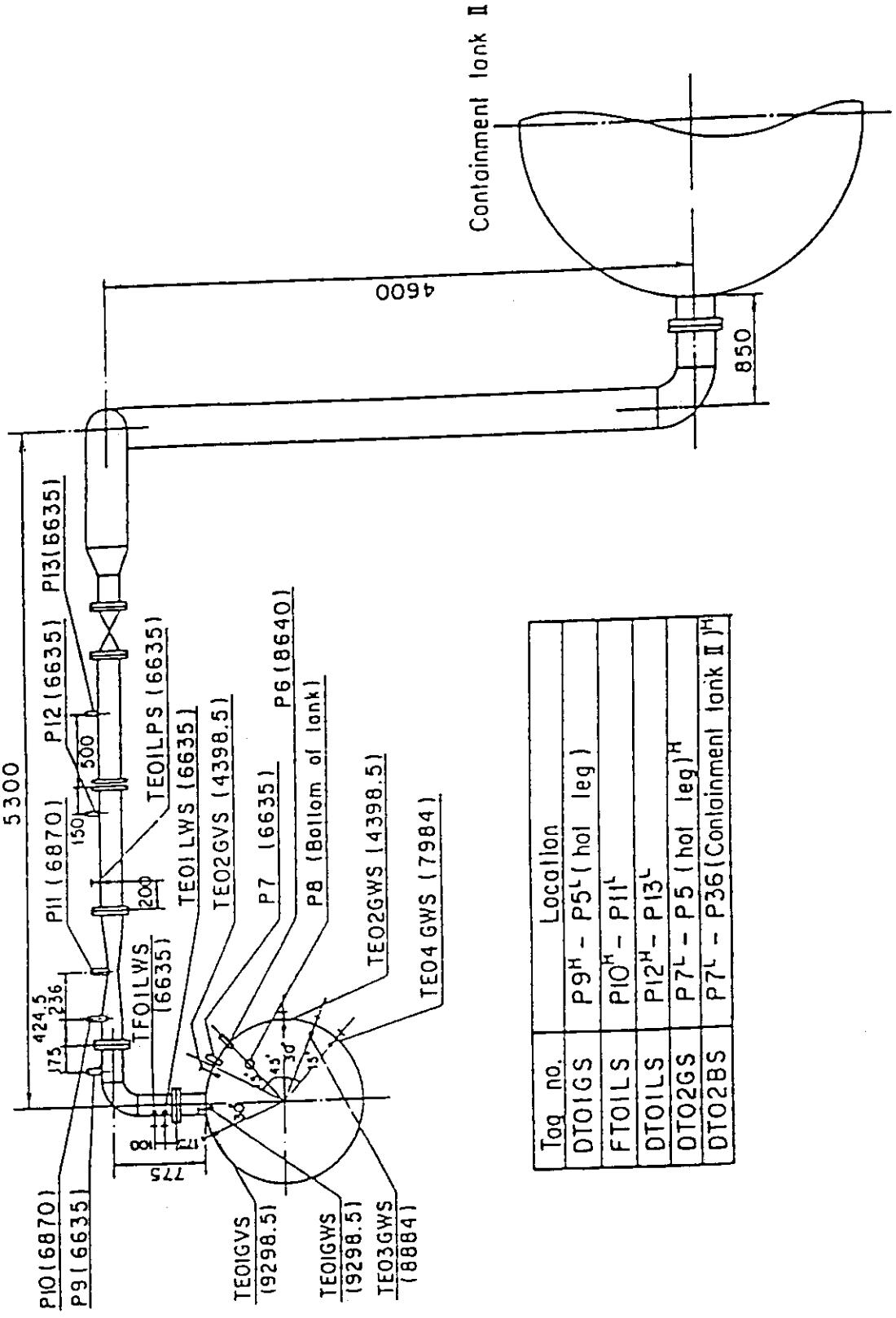

Tag no.	Location
DT01GS	$P9^H - P5^L$ (hot leg)
FT01LS	$P10^H - P11^L$
DT01LS	$P12^H - P13^L$
DT02GS	$P7^L - P5$ (hot leg)^H
DT02BS	$P7^L - P36$(Containment tank II)^H

Fig. A-26 Locations of steam-water separator side broken cold leg instrumentation

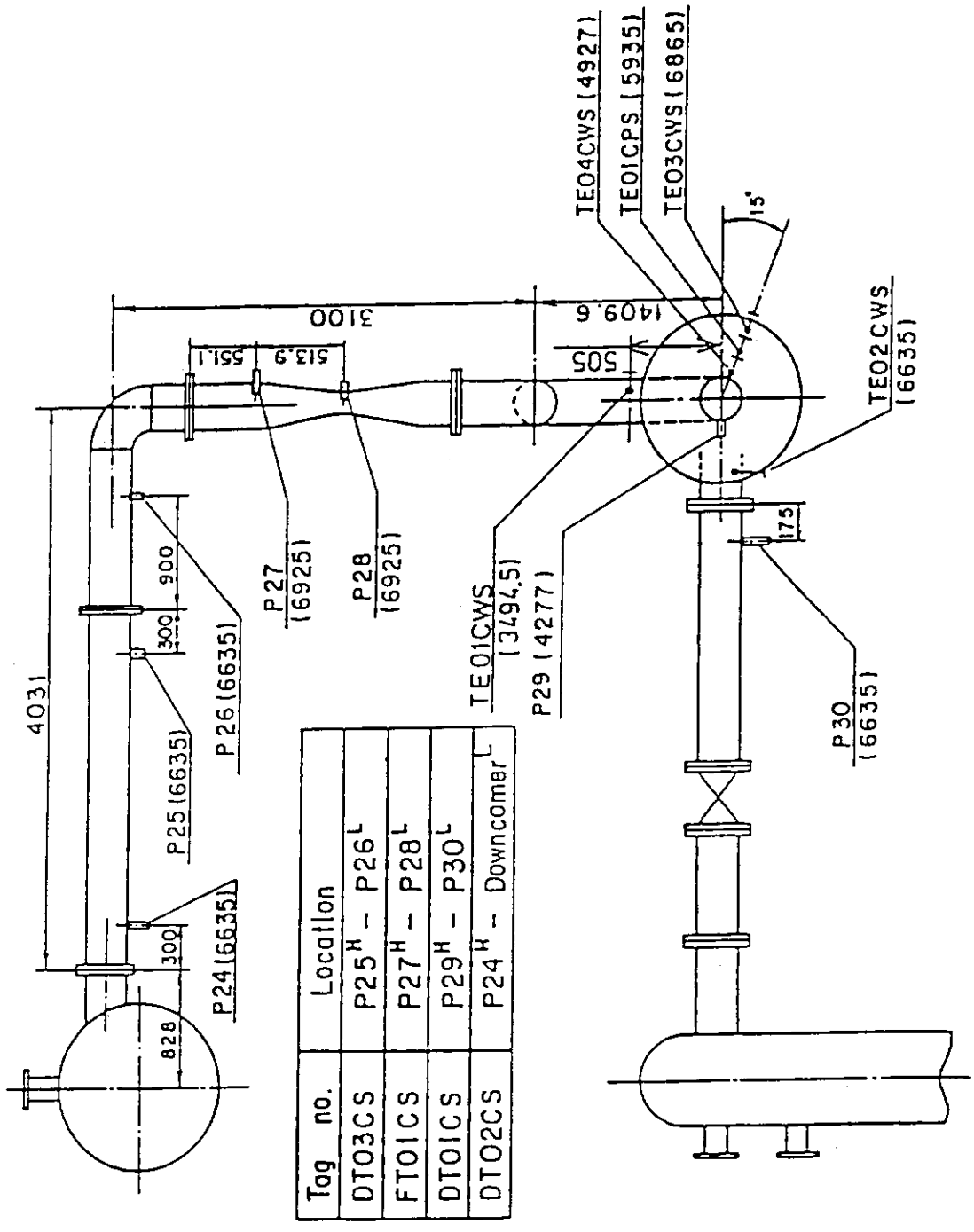

Fig. A-27 Locations of intact cold leg instrumentation

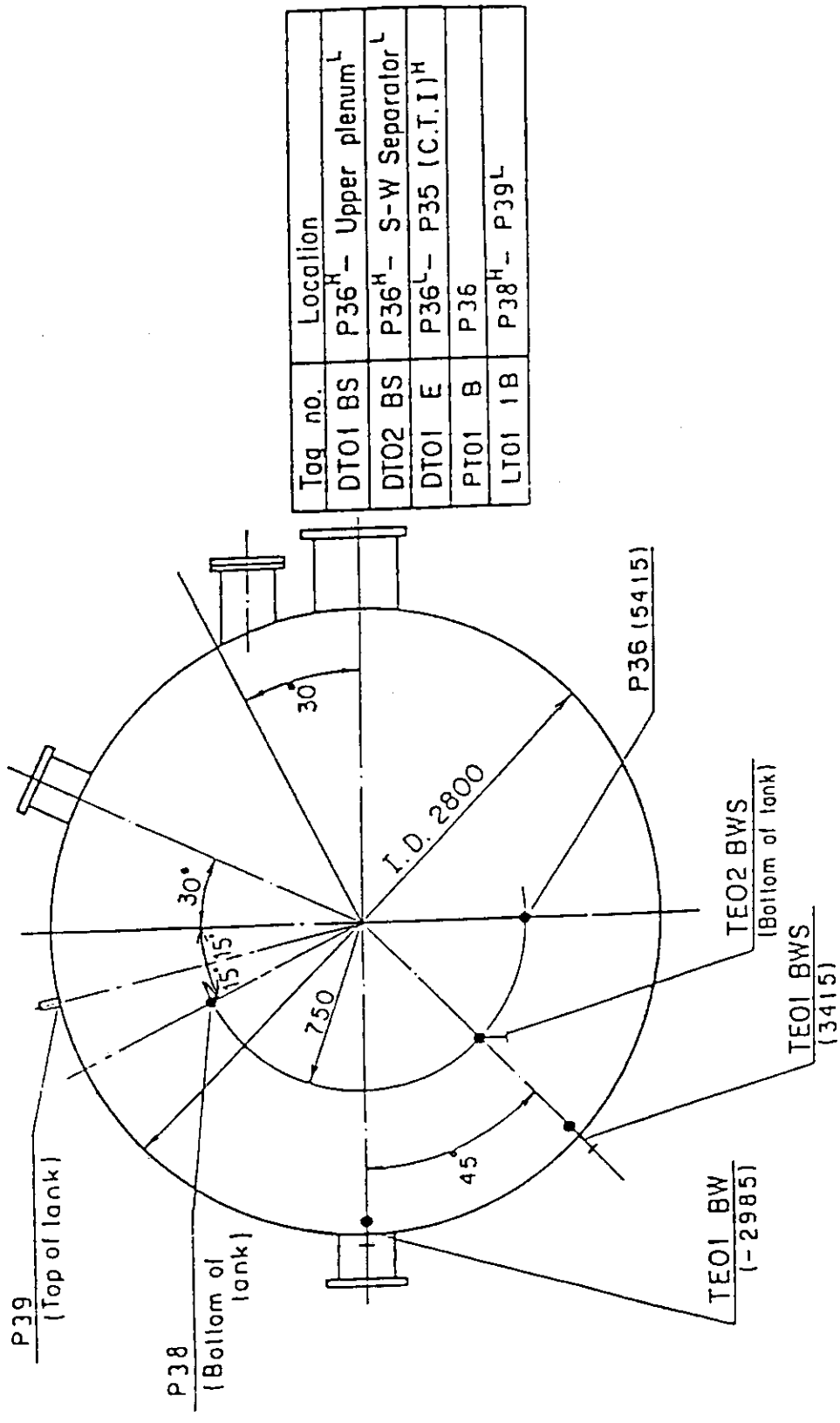

Fig. A-28 Locations of containment Tank-II instrumentation

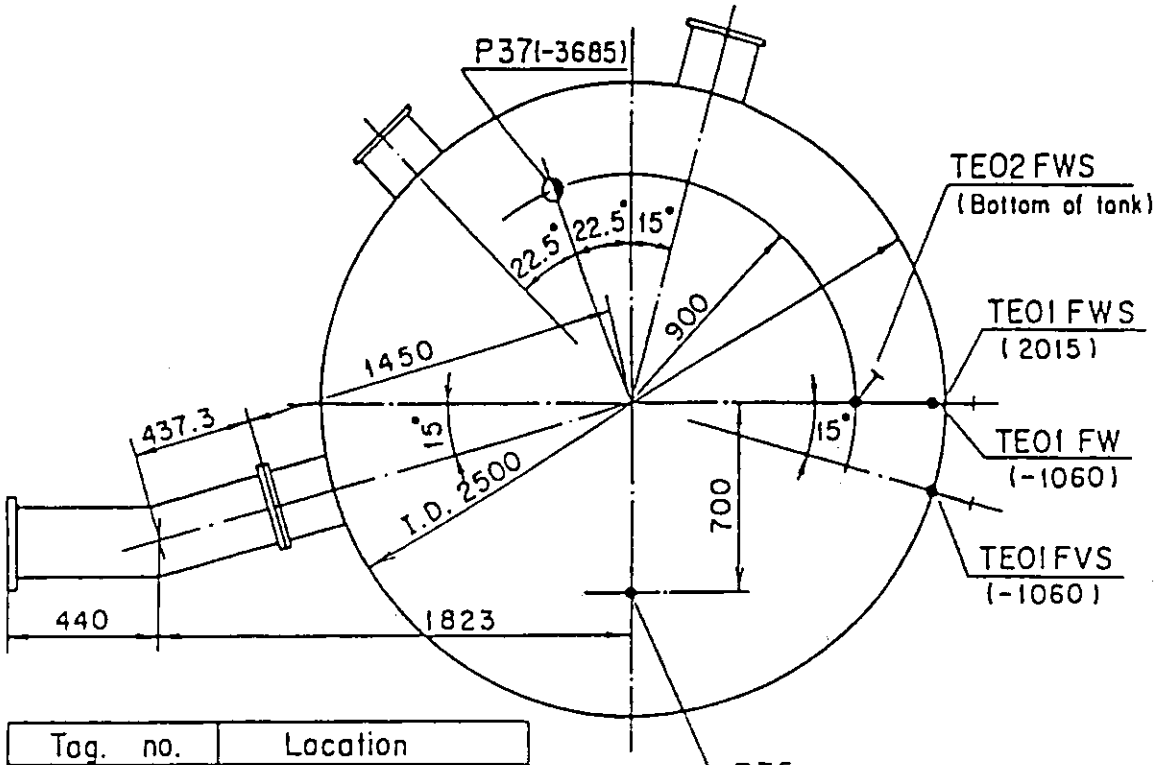

Tag. no.	Location
LT01 FS	$P35^{L}$ – $P37^{H}$
DT01 FS	$P35^{H}$ – $Downcomer^{L}$
DT01 E	$P35^{H}$ – P36(C.T. II)^{H}
PT01 F	P35

Fig. A-29 Locations of containment Tank-I instrumentation

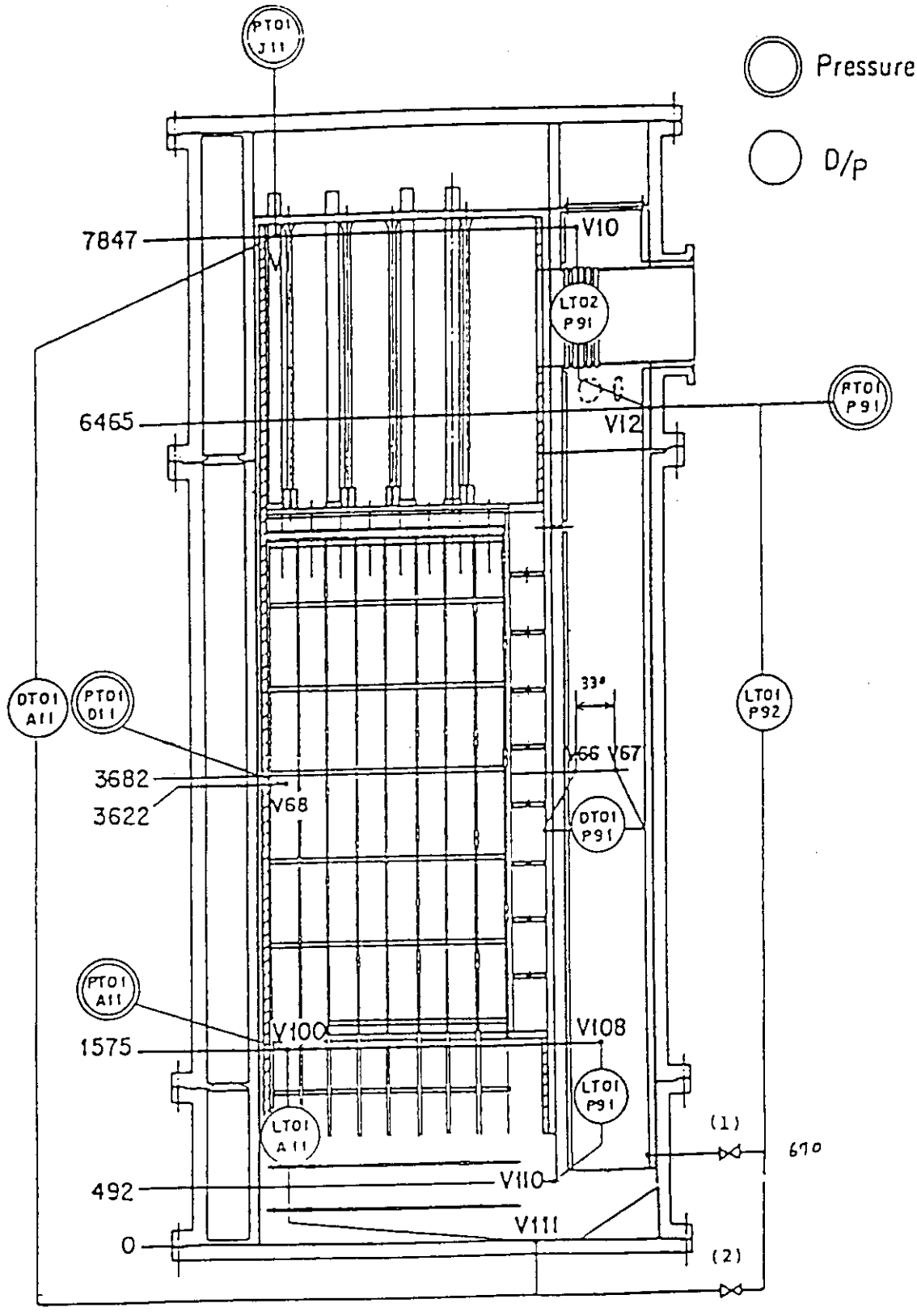

(1) used for lower plenum injection test
(the bottom of downcomer is blocked)
(2) used for the other tests

Fig. A-30 Location of pressure measurements in pressure vessel, differential pressure measurements between upper and lower plenums and liquid level measurements in downcomer and lower plenum

Appendix B Selected Data for Test S1-06 (Run 512)

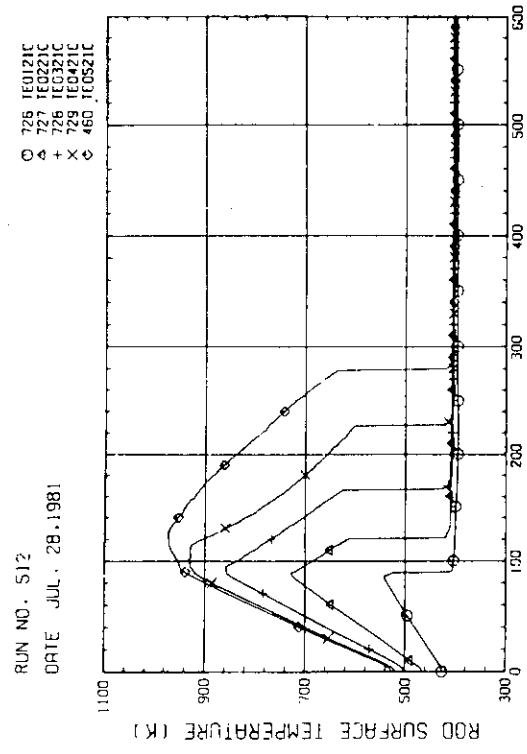

Fig. B-1 Heater rod temperature (Bundle 1-1C, Lower half)

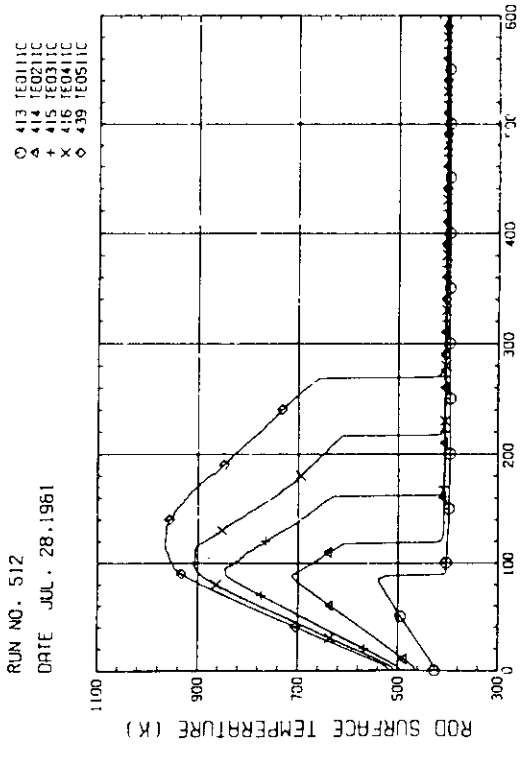

Fig. B-2 Heater rod temperature (Bundle 1-1C, Upper half)

Fig. B-3 Heater rod temperature (Bundle 2-1C, Lower half)

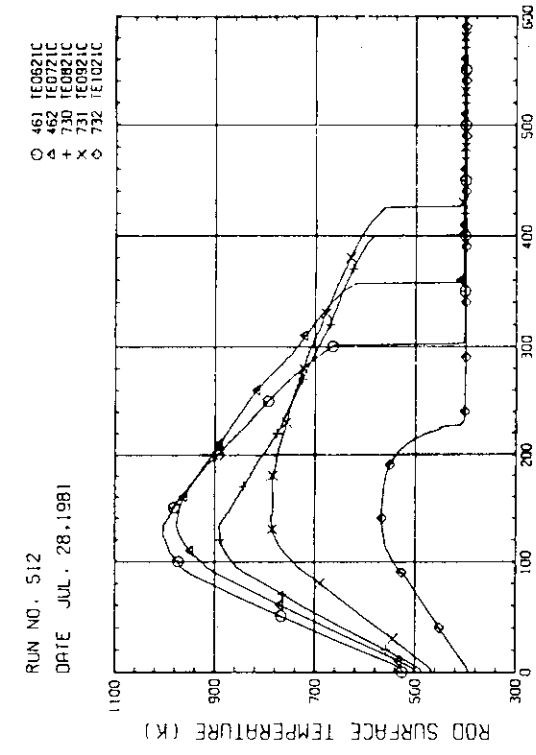

Fig. B-4 Heater rod temperature (Bundle 2-1C, Upper half)

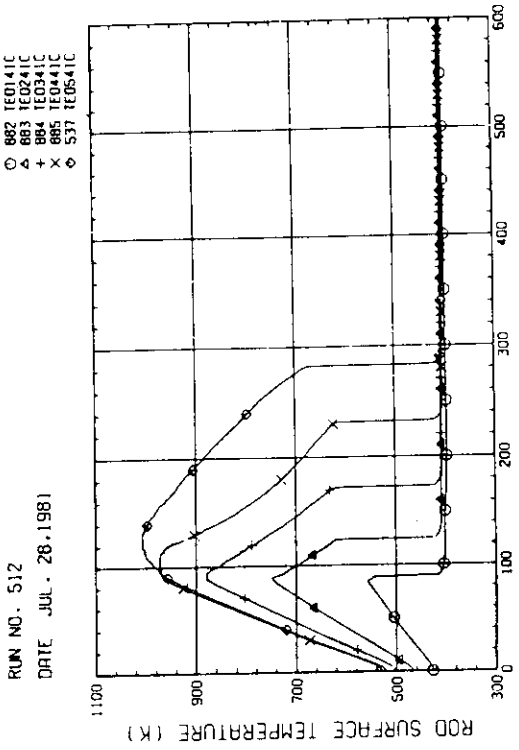

Fig. B-7 Heater rod temperature (Bundle 4-1C, Lower half)

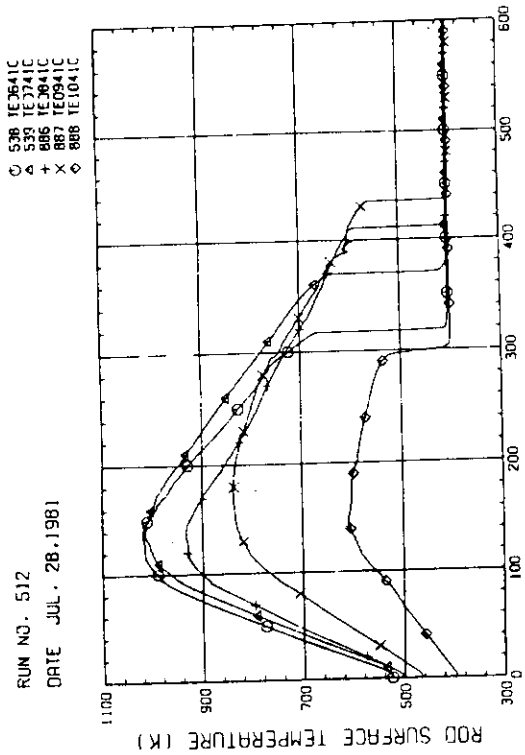

Fig. B-8 Heater rod temperature (Bundle 4-1C, Upper half)

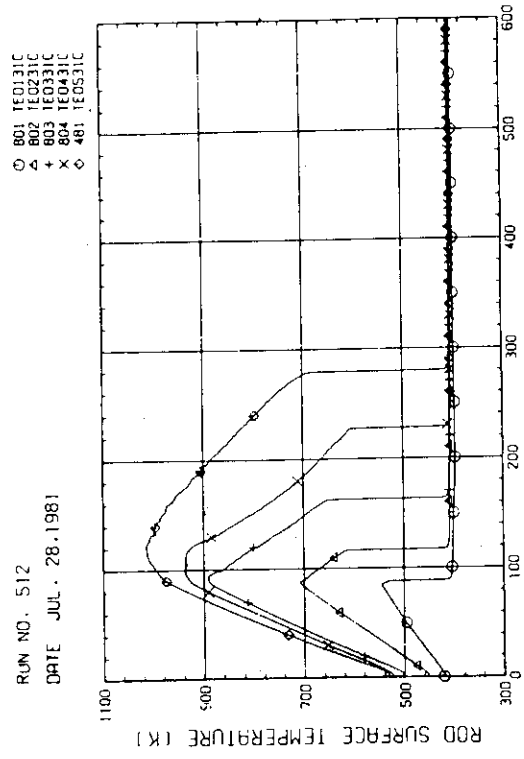

Fig. B-5 Heater rod temperature (Bundle 3-1C, Lower half)

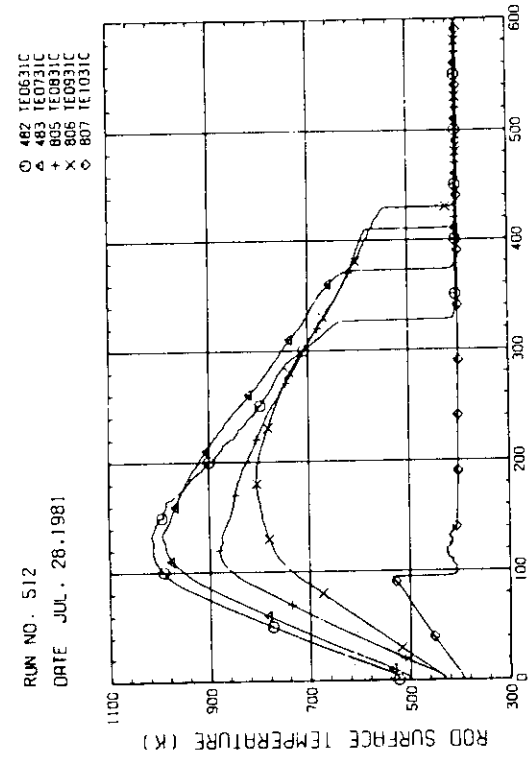

Fig. B-6 Heater rod temperature (Bundle 3-1C, Upper half)

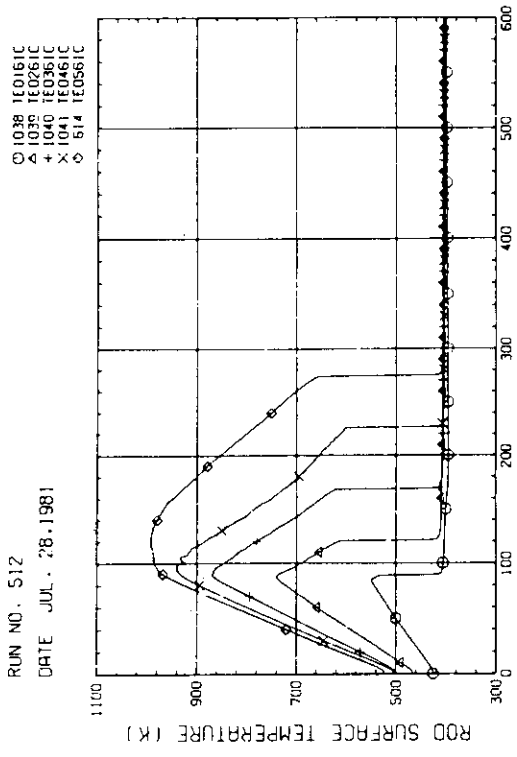

Fig. B-9 Heater rod temperature (Bundle 5-1C, Lower half)

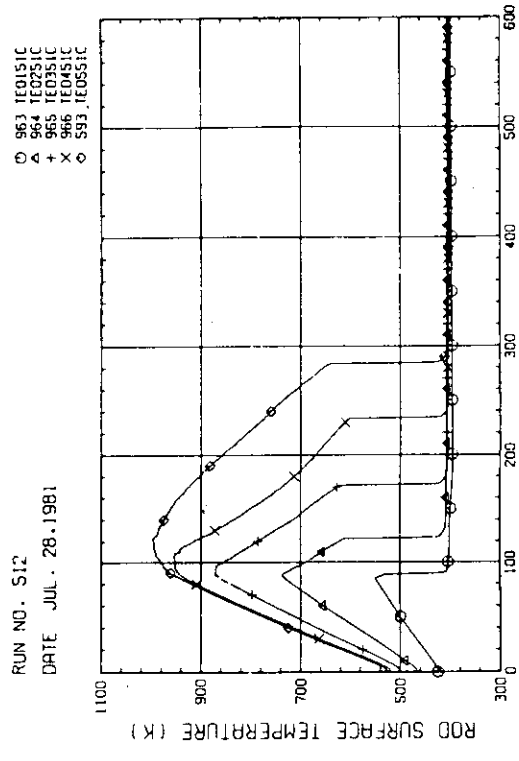

Fig. B-11 Heater rod temperature (Bundle 6-1C, Lower half)

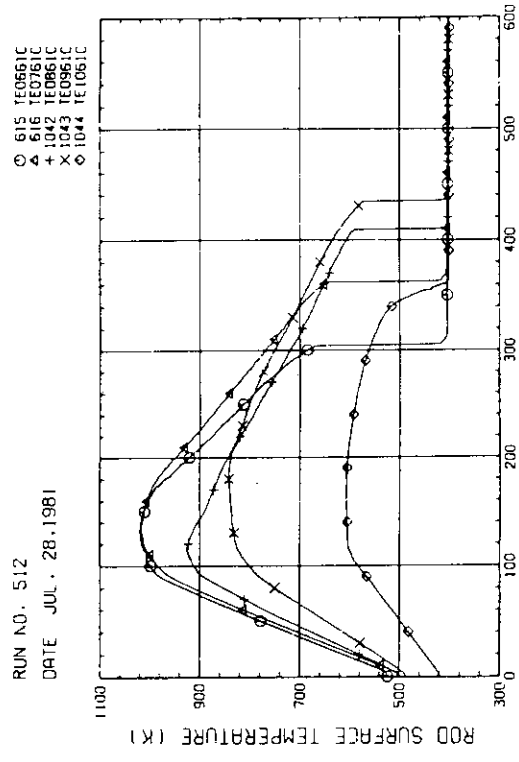

Fig. B-10 Heater rod temperature (Bundle 5-1C, Upper half)

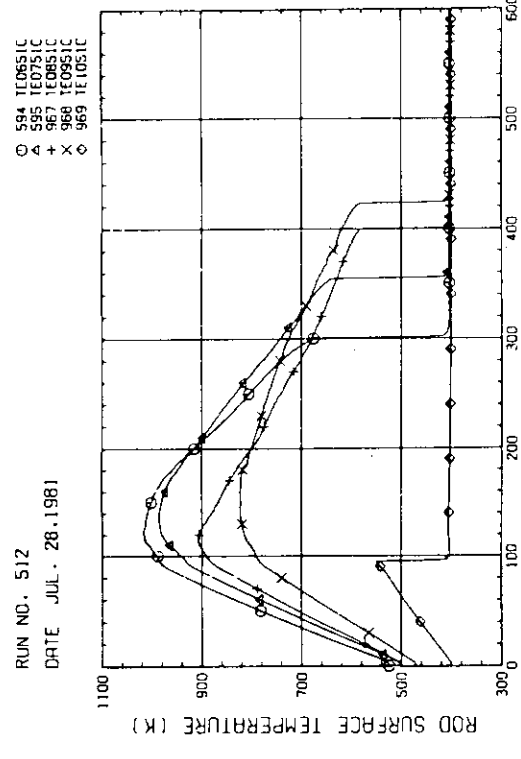

Fig. B-12 Heater rod temperature (Bundle 6-1C, Upper half)

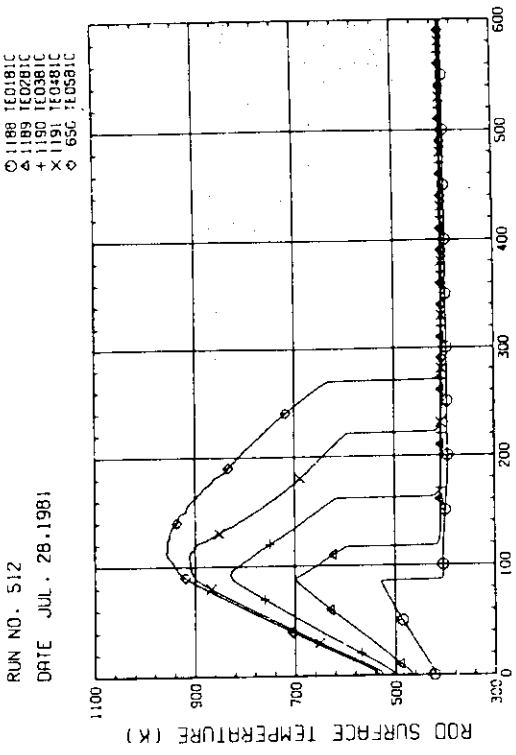

Fig. B-15 Heater rod temperature (Bundle 8-1C, Lower half)

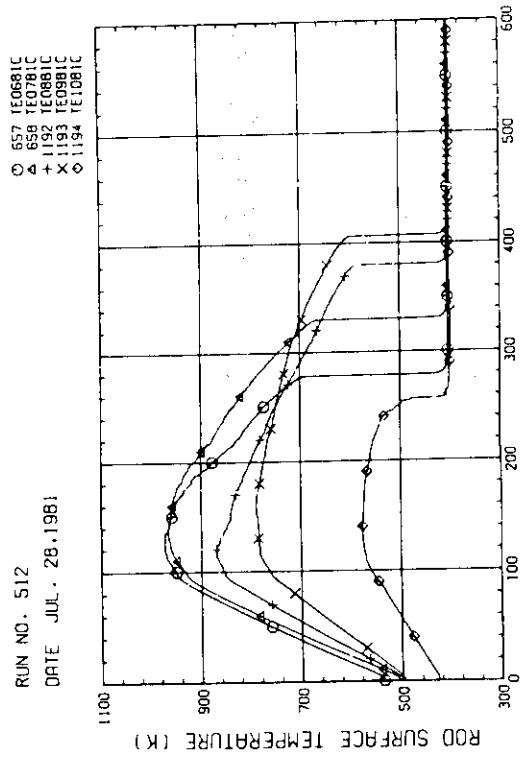

Fig. B-16 Heater rod temperature (Bundle 8-1C, Upper half

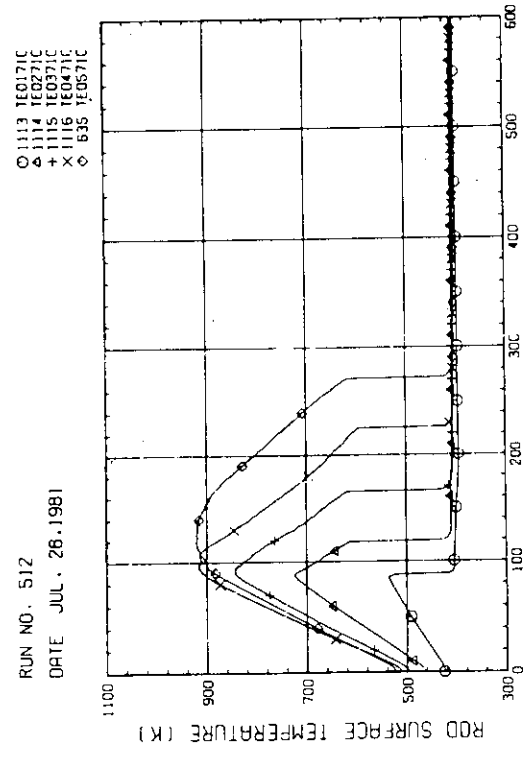

Fig. B-13 Heater rod temperature (Bundle 7-1C, Lower half)

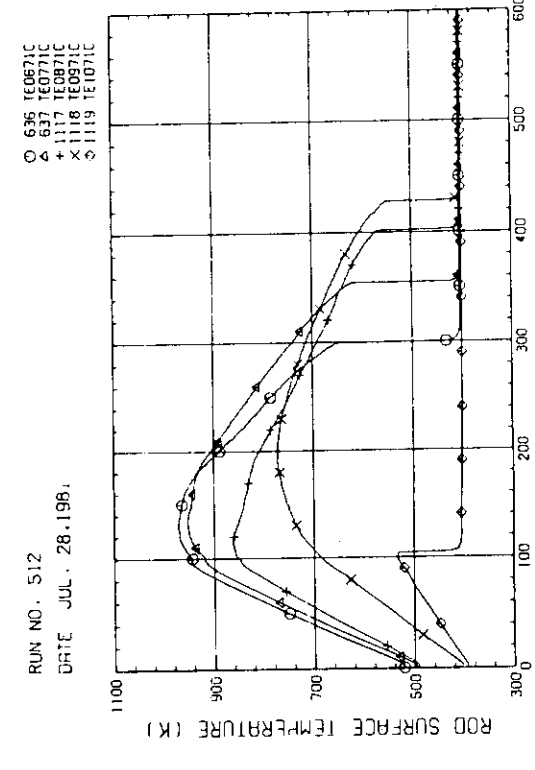

Fig. B-14 Heater rod temperature (Bundle 7-1C, Upper half)

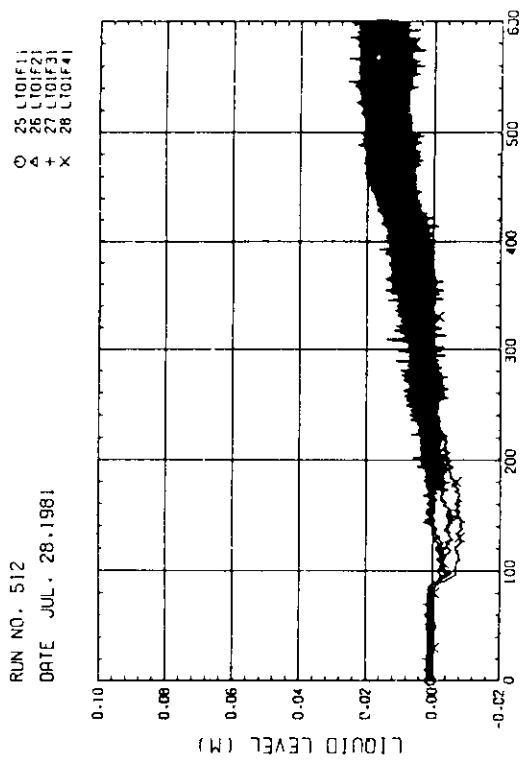

Fig. B-19 Liquid level above end box tie plate (Bundle 1,2,3,4)

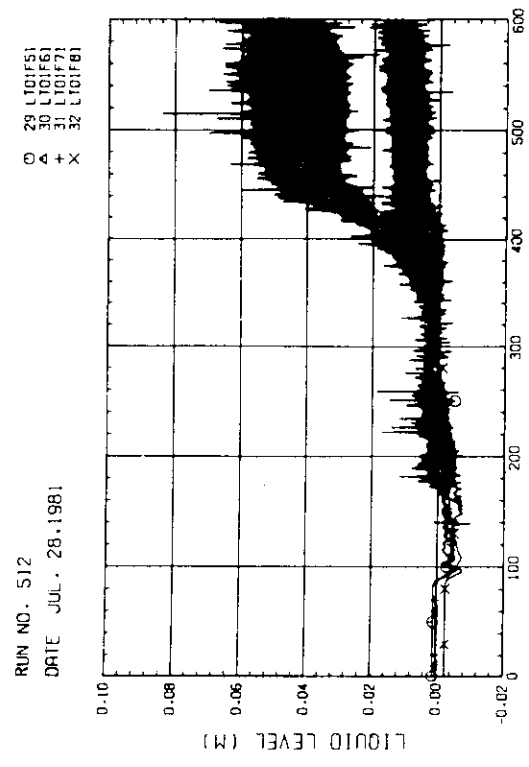

Fig. B-20 Liquid level above end box tie plate (Bundle 5,6,7,8)

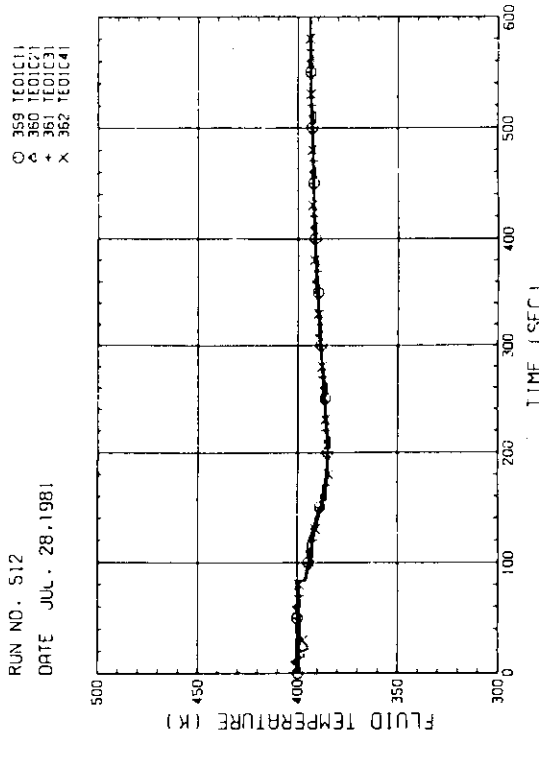

Fig. B-17 Fluid temperature at core inlet (Bundle 1,2,3,4,100mm below heated part)

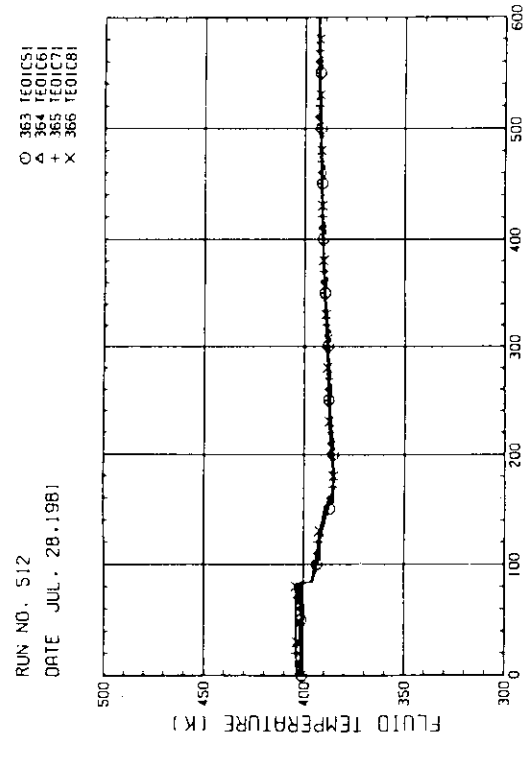

Fig. B-18 Fluid temperature at core inlet (Bundle 5,6,7,8,100mm below heated part)

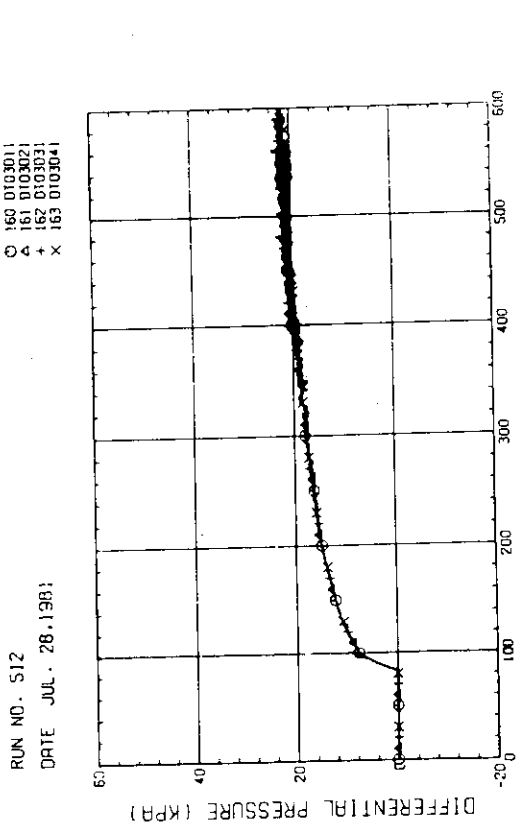

Fig. B-23 Differential pressure of core full height (Bundle 1,2,3,4)

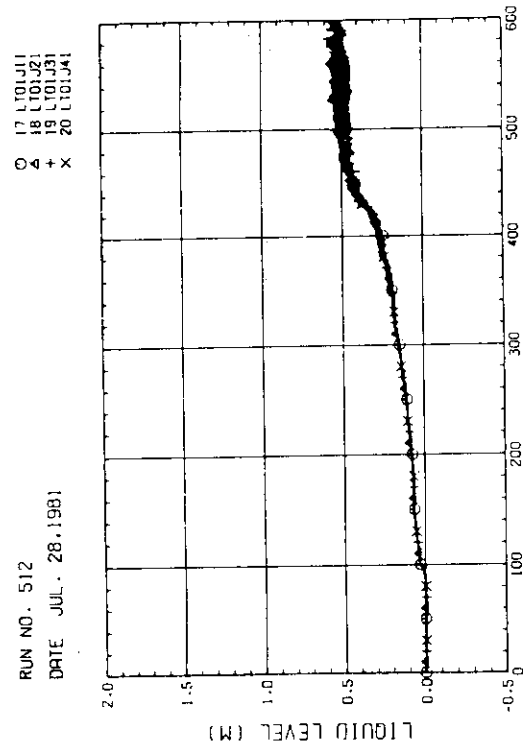

Fig. B-21 Liquid level above UCSP (Bundle 1,2,3,4)

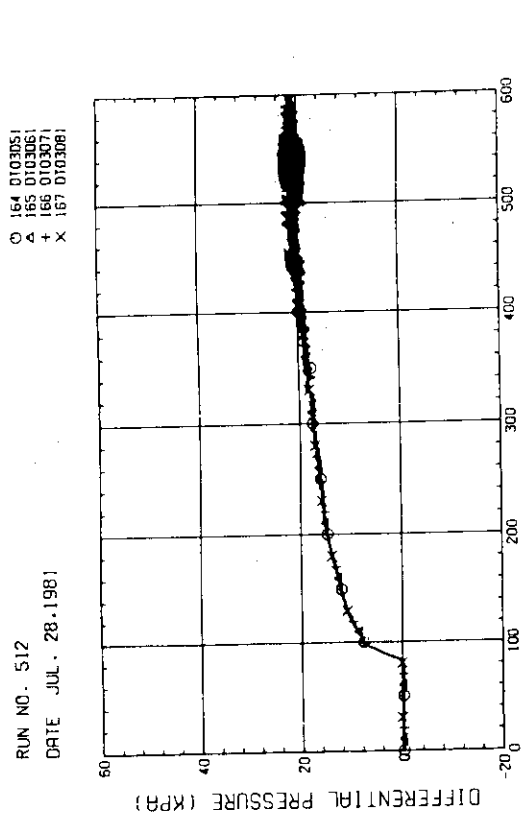

Fig. B-24 Differential pressure of core full height (Bundle 5,6,7,8)

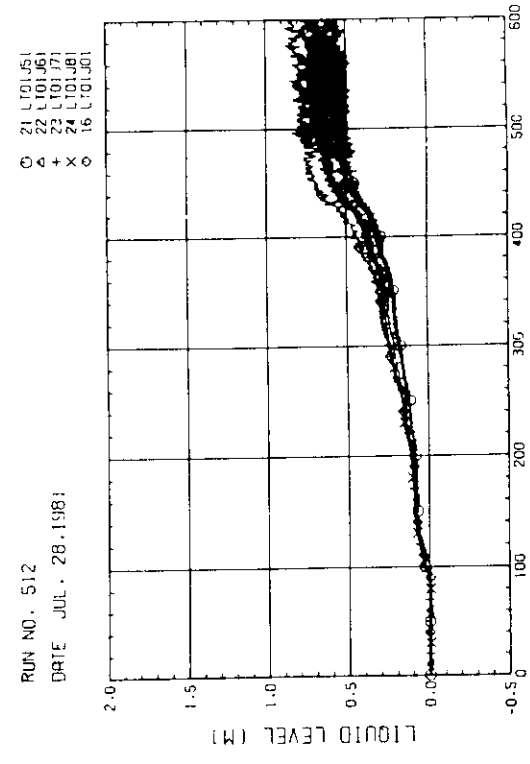

Fig. B-22 Liquid level above UCSP (Bundle 5,6,7,8 and core baffle)

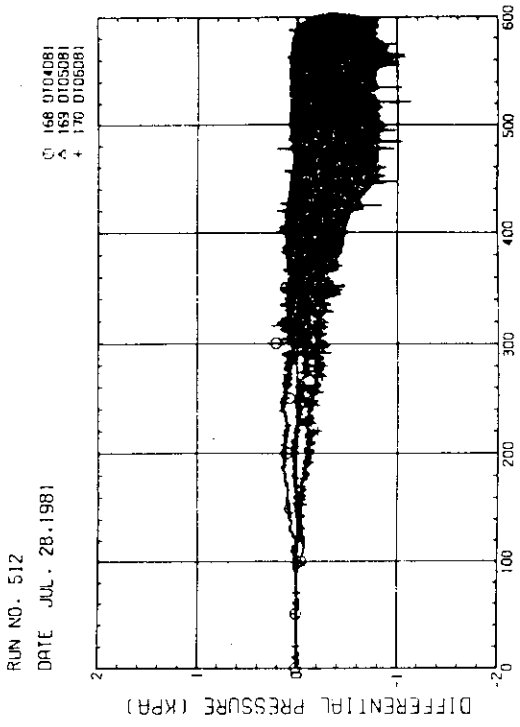

Fig. B-27 Differential pressure, horizontal, bundle 5-8 (04-below spacer 4, 05-below spacer 6, 06-below end box)

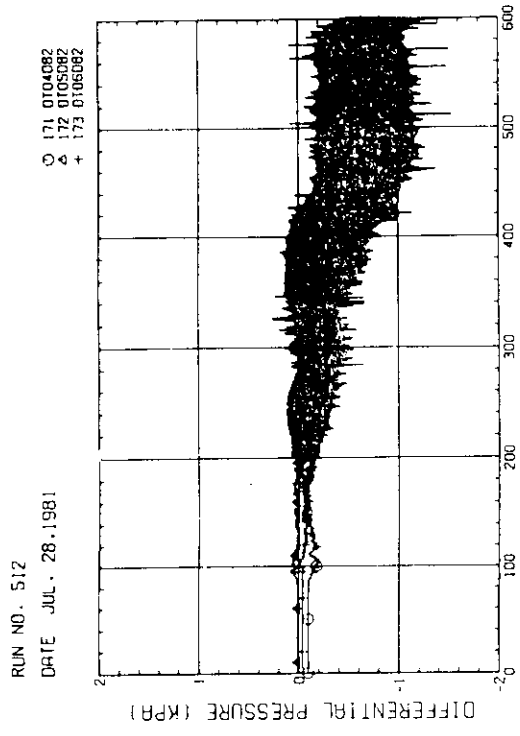

Fig. B-28 Differential pressure, horizontal, bundle 1-8 (04-below spacer 4, 05-below spacer 6, 06-below end box)

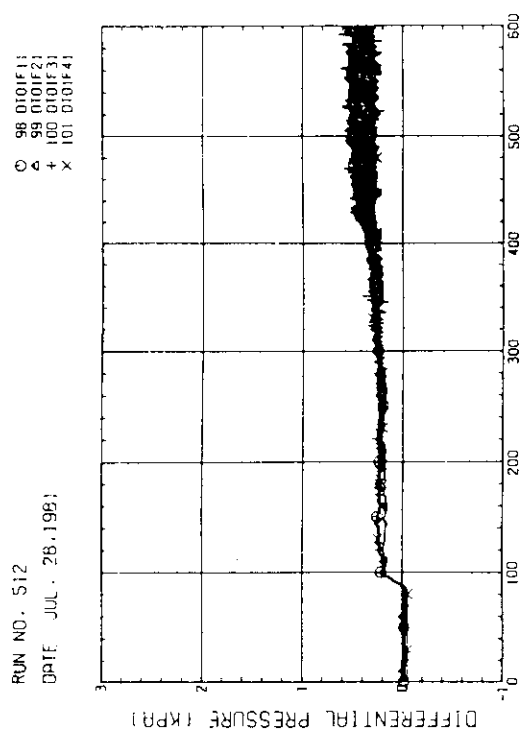

Fig. B-25 Differential pressure across end box tie plate (Bundle 1,2,3,4)

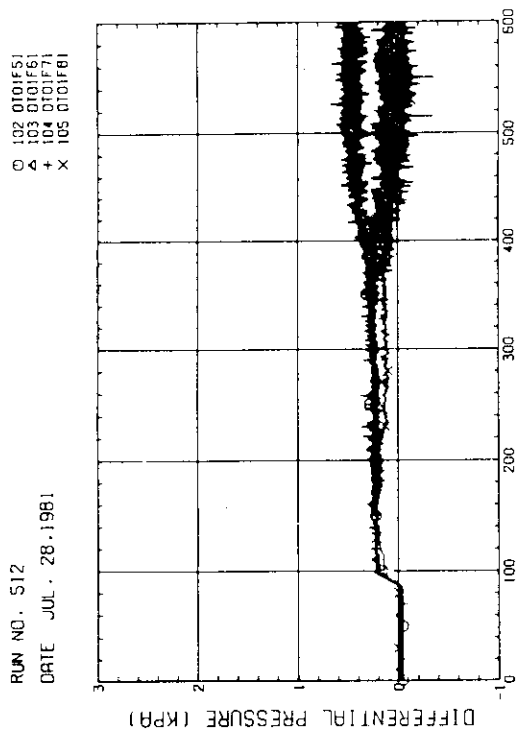

Fig. B-26 Differential pressure across end box tie plate (Bundle 5,6,7,8)

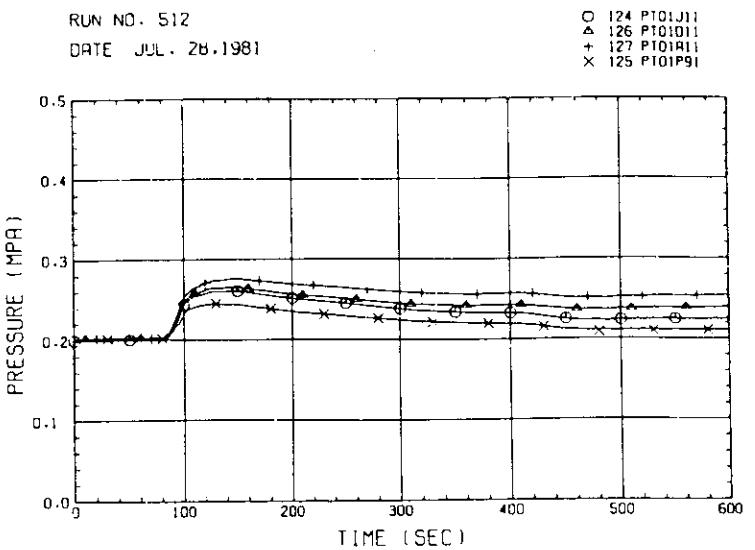

Fig. B-29 Pressure in PV (J-top of PV, D-core center, A-core inlet, P-below cold leg nozzle in downcomer)

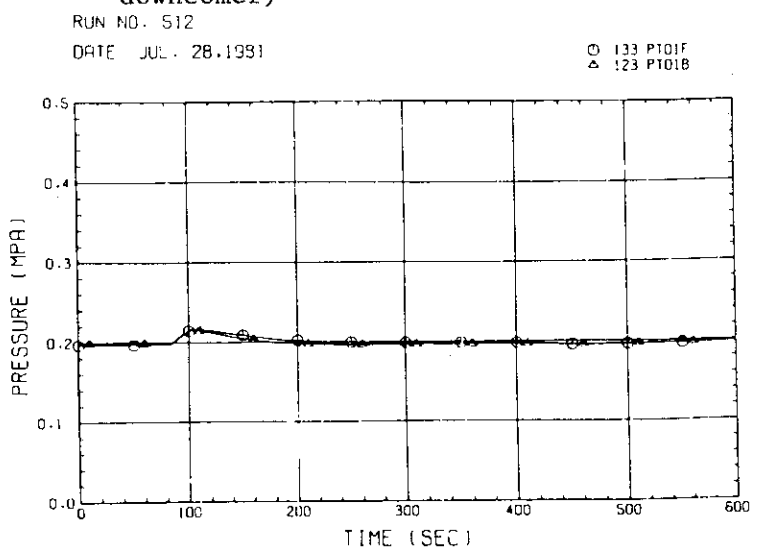

Fig. B-30 Pressure at top of containment tank-I and containment tank-II (F-con ainment tank-I, B-containment tank-II)

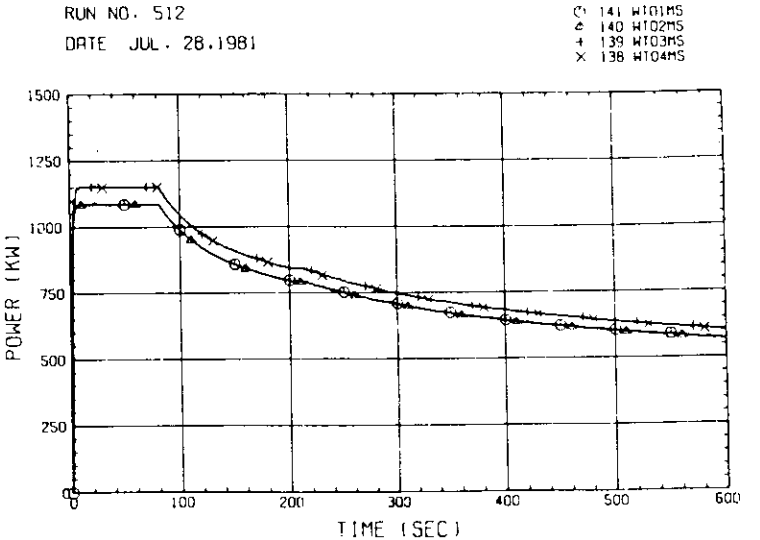

Fig. B-31 Bundle power (Bundle 1,2,3,4)

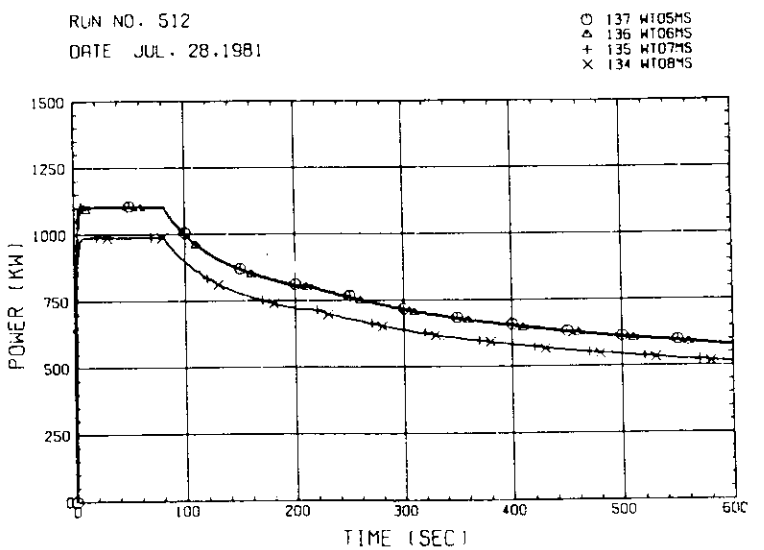

Fig. B-32 Bundle power (Bundle 5,6,7,8)

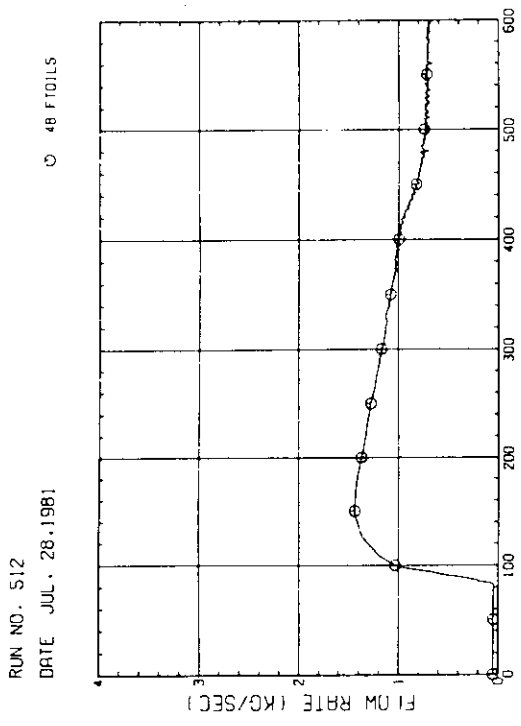

Fig. B-35 Mass flow rate of broken cold leg-steam/water separator side

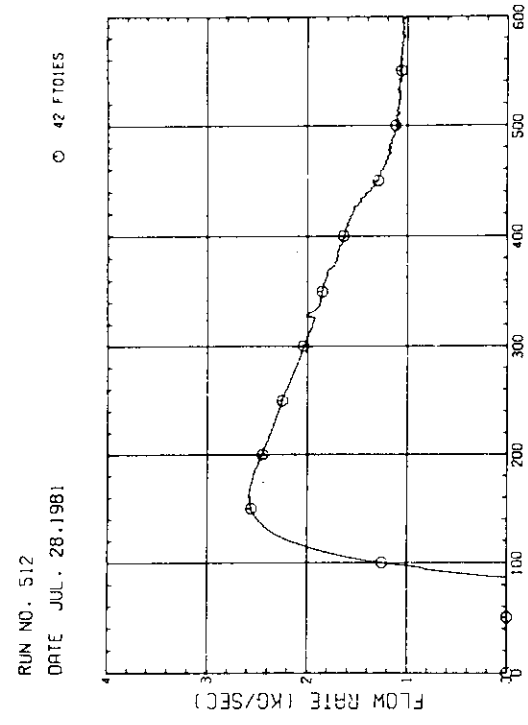

Fig. B-36 Mass flow rate from containment tank-I to containlent tank-II

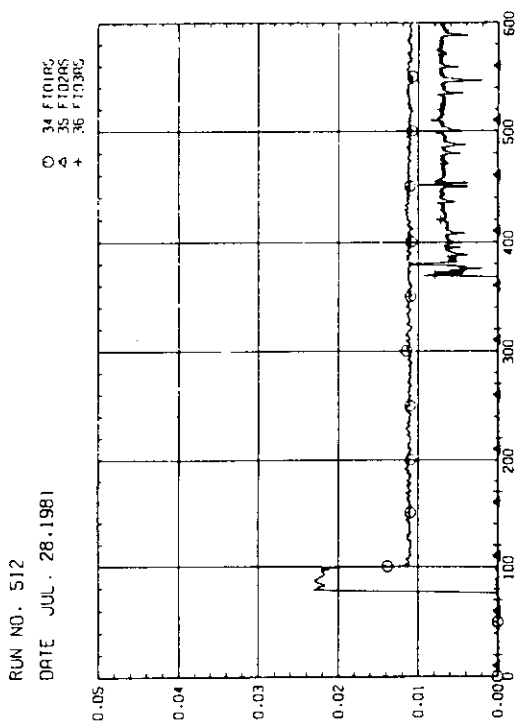

Fig. B-33 Flow rate of ECC water (01-Downcomer/Lower plenum/Hot leg, 02-Intact cold leg, 03-Broken cold leg)

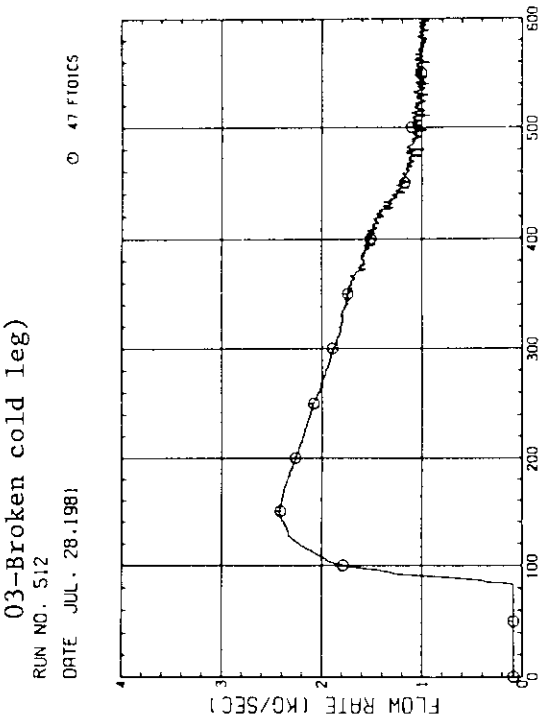

Fig. B-34 Mass flow rate of intact cold leg

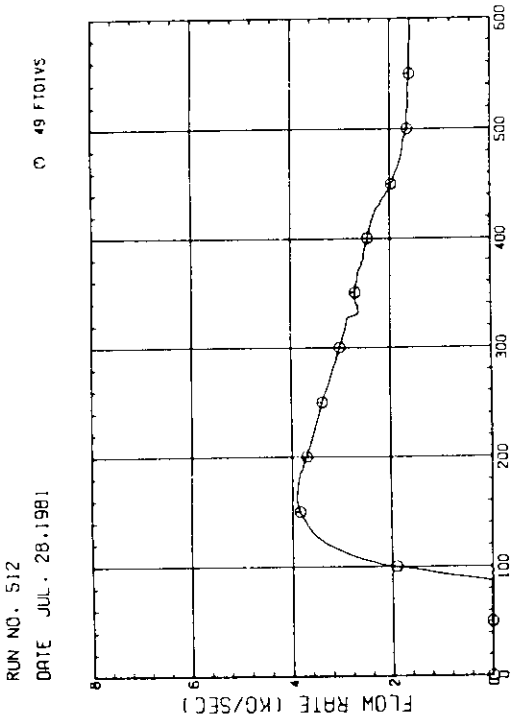

Fig. B-37 Steam flow rate of discharge from containment tank-II

Appendix C　Selected Data for Test S1-08 (Run 514)

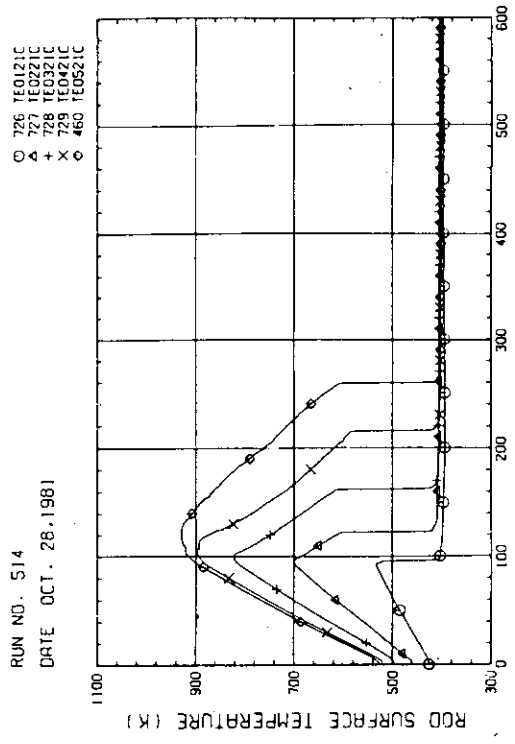

Fig. C-1 Heater rod temperature (Bundle 1-1C, Lower half)

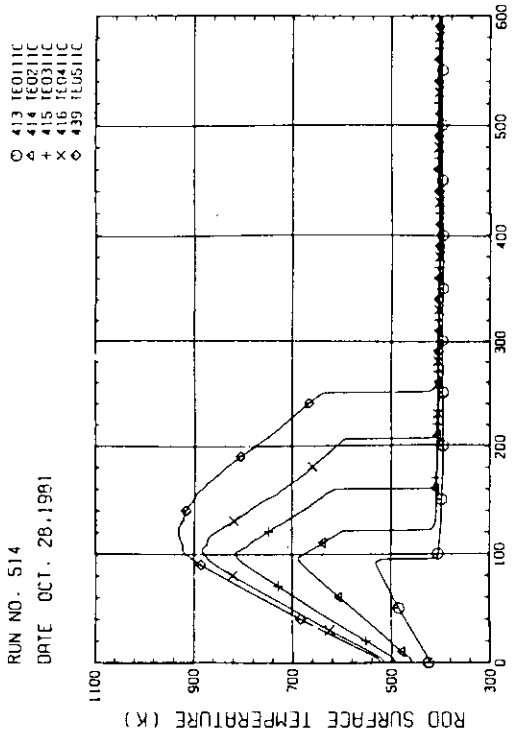

Fig. C-2 Heater rod temperature (Bundle 1-1C, Upper half)

Fig. C-3 Heater rod temperature (Bundle 2-1C, Lower half)

Fig. C-4 Heater rod temperature (Bundle 2-1C, Upperhalf)

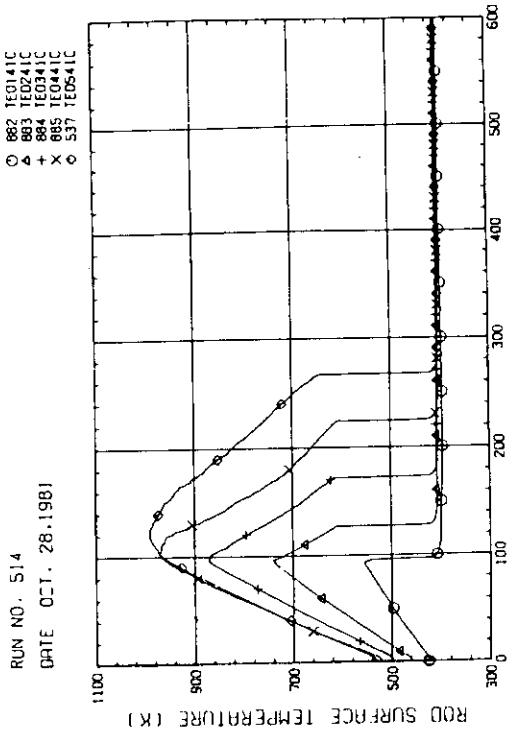

Fig. C-5 Heater rod temperature (Bundle 3-1C, Upper half)

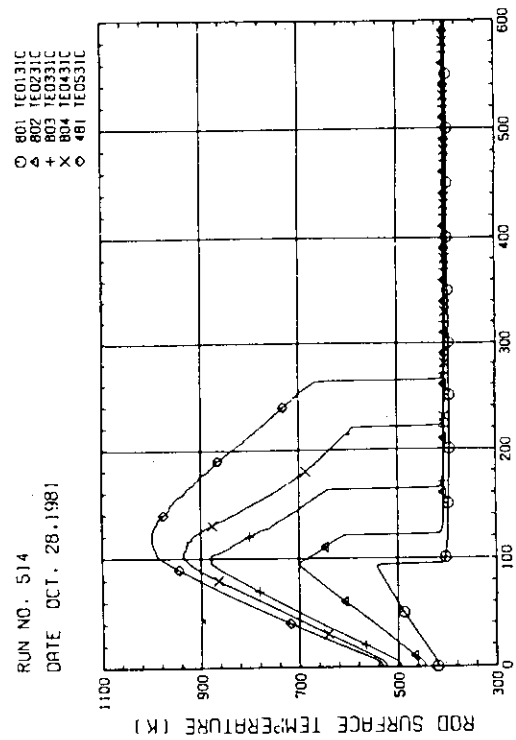

Fig. C-6 Heater rod temperature (Bundle 3-1C, Upper half)

Fig. C-7 Heater rod temperature (Bundle 4-1C, Lower half)

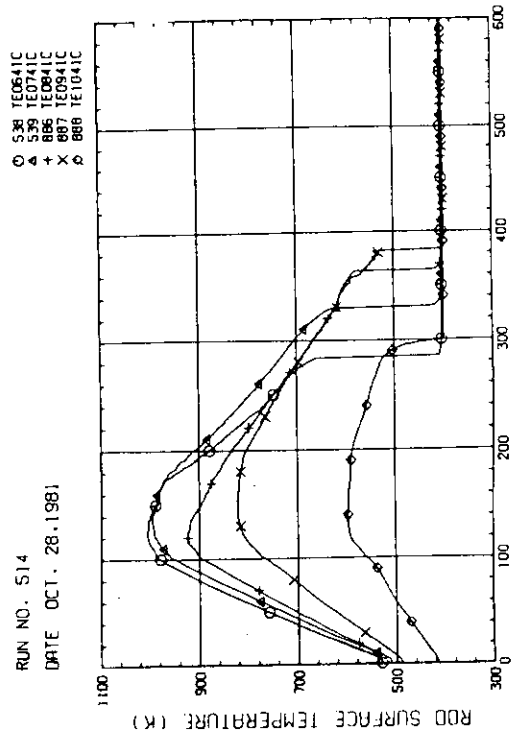

Fig. C-8 Heater rod temperature (Bundle 4-1C, Upper half)

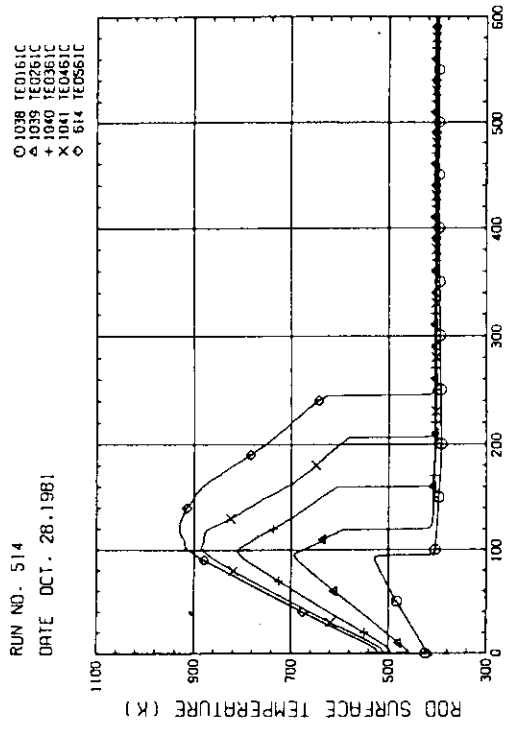

Fig. C-11 Heater rod temperature (Bundle 6-1C, Lower half)

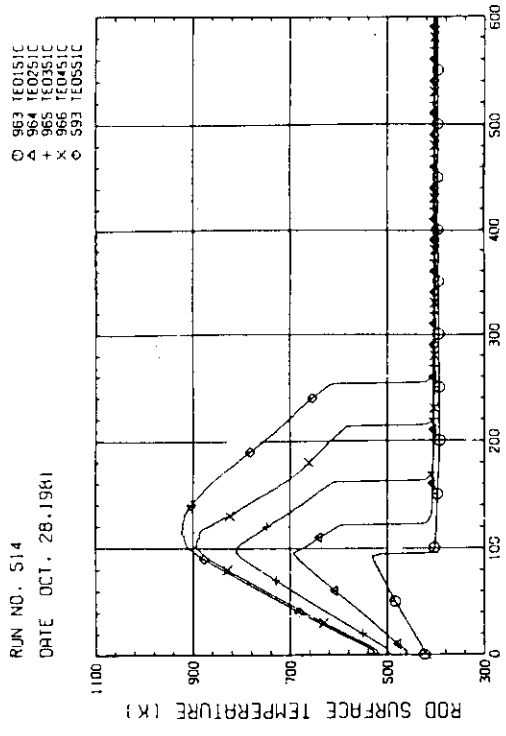

Fig. C-9 Heater temperature (Bundle 5-1C, Lower half)

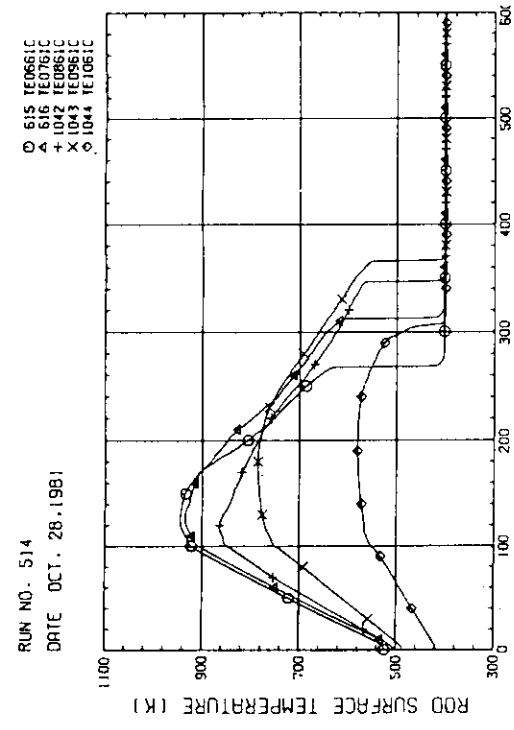

Fig. C-12 Heater rod temperature (Bundle 6-1C, Upper half)

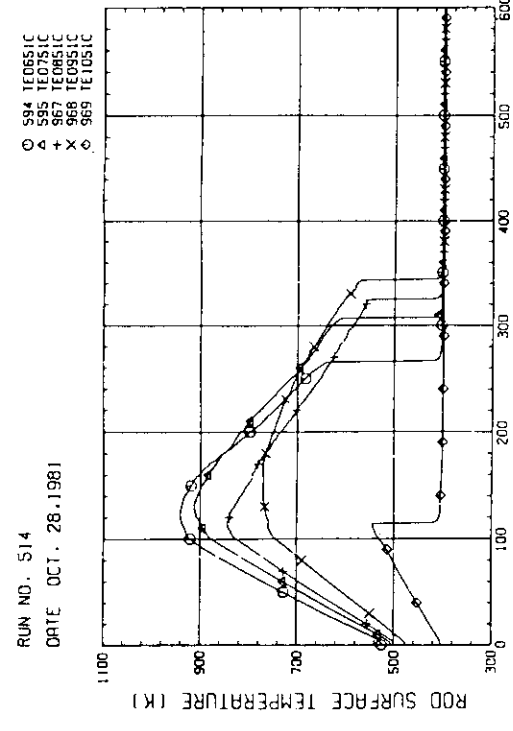

Fig. C-10 Heater rod temperature (Bundle 5-1C, Upper half)

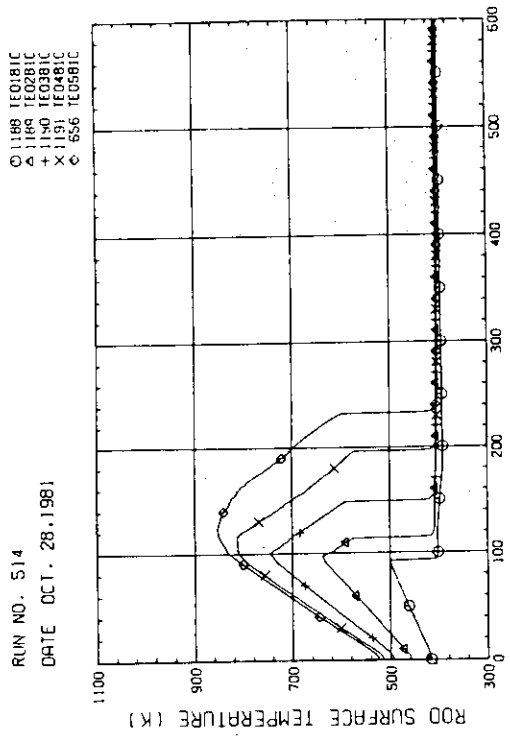

Fig. C-15 Heater rod temperature (Bundle 8-1C, Lower half)

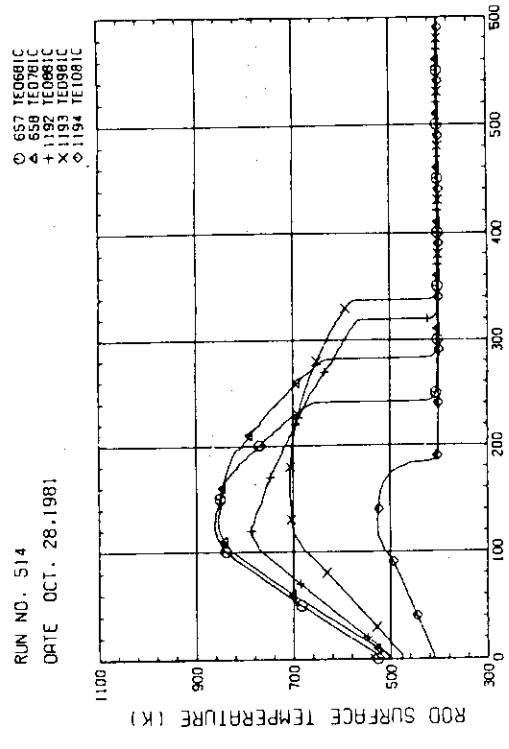

Fig. C-16 Heater rod temperature (Bundle 8-1C, Upper half)

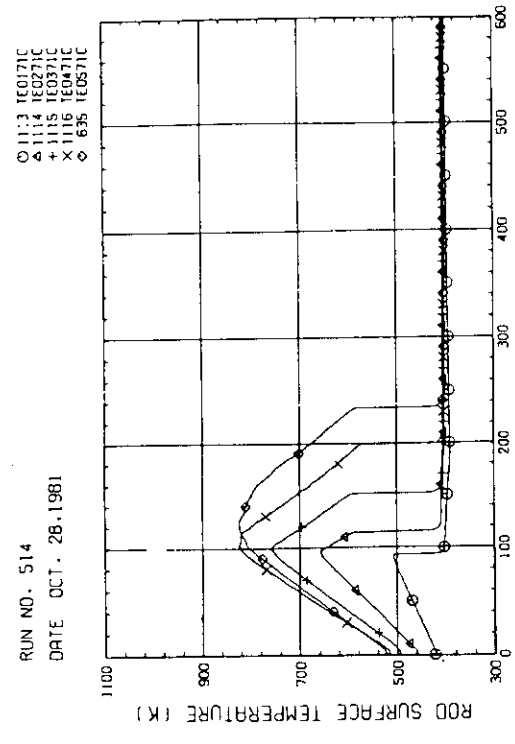

Fig. C-13 Heater rod temperature (Bundle 7-1C, Lower half)

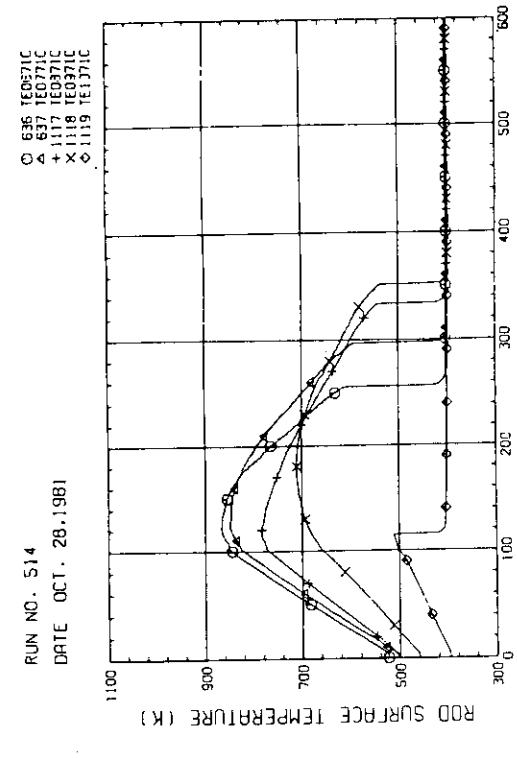

Fig. C-14 Heater rod temperature (Bundle 7-1C, Upper half)

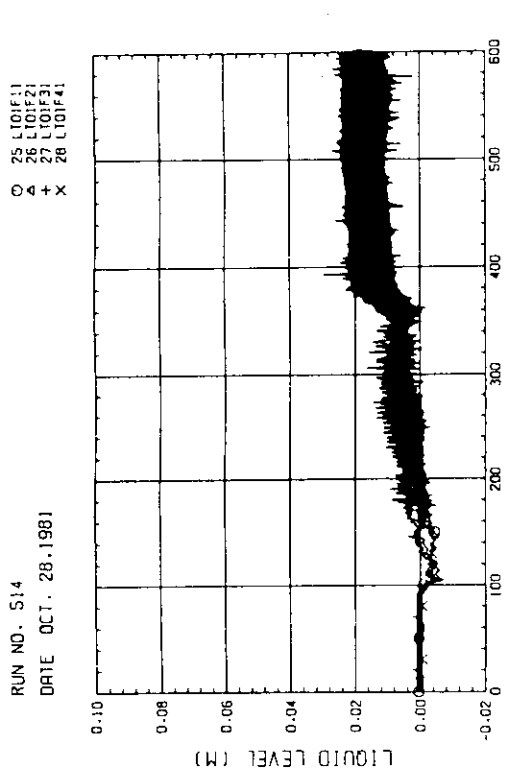

Fig. C-19 Liquid level above end box tie plate (Bundle 1,2,3,4)

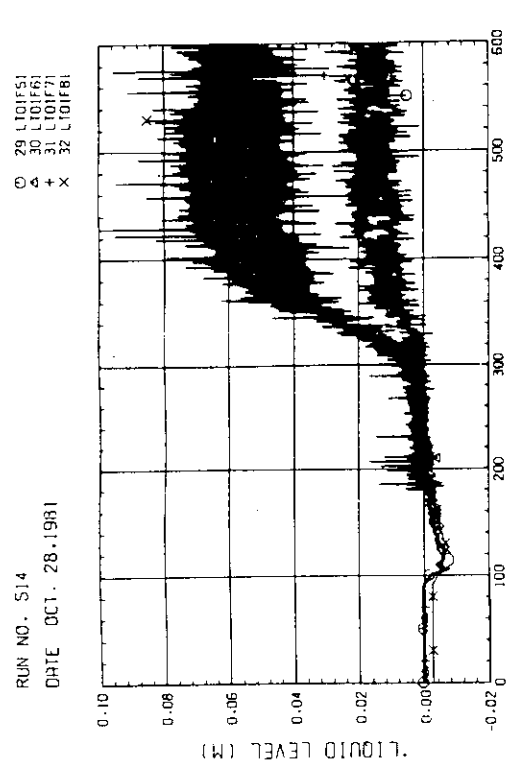

Fig. C-20 Liquid level above and box tie plate (Bundle 5,6,7,8)

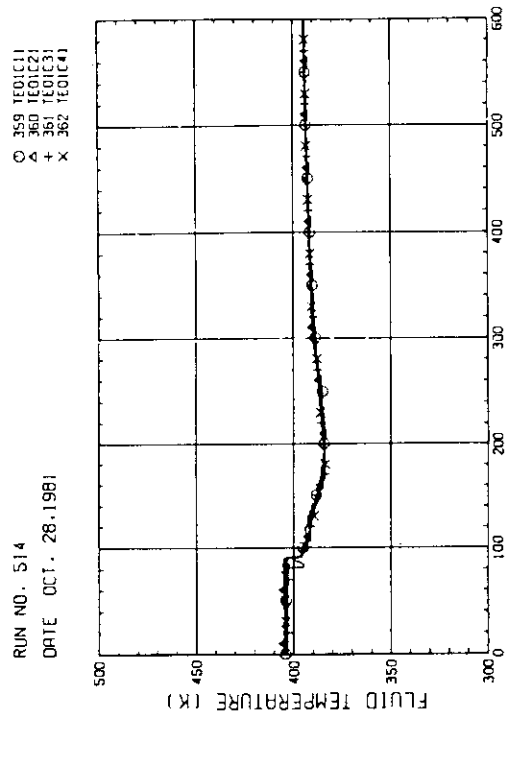

Fig. C-17 Fluid temperature at core inlet (Bundle 1,2,3,4,100mm below heated part)

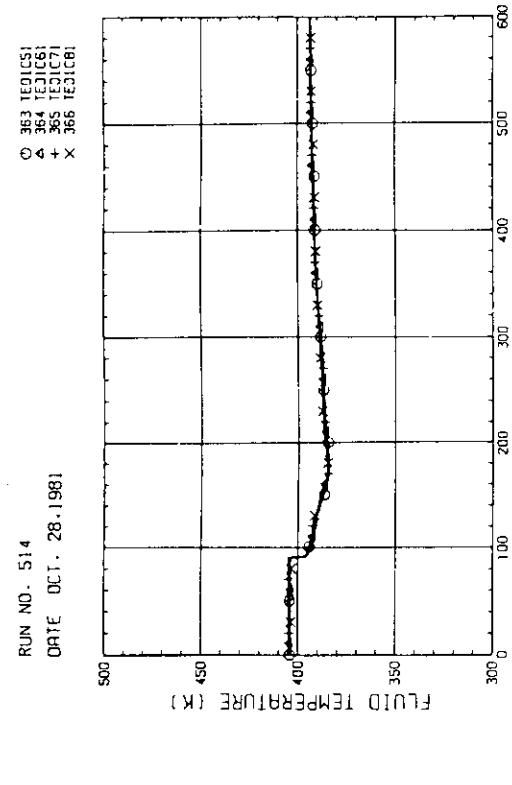

Fig. C-18 Fluid temperature at core inlet (Bundle 5,6,7,8,100mm below heated part)

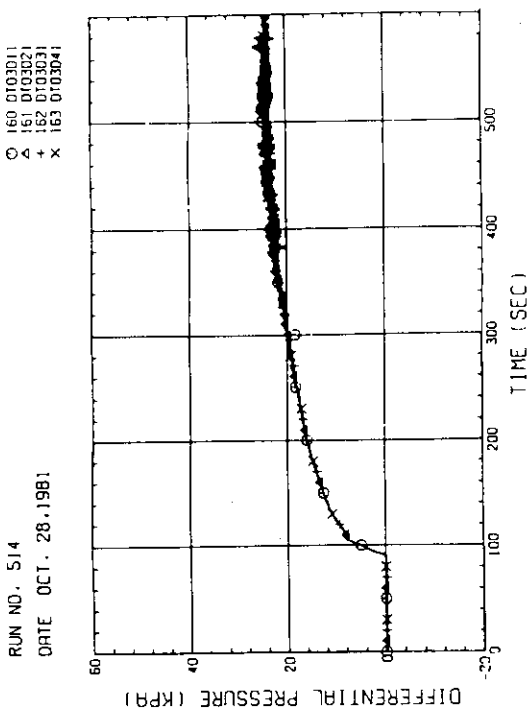

Fig. C-23 Differential pressure of core full height (Bundle 1,2,3,4)

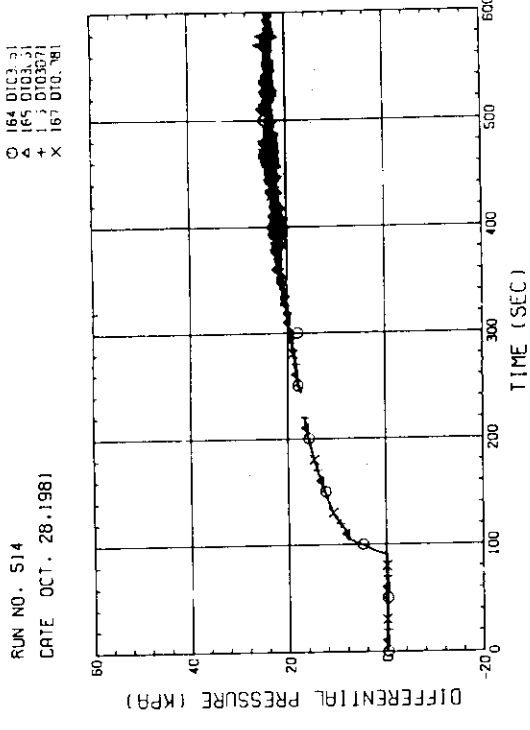

Fig. C-24 Differential pressure of core full height (Bundle 5,6,7,8)

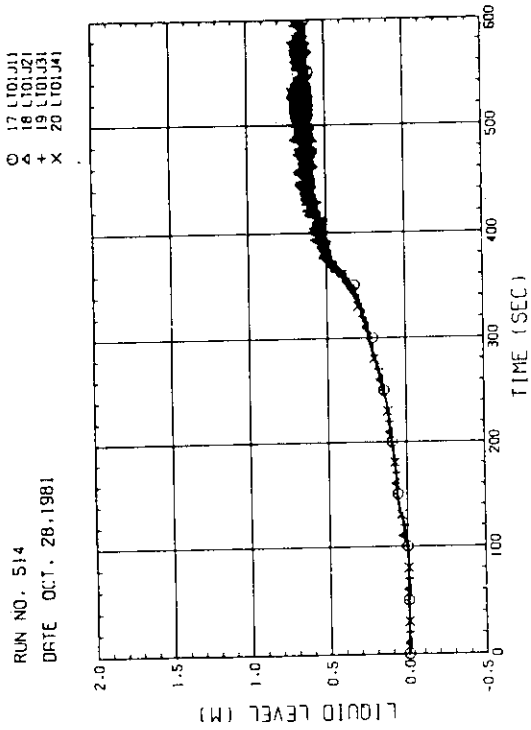

Fig. C-21 Liquid level above UCSP (Bundle 1,2,3,4)

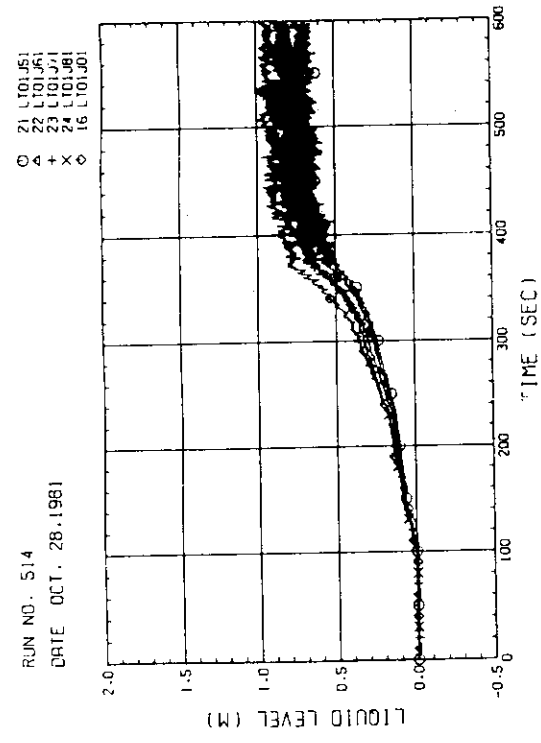

Fig. C-22 Liquid level above UCSP (Bundle 5,6,7,8 and core baffle)

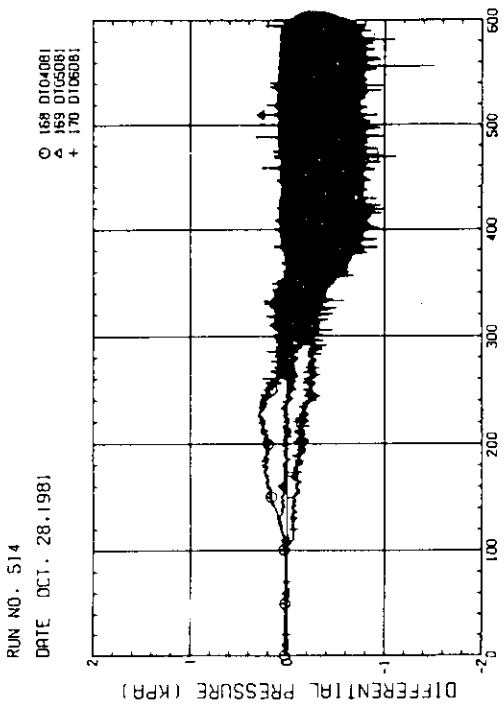

Fig. C-27 Differential pressure, horizontal, bundle 5-8 (04-below spacer 4, 05-below spacer 6, 06-below end box)

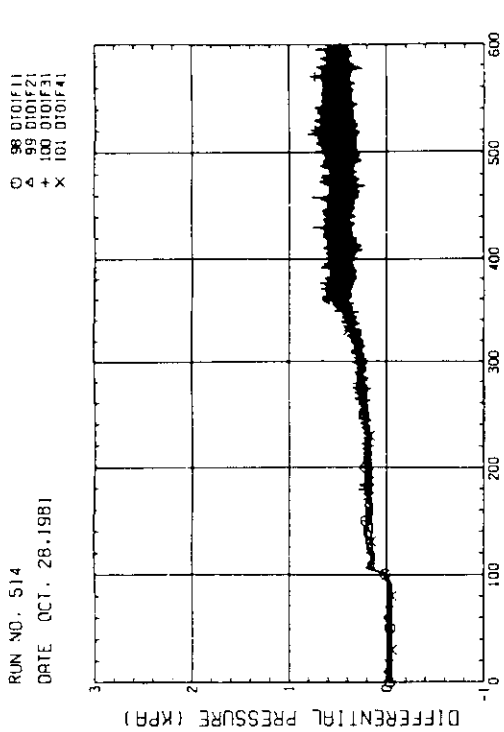

Fig. C-25 Differential pressure across end box tie plate (Bundle 1,2,3,4)

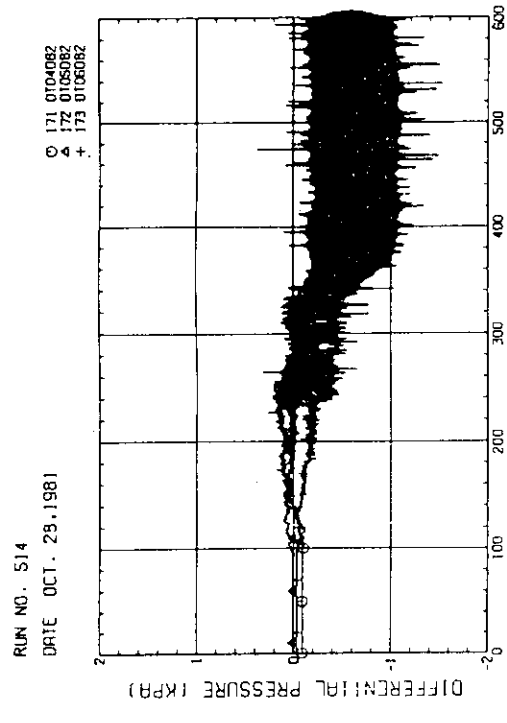

Fig. C-28 Differential pressure, horizontal, bundle 1-8 (04-below spacer 4, 05-below spacer 6, 06-below end box)

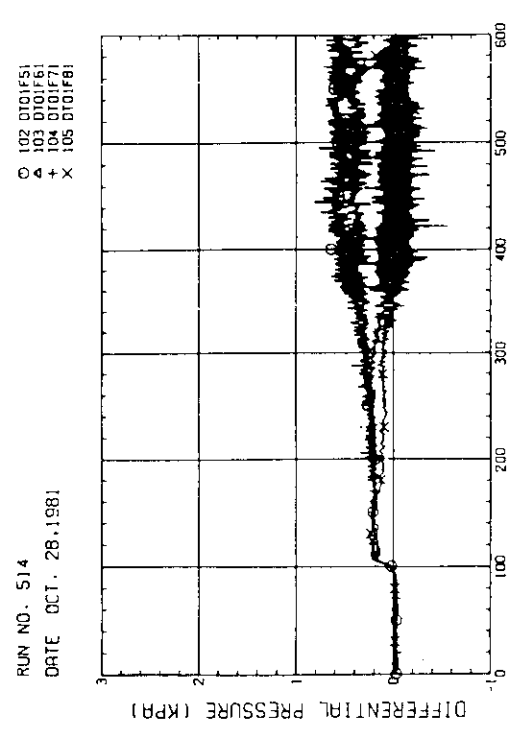

Fig. C-26 Differential pressure across end box tie plate (Bundle 5,6,7,8)

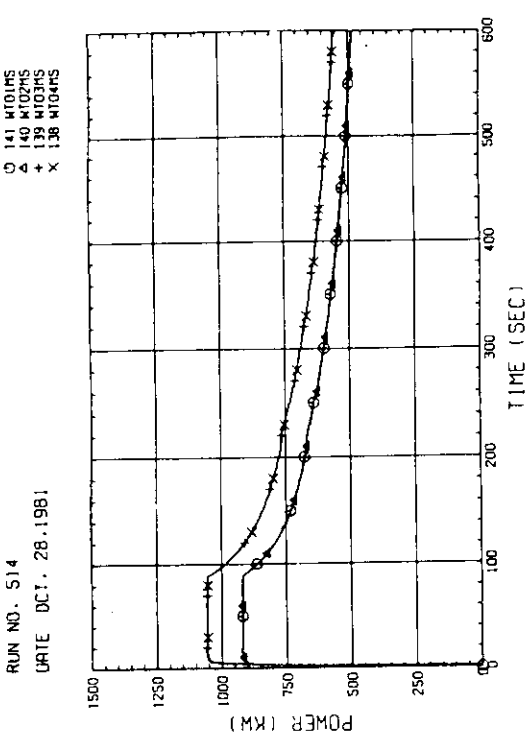

Fig. C-31 Bundle power
(Bundke 1,2,3,4)

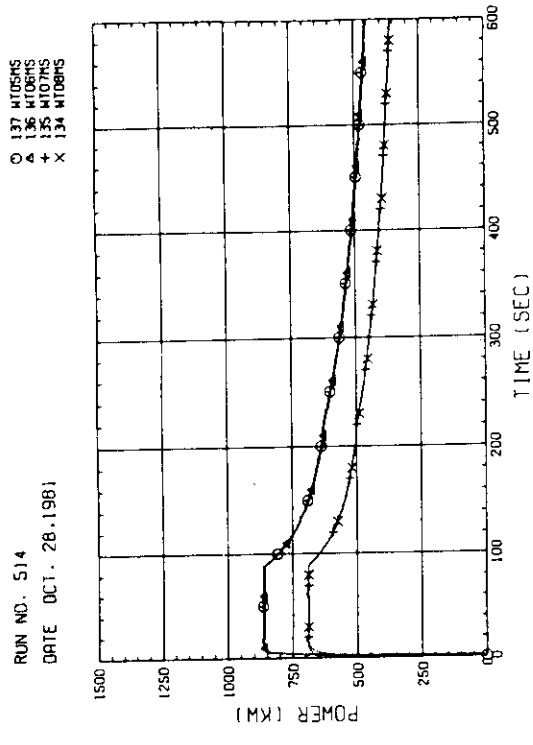

Fig. C-32 Bundle power
(Bundle 5,6,7,8)

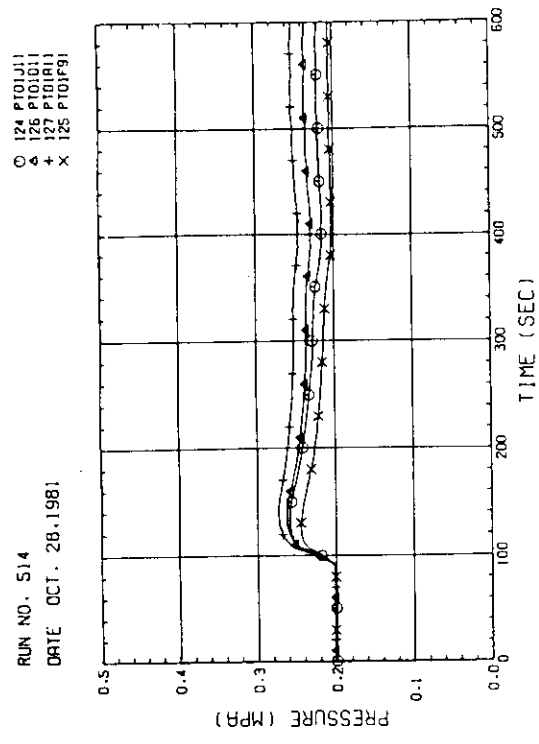

Fig. C-29 Pressure in PV (J-Top of PV, D-core center, A-core inlet, P-below cold leg nozzle in downcomer)

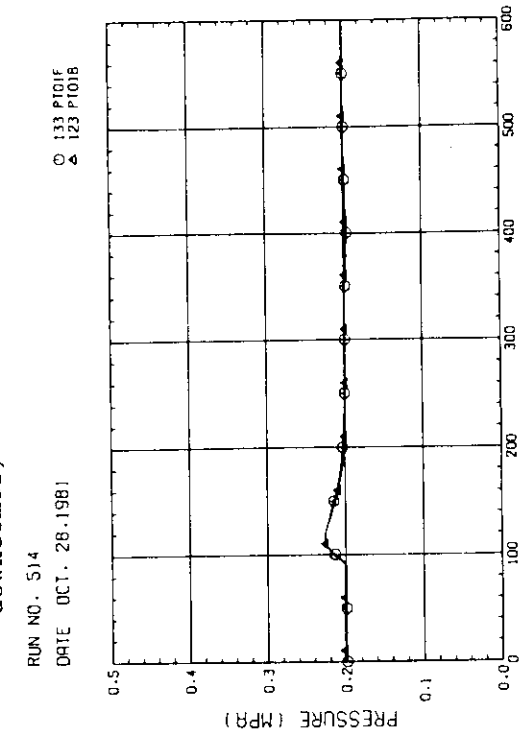

Fig. C-30 Pressure at top of containment tank-I and containment tank-II (F-containment tank-I, B-containment tank-II)

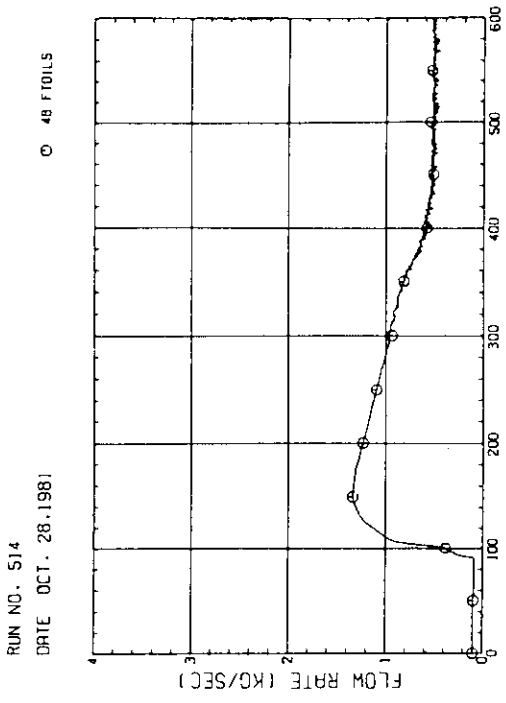

Fig. C-35 Mass flow rate of broken cold leg-steam/water separator side

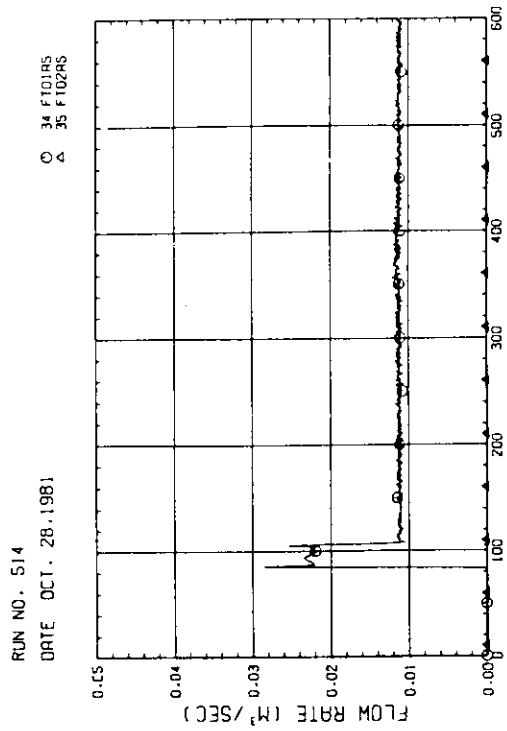

Fig. C-33 Flow rate of ECC water (01-Downcomer/Lower plenum/Hot leg, 02-intact cold leg, 03-Broken cold leg)

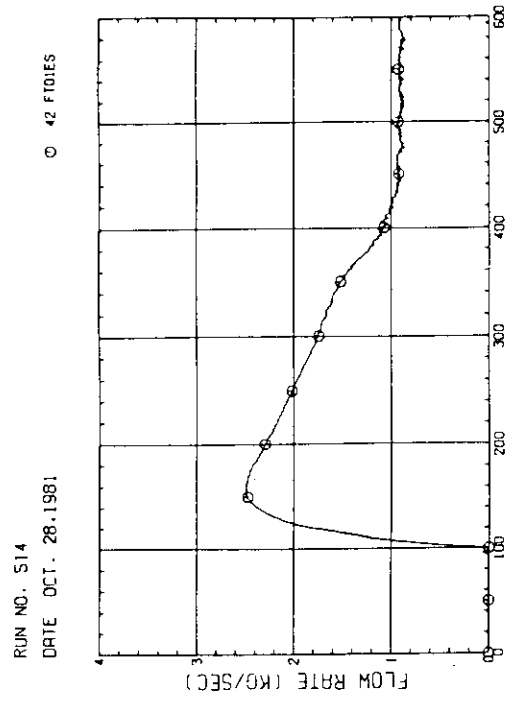

Fig. C-36 Mass flow rate from containment tank-I to containment tank-II

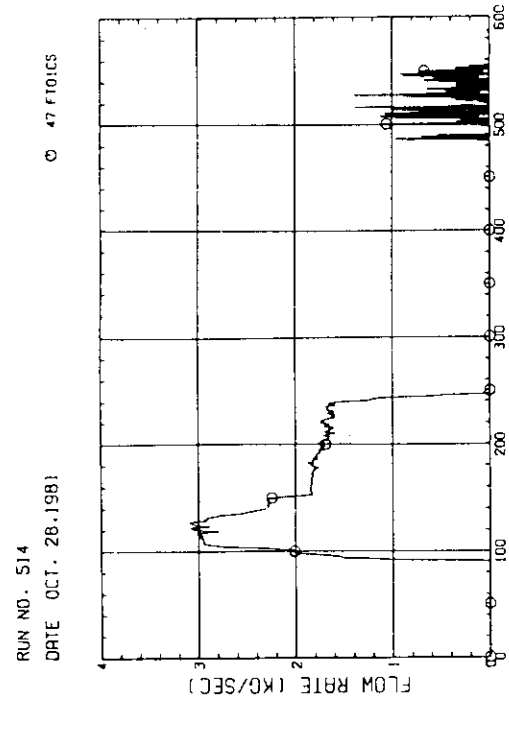

Fig. C-34 Mass flow rate of intact cold leg

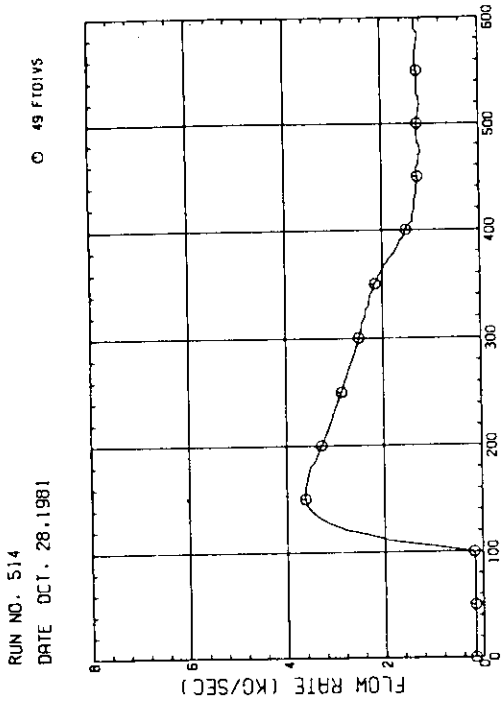

Fig. C-37 Steam flow rate of discharge from containment tank-II